A GLACIOCHEMICAL STUDY OF THE MILL ISLAND ICE CORE

by

Mana Inoue, B.Eng, B.AntStd. Hons

Submitted in fulfilment of the requirements
for the Degree of Doctor of Philosophy

Institute for Marine and Antarctic Studies
University of Tasmania
August, 2015

I declare that this thesis contains no material which has been accepted for a degree or diploma by the University or any other institution, except by way of background information and duly acknowledged in the thesis, and that, to the best of my knowledge and belief, this thesis contains no material previously published or written by another person, except where due acknowledgement is made in the text of the thesis, nor does the thesis contain any material that infringes copyright.

Signed:

Mana Inoue

Date: 12 January 2016

This thesis may be made available for loan and limited copying in accordance with the *Copyright Act 1968*

Signed:

Mana Inoue

Date: 12 January 2016

ABSTRACT

The IPCC 5th Assessment Report states that there are insufficient Southern Hemisphere climate records to adequately assess climate change in much of this region. Ice cores provide excellent archives of past climate, as they contain a rich record of past environmental tracers archived in trapped air and precipitation. However Antarctic ice cores, especially those from East Antarctica, are limited in quantity and spatial coverage. To help address this, a 120 m ice core was drilled on Mill Island, East Antarctica (65° 30' S, 100° 40' E). Mill Island is one of the most northerly ice coring sites in East Antarctica, and is located in a region with sparse ice core data.

The specific project aims were: 1) To produce a high resolution, well-dated record of water stable isotopes (δ^{18}O, δD), and trace ion chemistry (sea salts, sulphate, methanesulphonic acid); 2) to investigate the seasonal and interannual variability of sea salts, in order to reveal which climate factors influence the Mill Island record; 3) to perform a regional comparison of δ^{18}O and snow accumulation rate with nearby existing climate records from ice cores, observational stations, and atmospheric models, in order to seek the optimal method for temperature reconstruction using the Mill Island ice core record.

Hydrogen peroxide, water stable isotopes, and trace ion chemistry were measured at high resolution throughout the entire core. The ice core was dated using a combination of chemical species, but primarily using water stable isotopes. The Mill Island ice core contains 97 years of climate record (1913 – 2009), and has a mean snow accumulation of 1.35 metres (ice-equivalent) per year (mIE/yr). Concentrations of trace ions were generally higher than at other Antarctic ice core sites (e.g., mean sodium levels were 254 $\mu Eq/L$). The full trace ion record contained a mix of periods with well-defined seasonal cycles and periods with weak seasonality and a higher baseline. An abrupt change was observed in the sea salt record in the mid-1930s. This may be related to a significant change in the local ice-scape. Sea salts were compared with instrumental data, including atmospheric models and satellite-derived sea ice concentration, to investigate influences on the Mill Island ice core record. The mean annual sea salt record did not show a correlation with wind speed. Instead, sea ice concentration to the east of Mill Island was found to be likely influencing the annual mean sea salt record, at least during the period of 1979 to 2009. A mechanism involving formation of frost flowers on sea ice was pro-

posed to explain the extremely high sea salt concentration. Post-depositional migration of magnesium and methanesulphonic acid were observed in the trace ion record, and for the first time, migration of sodium and chloride were observed.

Snow accumulation rate was compared with snow accumulation or precipitation record from nearby sites. The Mill Island snow accumulation was found to be influenced by local orography, i.e., the annual snow accumulation record is not strongly related with precipitation in nearby sites. The Zonal Wave Three (ZW3), large scale atmospheric mode, modulates precipitation at nearby Law Dome, and to a lesser extent, modulates Mill Island precipitation.

Snow accumulation and δ^{18}O were compared with precipitation and temperature data from atmospheric models. The climatology of precipitation at Mill Island shows evidence of higher snowfall during winter, consistent with other Antarctic sites. The linear monthly ice core dating was adjusted using the precipitation climatology, and the adjusted δ^{18}O record resulted in a warmer annual signal. This finding indicates that without this adjustment, there is a small cold bias in annual temperature reconstructions from ice cores that share this elevated winter precipitation. This bias should be considered when reconstructing temperatures where climate trends differ with season and when comparing with other temperature reconstructions (e.g., terrestrial or ocean based records).

In situ temperature data (e.g., a co-located Automatic Weather Station) are not available at Mill Island. Instead, the annual mean δ^{18}O record was compared with atmospheric reanalysis model output temperature at Mill Island. The correlation was found to be statistically insignificant. To attempt a more accurate palaeothermometer reconstruction, the annual record was divided into summer and winter "windows" with the maximum δ^{18}O value set as the summer window centre, and the minimum δ^{18}O value set as the winter window centre. It was found that when using narrow summer and winter windows, the δ^{18}O value was significantly correlated with December to April mean model temperatures and May to July mean model temperatures, respectively.

ACKNOWLEDGEMENTS

Firstly, I would like to thank all of my supervisors: Mark Curran, Andrew Moy, Tas van Ommen, Alex Fraser, Helen Phillips, and Ian Goodwin. Especially, huge appreciation to Alex for your lightning speed responses any time, and for wise suggestions not only as a supervisor but also as a good friend; also to Mark for giving me many opportunities during my Ph.D., and such an amazing field work experience. I also would like to thank the glaciology team, Meredith Nation, Sam Poynter, Jason Roberts, Alan Elcheikh, Tessa Vance, Chris Plummer, Shavawn Donoghue, and Ben Domensino for their support; and to the Mill Island field work (AAS project 1236) crew, including Mark Curran, Ian Goodwin, Andrew Moy, Ben Domensino, Troy Baker, and Tim Gill, for their hard work.

My appreciation also goes to Andrew Klekociuk for the HYSPLIT support; Jan Lieser for the sea ice data; Scott Carpentier for useful and helpful climate discussions; Melissa Nigro for the AMPS data; Jan Lenaerts for the RACMO data; Mike Summer and Tom "Tank" Remenyi for the LaTeX support; the ACE CRC and IMAS administration teams, especially Wenneke ten Haout and Kate Maloney for their amazing support and leadership; Guy Williams and the Young Antarctic Scientist (YAS) team (Ben, Nick, Eva, Julie, Molly, Margaux, David, Lavy, Tom, Delphi, Merel, Pearse), it was great fun to visit schools and talk about Antarctic science to kids! Christine Weldrick for proofreading, your fresh eye saved me a lot of work!

Huge thank to the Aurora Basin North (ABN) ice core drilling project crew: Mark Curran (Science leader), Sharon Labudda (Field leader), Tas van Ommen, Noel Paten, Malcolm Arnold, Simon Sheldon, Trevor Popp, Jerome Chappellaz, David Etheridge, Chunlei An, J. P. Steffensen, Andrew Moy, Meredith Nation, Jenny Carlisle, Tony Fleming, Joe "captain" McConnell, Wang Feiteng, Peter Campbell "Bloo", Jason Roberts, Olivia Maselli, Nerilie Abram, Holly Winton, Chris Plummer, Olivier Alemany and Tessa Vance; all the people who supported us from Casey, Kingston, Hobart and all over the world. I had such a great experience during the field work. This was definitely a highlight of my life, and strong motivation for the next steps.

I would like to acknowledge the International Postgraduate Research Scholarship (IPRS), the Australian Postgraduate Awards (APA), and the Antarctic Climate & Ecosystems Cooperative Research Centre (ACE CRC)

for my Ph.D. scholarship, and the Institute for Marine and Antarctic Studies (IMAS) for travel funds.

And of course, enormous thank to all my friends. My Ph.D. life would not be this colourful, meaningful, or joyful without your laughs, love and happiness. In particular, Lucho, my Chilean brother and best friend, thank you very much for looking after me, for all your support, suggestions, help, and for hiking, cooking, movie, playing music, drinking, chatting, everything. What you have done for me is way more worthy than quite few bottles of whisky and shochu! I can't express enough how much I appreciate you. Thank you.
Manu, my French brother, thank you for caring for me, listening all my complaints and giving me French solutions which opened my eyes many times!
Without my two brothers, the last six month of my Ph.D. would have been much harder. I loved the swimming time with you two. Thank you, Onichans.
Eva, thank you for the multiple tea times, complaining together about everything, and kidnapping me for breaks. Julie, thank you for making me laugh and encouraging me when I was really down. You rescued me from darkness many times. Nicole, thanks for the connection between us, laughing and smiling. I miss you and love you so much. You are just amazing! Maurito, Andre, thank you for the countless precious evenings. I miss those times with you guys in Lower Sandy Bay and in Japan! Molly and Lara, the "original friends", thank you for your endless love since my Honours degree. You have been always there when I needed you. Thank you. Amelia, Tania, Nick, Daniela, Malinda, Camila, Max, Pearse, PaPas (Pablo and Pamela), Giulia, and Luchita, thank you for feeding me both food and love. Ramos, Shihong, thank you for your patience. You are the best driving instructors!
Big thanks also go to Alyce, Laura, Jane, Rob, Jessica, Felipe, Gaspar, Elsa, Martin, Martin, Mario, Rob, Fabien, Veronique, Abby, Kathleen, David, Roser, Elias, Malou, Sjoerd, Lev, Alinta, Jake, Ziya, Mr King, Jennifer, Eric, Cecilia, Cedric, Marcelina, Mono, Claudio, Ivan, Fernanda, Gigi, Raphael, Alina, Jessica, Andres, Waldo, Carla, Beltran, Martha, Hiromi, Mao, Maki, Margaux, Nina, Karine, Roland, Axel, Delphi, Cesar, Eric, Marion, Elena, Alice, Kate, Sarah, Kathy, Andreas, Manuel, Camila, Jimmy, Merel, Indi, Lavy, Tom, Christine, Thibaut, Ana, Javier, Leo, Sandra, Jan, Sally, Seb, Julien, Anicee, Rowena, and more! It is nearly impossible to list all of you. Thank you.

Thanks to my sister for encouraging me to back to uni, and to my parents for your support. I'm sorry that my life is not a "normal" Japanese life as you expect. I hope you understand.

Lastly, to GK, no matter what, this whole thing wouldn't have even started without you. Thanks for bearing with my selfishness, thanks for all your time. Thank you.

TABLE OF CONTENTS

LIST OF FIGURES

LIST OF TABLES

Chapter 1

Introduction

1.1 Basis of the study

Climate change is one of the most important and urgent issues facing humankind. Despite recent intensive, globally-coordinated research efforts, key aspects of the climate system are still poorly understood (IPCC, 2014). Antarctica and the Southern Ocean play a critical role in the global climate system. Understanding past climate variability is crucial for interpreting the present climate and understanding the future state of the global climate system. Highly valuable historical records of several key climate parameters are contained within chemical records of Antarctic ice cores, e.g., sea ice extent (e.g., Curran et al., 2003; Abram et al., 2013), the dominant modes of large-scale atmospheric variability in the high-latitude Southern Hemisphere (e.g., Goodwin et al., 2004; Steig et al., 2013), and past temperature (e.g., van Ommen and Morgan, 1997; Schneider et al., 2006). One aim of this thesis is to

extend studies such as these using high resolution records from Mill Island, a new ice core site in East Antarctica. The Mill Island site was selected based on an expected high accumulation rate, and was expected to provide a straightforward high resolution climate record.

1.2 Significance and aims

Mill Island (65° 30' S, 100° 40' E) is situated in East Antarctica, at a location experiencing high and consistent precipitation, making it an ideal location for producing high-resolution and high-quality proxy climate records. A thorough glaciochemical investigation of the Mill Island ice core will contribute to answering the key questions, "What changes are occurring in the climate of Antarctica and the Southern Ocean?" and "What are the links between these changes and the global climate system?" Records of these climate proxies will contribute to improving models of the climate system and projections of the future state of the climate.

This project addresses a knowledge gap identified in the most recent Intergovernmental Panel on Climate Change (IPCC) report: A lack of high-resolution climate records from the Southern Hemisphere. The international ice core community peak planning body, International Partnerships in Ice Core Science (IPICS), has developed scientific goals to address the aformentioned

knowledge gap, and this project contributes to that plan (PAGES 2k Consortium et al., 2013).

The aims of this thesis are:

1. To produce high resolution, well-dated records of water stable isotopes (δ^{18}O, δD), and trace ion chemistry (sea salts, sulphate, methanesulphonic acid) at Mill Island;

2. To investigate the seasonal and interannual variability of sea salts, in order to understand climate factors influencing Mill Island; and

3. To perform a regional comparison of δ^{18}O and snow accumulation rate with nearby existing climate records from ice cores, observational stations, and atmospheric models, in order to determine the optimal method for temperature reconstruction at Mill Island.

This thesis will show that the Mill Island ice core records are unexpectedly complex, with strong modulation of the trace chemistry on long timescales. While this makes interpretation of the record challenging, this thesis will examine potential reasons for the complexity and provide evidence for significant regional influence as a result of long term variability of regional sea ice cover.

This chapter provides the background information for the thesis. Site information about Mill Island, the field season, and details on the ice cores

collected from Mill Island are presented here. The following literature review focuses on snow accumulation, water stable isotopes and trace ion chemistry, particularly sea salts, non sea salt sulphate ($nssSO_4^{2-}$), and methanesulphonic acid (MSA). The review provides background information and discussion of relevant issues that are important in the chapters that follow.

1.3 Site information

Mill Island (65° 30' S, 100° 40' E) is a small island ($\sim 45 \times 35$ km), rising ~ 500 m above sea level, located in East Antarctica. It is connected to the Antarctic continent by the Shackleton Ice Shelf. The relatively low elevation and close distance to the ocean suggests the potential for significant input of maritime air to the snow falling at Mill Island. Mill Island is located approximately 500 km east of Law Dome, 350 km west of Mirny Station, 60 km north of the exposed rock formation known as Bunger Hills, and lies at the northern edge of the Shackleton Ice Shelf in Queen Mary Land (Figure 1.1). The Shackleton Ice Shelf has experienced large changes in the past (Young and Gibson, submitted, 2013) which are likely periodic in nature, and not necessarily forced by changes in the local climate.

Mill Island is the most northerly Antarctic ice core site outside of the Antarctic Peninsula, and therefore the Mill Island ice core comprises the most

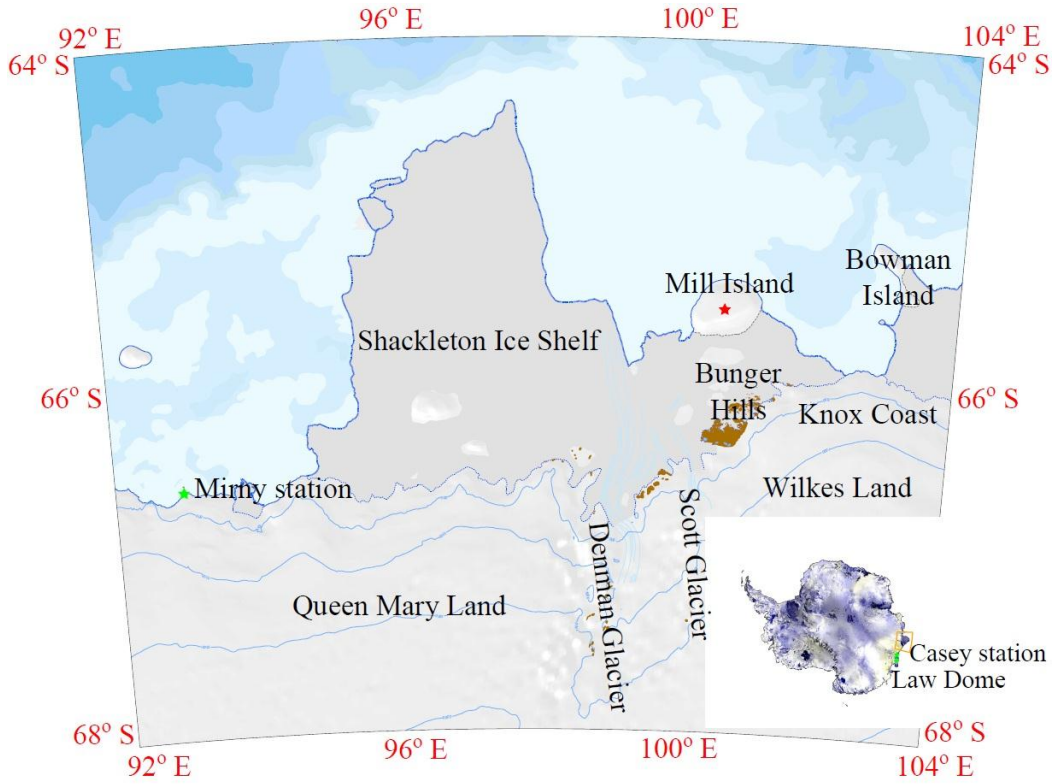

Figure 1.1: A map of the Shackleton Ice Shelf region. This map is modified from map number 13976 produced by the Australian Antarctic Data Centre, courtesy of the Australian Antarctic Division, © Commonwealth of Australia, 2012.

northerly climate record for East Antarctica (Roberts et al., 2013). Mill Island experiences a polar maritime climate and high precipitation, particularly on its eastern flank, due to moist and warm air masses from the Southern Ocean brought onshore by low pressure systems. The site also experiences dry and cold air associated with strong katabatic winds from the continent and low level cloud, fog and rime formation over the summit caused by localised summer sea-breezes associated with nearby sea-ice breakout (Roberts et al., 2013). Records from Mirny Station show that the monthly mean temperature is below zero throughout the year (Turner and Pendlebury, 2004), suggesting that Mill Island has only a small chance of experiencing melt, particularly at the ∼500 m elevation summit. The high precipitation rate and minimal melt makes Mill Island an ideal site from which to extract high resolution climate records for the Southern Hemisphere.

1.3.1 Drilling campaign

In the 2008/2009 summer, one shallow core was recovered during a reconnaissance expedition in preparation for the 2009/2010 drilling program. The main ice core drilling campaign was carried out during the 2009/2010 Australian Antarctic field season as part of a collaboration between Macquarie University, the Antarctic Climate & Ecosystems Cooperative Research Centre (ACE CRC), and the Australian Antarctic Division (AAD) (AAS project

1236). The team spent three weeks in the field, and drilled one 120 m main ice core (MI0910) and seven shallow (from ∼5 m to 10 m) firn ice cores. However, due to harsh weather conditions, other observational data such as snow pit and ground penetrating radar (GPR) data were not acquired. Table 1.1 gives information on each of the ice cores. Figure 1.2 shows the location of each ice core site. Two shallow cores, MIp0910 and MI0kp0910, were derived from the same site as the main core, MI0910. Other shallow cores were taken at a 5 km distance from MI0910 in directions of north, north-east, east, south, and west (MIN5kp0910, MINE5kp0910, MIE5kp0910, MIS5kp0190, MIW5kp0910, respectively).

This thesis focuses on the main (MI0910) ice core record, with the support of two shallow ice cores MIp0910 and MIp0809. The Eclipse ice core drill, an electromechanical dry ice-coring drill detailed in (Blake et al., 1998), used for the main core required ∼2 m of trench for operation. Thus, the main core does not have samples from the surface to the base of the trench. This section of the record was obtained from shallow ice cores drilled with a different drill. The MI0910 record is supplemented at the top by the MIp0910 record.

1.3.2 Previous studies using the Mill Island shallow ice cores

Domensino (2010) used the MIp0910 ice core (spanning 2006 – 2009) in a study aiming to resolve the synoptic climate variability of the Southern Ocean.

Ice core	Latitude	Longitude	Relative location to MI0910 main core	Depth (m)	Drill date
MI0910	65º 33' 10" S	100º 47' 06" E	-	120	2010-01-18
MIp0910	65° 33' 10" S	100° 47' 06" E	0	10.57	2010-01-15
MI0kp0910	65° 33' 10" S	100° 47' 06" E	0	5.13	2010-01-18
MIN5kp0910	65° 33' 10" S	100° 47' 06" E	5km north	5.80	2010-01-18
MINE5kp0910	65° 33' 10" S	100° 47' 06" E	5km north-east	10.50	2010-01-29
MIE5kp0910	65° 33' 10" S	100° 47' 06" E	5km east	10.25	2010-01-29
MIS5kp0910	65° 33' 10" S	100° 47' 06" E	5km south	10.74	2010-01-24
MIW5kp0910	65° 33' 10" S	100° 47' 06" E	5km west	10.14	2010-01-24
MIp0809	65° 33' 25" S	100° 33' 26" E	10km west	16.69	2009-01-22

Table 1.1: The location, depth, and drill date of ice cores recovered from Mill Island.

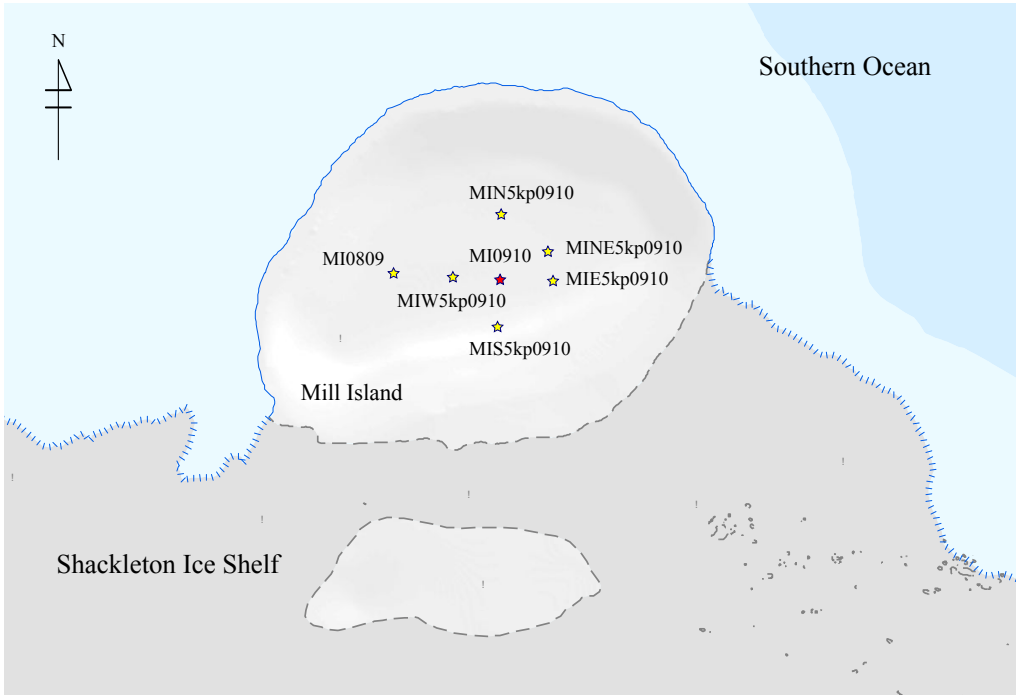

Figure 1.2: The location of the Mill Island ice cores. Two shallow cores, MIp0910 and MI0kp0910, were drilled from same site as the main core MI0190. Map modified from map number 13976 produced by the Australian Antarctic Data Centre, courtesy of the Australian Antarctic Division, © Commonwealth of Australia, 2012.

Sodium (Na^+) originates from open water sea salts and frost flowers on the surface of sea ice. Seasonal variations in Na^+ concentrations were linked to synoptic storm variability, and the partitioning between Na^+ sources within each season was determined by sea ice extent and the dominant synoptic conditions. A higher contribution from frost flowers was evident in seasons where increased sea ice was coupled with synoptic conditions that promote their formation and transportation. Snow accumulation at MIp0910 was found to be ∼42% higher than at MIp0809 in the winter of 2008, due to the location of MIp0809 location on the leeward slope of Mill Island. Summer accumulation variability was found to be linked to the blocking of circumpolar westerlies, with enhanced northerly flow generating a higher snow accumulation rate at Mill Island. Domensino (2010) concluded that there was no significant snow accumulation variability within the spatial array of shallow core sites (representing a spatial separation of ∼15 km). Snow accumulation differences across the island are the result of topographic variations, not spatial variability of precipitation.

1.4 Background on ice core proxies

The following section introduces the background of glaciochemical studies of ice cores related to this thesis. It discusses the use of annual snow accumulation rate, water stable isotopes, trace ion sea salt species, nssSO_4^{2-}, and MSA as

climate proxies.

1.4.1 Snow accumulation

Melting of the Antarctic Ice Sheet plays an important role in sea level rise, however, it is difficult to assess the current contribution of the Antarctic Ice Sheet to sea level rise due to uncertainties in net surface mass balance (SMB) over most of the continent. SMB data are often of limited spatial and temporal representativeness, and current knowledge of SMB is confounded by measurement inaccuracy, and lack of quality control (Magand et al., 2007).

SMB data can be derived from several techniques including precipitation gauges, snow stake measurements, ultrasonic range detectors, and annual snow accumulation records from ice cores. By measuring annual layer thickness and density of the ice core, it is possible to retrieve long-term mean and reliable annual snow accumulation records (e.g., Goodwin et al., 2003; Magand et al., 2007). Collections of reliable long-term snow accumulation point records have been used to construct large-scale, continuous SMB datasets using remote sensing datasets to interpolate between points (e.g., Arthern et al., 2006). Such high quality point SMB collections (e.g., Favier et al., 2013) have also been used to validate the SMB component of atmospheric models (e.g., Lenaerts et al., 2012). Validated SMB models can then be used for sea level rise model projections under various warming scenarios into the 21st century

(e.g., Lenaerts et al., 2013).

The snow accumulation record is also a proxy for circumpolar atmospheric circulation (Goodwin et al., 2003), and for synoptic scale storm events, not only at the ice core site but also in the wider area (Cohen and Dean, 2013). A link between snow accumulation at Law Dome (LD) and precipitation in south-west Western Australia was also identified (van Ommen and Morgan, 2010).

1.4.2 Water stable isotopes

The ratio of water stable isotopes in firn/ice is known to be a proxy for temperature. Temperature is a key parameter in driving water stable isotope fractionation in condensation and evaporation processes as well as transport processes (Dansgaard, 1964). Therefore the ratio of water stable isotopes has been used in earlier ice core studies as a "palaeothermometer" (e.g., Paterson, 1994; van Ommen and Morgan, 1997; PAGES 2k Consortium et al., 2013). The mechanism of water isotopic fractionation, the character of each species, and the relationships between water stable isotope ratio and temperature are described in this section.

Mechanism of water isotopic fractionation, and the role of δ^{18}O, δD, D-ex, and δ^{17}O

The proportions of water stable isotopes, $H_2{}^{16}O$, $H_2{}^{17}O$, $H_2{}^{18}O$ and $HD^{16}O$, are generally uniform throughout the ocean (Dansgaard, 1964; Angert et al., 2004). When water evaporates from the surface of the ocean, heavier isotopes (i.e., $H_2{}^{17}O$, $H_2{}^{18}O$ and $HD^{16}O$), tend to preferentially remain in the ocean. Thus, the water vapour above the surface of the ocean is enriched in $H_2{}^{16}O$ and other light isotopic variants. As the water vapour is transported to higher latitudes, the airmass cools down, and molecules with heavier isotope preferentially precipitate to avoid supersaturation. Thus, the water vapour becomes more depleted in heavier isotopes molecules as the surrounding air temperature cools (Morgan, 1982). The ratio of heavier isotopes (δ) relative to Standard Mean Ocean Water (SMOW), is calculated with the following equation (Dansgaard, 1964; Paterson, 1994)

$$\delta = \frac{\alpha_{sample} - \alpha_{SMOW}}{\alpha_{SMOW}} \times 10^3 \text{ ‰} \tag{1.1}$$

where α is the concentration of the isotopes in sample (α_{sample}), and in SMOW (α_{SMOW}). The final δ values in precipitation at the site depend mainly on the total amount of water vapour lost from the air mass, and this is largely controlled by temperature via its effect on the saturation vapour pressure (Morgan, 1985). As the δ values in precipitation relate closely to temperature, the ratios of oxygen isotope (δ^{18}O) and deuterium (δD) have both been used

as proxies for site temperature.

While δ^{18}O and δD both give past temperature information, the combination of these two isotopes and deuterium excess (D-ex), provides additional information on past temperature and evaporative conditions over the ocean (Bradley, 1999; Delmotte et al., 2000). D-ex reflects the different behaviours of $HD^{16}O$ and $H_2{}^{18}O$ occurring during the processes of evaporation and condensation (Delmotte et al., 2000), and thus has been used for deriving moisture source information. However D-ex is influenced by the relative humidity of the oceanic source region as well as sea surface and site temperatures, making it difficult to use as a sole indicator for moisture source conditions (Landais et al., 2008). D-ex is calculated with the equation

$$D\text{-}ex = \delta D - 8\,\delta^{18}O$$

(Paterson, 1994; Delmotte et al., 2000).

Until recently, the depletion of $H_2{}^{17}O$ in precipitation was assumed to carry no additional information to that of $H_2{}^{16}O$ and $H_2{}^{18}O$ (Angert et al., 2004). Furthermore, measurement of δ^{17}O was impractical until recently (Landais et al., 2008). Angert et al. (2004) suggested the potential use of δ^{17}O, and recent analytical improvement has made the measurement of δ^{17}O possible (Barkan and Luz, 2005; Landais et al., 2008). Together with δ^{18}O and D-ex, δ^{17}O from coastal ice core sites may be used as a proxy for relative humidity at the moisture source (Landais et al., 2012).

δ^{18}O as a temperature proxy

Since δ^{18}O and δD values in precipitation depend on the temperature at the moisture source (i.e., the sea surface temperature, SST) and at the precipitation site, and because the SST is more stable than the air temperatures at high latitudes, the dependence on SST is relatively smaller, so values of δ^{18}O and δD in polar snow both strongly reflect the temperature at the site and time of precipitation. Thus, measuring these ratios as a function of depth in an ice core can be interpreted as a record of site temperature (Paterson, 1994). δ^{18}O and temperature generally display a linear relationship, given by the following empirical equation

$$\delta^{18}O = \alpha T + \beta \tag{1.2}$$

where T is the site temperature and the parameters $\alpha = \mathrm{d}\delta/\mathrm{dT}$ and β are calibration constants for the isotope thermometer (van Ommen and Morgan, 1997). Whilst the parameter α, i.e., the calibration slope, typically lies within the range of 0.6 to 0.7 ‰/K in Greenland and inland Antarctica (Dansgaard, 1964; Paterson, 1994; van Ommen and Morgan, 1997), the calibration slope, however, can be different at each site. This is due to other processes such as changes in the moisture source, and transport processes may also influence the isotopic signal for that site. For example, van Ommen and Morgan (1997) found $\alpha = 0.44$ ‰/K from the Law Dome ice core.

1.4.3 Trace ion chemistry

The atmosphere contains various soluble and insoluble impurities originating from three sources: The ocean (e.g., sea salt); the surface of the continents (e.g., terrestrial dust); and biogenic or anthropogenic gas emissions (e.g., dimethyl sulphide [DMS] and hydrogen chloride [HCl]) (Legrand and Mayewski, 1997). Primary aerosols, e.g., sea salt and dust, are directly introduced into the atmosphere by wind from marine and continental surfaces. Secondary aerosols are produced within the atmosphere during oxidation of trace gases (Legrand and Mayewski, 1997). Trace ion records represent a wide range of environmental information. For example, Plummer et al. (2012) investigated nssSO_4^{2-} from the Law Dome ice core to determine the timing of volcanic eruption events over the past 2000 years. Also, Goodwin et al. (2004) and Vance et al. (2013) used sea salt (sodium [Na^+]) to investigate large-scale climate phenomena such as the Southern Annular Mode (SAM) and El Niño, respectively. Moreover, sea salt and methanesulphonic acid (MSA) have been studied as proxies for sea ice (Curran et al., 2003; Wolff et al., 2003; Abram et al., 2013). The trace ions measured in this thesis can broadly be categorised into two groups: Sea salt species (Na^+, Cl^-, Mg^{2+}, Ca^{2+} and a part of SO_4^{2-}); and non sea salt species (MSA, nssSO_4^{2-}, and NO_3^-). This section introduces sea salt, nssSO_4^{2-} and MSA, which are a focus of this thesis.

Sea salt: Open ocean and frost flower

Sea salt concentration in Antarctic ice cores is characterised by a winter maximum and a summer minimum, despite the closer distance to the open ocean during summer (Legrand and Mayewski, 1997). This apparent contradiction leads to a discussion of the source of sea salt. Sea spray (i.e., bursting of air bubbles during wave breaking) from the open ocean is the main source of sea salt, and the increased storm activity during winter causes the winter time maximum (Wagenbach et al., 1998a; Benassai et al., 2005). Snow pit studies have also shown high sea salt concentrations in snow following the passage of marine air advected to higher latitudes via cyclonic systems (McMorrow et al., 2001). During winter, the ratio of chloride (Cl^-) to Na^+ in ice cores is close to that of bulk seawater, suggesting that both Na^+ and Cl^- originate from sea salt. This ratio changes in summer due to additional Cl^- input from (HCl), especially farther inland (Legrand and Mayewski, 1997). Therefore, Na^+ is generally used as a representative of sea salt, and it has also been considered as a proxy of wind speed and storminess (Legrand and Mayewski, 1997; Curran et al., 1998; Wagenbach et al., 1998a).

It has also been suggested that frost flowers play an important role as a sea salt origin (Rankin et al., 2002). Frost flowers are ice crystals that grow on the upper surface of young sea ice. Frost flowers are highly saline and highly fractionated in sea salt ions, with sulphate being strongly depleted relative to

Na^+ (Rankin et al., 2002). There are four steps for frost flower formation. Firstly, the brine in thin young sea ice is transported toward the relatively colder surface due to the thermomolecular pressure gradient (Martin et al., 1996). The brine accumulates as both a liquid and a slushy layer on the surface of newly formed sea ice. Secondly, the surface brine evaporates into the colder atmospheric boundary layer which creates a thin (1 – 3 cm thickness) layer of water vapour just above the surface. This water vapour layer is supersaturated with respect to ice, and promotes deposition of crystal growth i.e., frost flowers (Rankin et al., 2002). Next, beneath the frost flowers, a saturated brine slush layer forms (2 – 4 mm thickness). Finally, surface tension effects cause the incorporation of the surface brine onto the frost flowers, resulting in high salinity on the frost flowers (Hall and Wolff, 1998; Rankin et al., 2002). These fragile frost flowers are expected to efficiently aerosolise (Rankin et al., 2002). Frost flowers have a salinity of almost three times the concentration of sea water attributing to the high salt concentration in the ice core during winter (Rankin et al., 2000). Thus, the sea-ice zone around Antarctica (particularly coastal regions) is an important source of sea salt aerosols (Abram et al., 2013).

Another important sea salt source could be the sublimation of salty blowing snow on sea ice (Yang et al., 2008). Dry, small particles of condensed sea salt snow are easily mobilised in strong winds, and this salty blowing snow may sublimate to produce salty aerosols. Therefore, the sea-ice zone

around Antarctica may be an important source of sea salt aerosols, especially in coastal Antarctica, and thus the sea salt record may be useful as a sea ice proxy (Wolff et al., 2003; Abram et al., 2013).

Non sea salt sulphate

Sulphate in ice cores originates from several sources. They include sea salt as a primary source, continental dust, large volcanic eruptions, and biological activity (Legrand and Mayewski, 1997; Curran et al., 1998). $\mathrm{nssSO_4^{2-}}$ is produced by the oxidation of sulphur dioxide (SO_2), which is derived from the oxidation of reduced organic sulphur gases, emitted mainly from the ocean and volcanoes. Thus, $\mathrm{nssSO_4^{2-}}$ is believed to indicate marine biogenic activity as well as being a volcanic activity indicator (Curran et al., 1998). $\mathrm{nssSO_4^{2-}}$ is calculated by subtracting sea salt sulphate from total sulphate.

$$[\mathrm{nssSO_4^{2-}}] = [\mathrm{totalSO_4^{2-}}] - k * [X] \tag{1.3}$$

where X is the reference sea salt component, usually $\mathrm{Na^+}$ (sometimes $\mathrm{Cl^-}$), and k is the bulk sea water ratio of $[\mathrm{SO_4^{2-}}]/[\mathrm{Na^+}]$ (Hall and Wolff, 1998). If all of the sulphate in the ice core originated from seawater, the ratio of sulphate to $\mathrm{Na^+}$ (or $\mathrm{Cl^-}$) in the ice core should be equal to the bulk seawater ratio, and the $\mathrm{nssSO_4^{2-}}$ value would be zero. If there are other sulphate sources such as marine biogenic or volcanic emissions, $\mathrm{nssSO_4^{2-}}$ becomes positive (Wagenbach et al., 1998a; Hall and Wolff, 1998). Negative values are often observed in ice

core nssSO_4^{2-} concentration records during winter (Wagenbach et al., 1998a; Curran et al., 1998). These deficiencies are generally well correlated with sea salt (Na^+ or/and Cl^-) concentration (Wagenbach et al., 1998a), and generally occur when the wind blows from a new sea-ice formation area (Hall and Wolff, 1998). These SO_4^{2-} depleted aerosols originate from frost flowers.

Methansulphonic acid (MSA)

MSA has only one source: Oxidation of DMS. DMS is a volatile sulphur gas produced by oceanic phytoplankton (Legrand and Mayewski, 1997; O'Dowd and de Leeuw, 2007). Those phytoplankton are particularly abundant in the sea ice zone, and produce DMS during summer months (Curran et al., 2002). Therefore, MSA is deposited in summer, and is used as a proxy for marine biogenic activity as well as sea ice extent (Welch et al., 1993; Legrand and Mayewski, 1997; Curran et al., 2003; Abram et al., 2013). Although the mechanism of MSA production within the sea ice zone is not yet fully understood, MSA is the most robust sea ice proxy at high accumulation coastal ice core sites (Abram et al., 2013).

Post-depositional MSA migration is frequently observed in ice core records (e.g., Wolff, 1996; Pasteur and Mulvaney, 2000; Curran et al., 2002). MSA generally shows a peak in summer in the top part of ice cores, in phase with nssSO_4^{2-}. However with increasing depth, MSA peaks gradually become out

of phase with nssSO_4^{2-} and finally peak in winter ice (Mulvaney et al., 1992; Wolff, 1996). This winter MSA peak is thought to migrate from summer snow, since MSA deposition in winter is highly unlikely (because MSA depends on production of marine biological activity, and nssSO_4^{2-} peaks remain in summer layers). Possible MSA migration occurs when MSA diffuses in either a vapor or liquid phase, and becomes locked in a winter layer by forming an insoluble salt with a cation (Pasteur and Mulvaney, 2000). Therefore, special attention is required to interpret the MSA record. However, because migration is likely contained within a single annual layer, such migration should not affect multi-year average MSA values (Curran et al., 2002).

1.5 Thesis structure

The background information for this thesis was provided in this chapter, including information about Mill Island, the ice core drilling campaign and the methodology for the laboratory procedures. Chapter 2 presents the measurement results of H_2O_2, water stable isotopes, and trace ion chemistry. Dating of Mill Island main ice core and a discussion of sulphate fractionation are also given in Chapter 2. The relationship between sea salt trace ion species and the local and regional environment of Mill Island are investigated in Chapter 3. Snow accumulation and temperature reconstructions using oxygen isotopes are presented in Chapter 4. Finally, Chapter 5 concludes the thesis, and suggests

future directions for the Mill Island ice core processing and interpretation. In addition, an appendix describing ice core dating uncertainties is included at the end of the thesis.

Chapter 2

Dating and glaciochemistry of the high resolution Mill Island ice core

2.1 Introduction

This chapter presents high resolution, well-dated records of water stable isotopes and trace ion chemistry from the main Mill Island 120 m ice core (MI0910) which will be used as climate proxies in the following chapters. The visual stratigraphy of MI0910 is documented in order to investigate the influence of coarse-grained layers on the measurement results. Sea salt fractionation is also investigated, in order to calculate non sea salt sulphate ($nssSO_4^{2-}$).

Accurate ice core dating is crucial for calibration and interpretation of ice core records. Many different dating methods have been used in the past including counting seasonal variations, radioisotopic methods, and reference horizons (Legrand and Mayewski, 1997; Bradley, 1999). In cores with sufficient accumulation rate, many trace records show distinct seasonal varieties which can be used to identify annual layers. For example, hydrogen peroxide (H_2O_2) shows clear seasonal variability in Antarctic snow due to its dependence on

tropospheric photochemistry formation processes (Logan et al., 1981; Sigg and Neftel, 1988; van Ommen and Morgan, 1996). Water isotope ratios (e.g., $\delta^{18}O$) also show seasonal cycles with more highly fractionated values in winter snow than in summer snow due to the close relationship with atmospheric temperature, as discussed in Chapter 1 (Bradley, 1999). Major trace ion chemicals (e.g., sodium [Na^+], chloride [Cl^-], nitrate [NO_3^-], calcium [Ca^{2+}]) also generally show pronounced seasonal variations and can be used for annual layer counting (Curran et al., 1998; Bradley, 1999). Various dating methods are used depending on the required accuracy and snow accumulation rate (Legrand and Mayewski, 1997). Using several records for dating is an effective method for counting annual layers, because different mechanisms express the seasonal cycle in different parameters. Multi-record layer counting can minimise dating uncertainties (e.g., Dansgaard et al., 1982; Morgan et al., 1997).

The stratigraphy of the MI0910 ice core shows higher density layers distributed occasionally throughout the entire ice core (Roberts et al., 2013). Layered structures such as these can be formed due to variations in meteorological conditions during precipitation processes, high surface temperatures inducing melt or enhanced grain metamorphism, or strong wind conditions during precipitation hiatuses (Langway, 1970; Alley et al., 1997). Warmer surface snow quickly covered by colder snow can eventually produce depth hoar, a consequence of restricted upward heat transfer and vapour migration

(Langway, 1970). Such layers can form from a small amount of liquid water condensing onto a surface or near-surface crust (Das and Alley, 2005). Hence the presence of fog may cause such a layer. Strong seasonal and diurnal temperature gradients drive grain-size growth (Linow et al., 2012). Strong continuous wind during precipitation hiatuses can remove surface snow. As a consequence, larger grains of near-surface snow are exposed, absorbing more solar radiation and accelerating grain growth and metamorphosis of the near-surface snow (Goodwin, 1990; Das et al., 2013). These grain metamorphism processes can occur rapidly (Langway, 1970; Alley, 1988). The cause of each layer is difficult to explicitly investigate by close inspection alone (Kinnard et al., 2008). Thus all such layers observed in MI0910 are here termed "crust layers" for convenience.

Non sea salt sulphate ($\mathrm{nssSO_4^{2-}}$) is sulphate which has not originated from sea salt. The main source of $\mathrm{nssSO_4^{2-}}$ in coastal Antarctic ice cores is from oxidation of sulphur dioxide from biogenic production in the ocean (Curran et al., 1998). Volcanic sulphate deposition is also seen in the $\mathrm{nssSO_4^{2-}}$ record. Generally, $\mathrm{nssSO_4^{2-}}$ is calculated by subtracting the total sea salt originated sulphate from total sulphate. The total sea salt sulphate is estimated from the concentration of a "conservative" sea salt ion such as sodium along with an assumed sea water ratio (see below). Occasionally, calculated $\mathrm{nssSO_4^{2-}}$ values in Antarctic snow and ice cores are negative due to sea salt fractionation (Hall

and Wolff, 1998; Wagenbach et al., 1998a). Fractionation of sea salt happens when a constituent of sea water is removed, leaving behind a deficit of that species (Hall and Wolff, 1998). Sea salt fractionation is the depletion of sea salt sulphate relative to sodium in snow and ice cores and has been identified at many coastal Antarctic sites during winter period (Minikin et al., 1998; Rankin et al., 2002). These depleted aerosols most likely originate from frost flowers which form on the surface of new sea-ice when the surface temperature is below -8 ℃, and the surface wind speed is low (Perovich and Richter-Menge, 1994; Rankin et al., 2000). Mirabilite ($Na_2SO_4{\cdot}10H_2O$) crystallises below -8 ℃ in brine which accumulates at the top of the sea ice surface. Hence the remaining brine becomes depleted in SO_4^{2-} (Wagenbach et al., 1998a). As a consequence, frost flowers which form in surface temperatures below -8 ℃ are depleted in SO_4^{2-} (Rankin et al., 2000). Details of frost flower formation are described in Section 1.4.3.

This chapter presents the dating of the MI0910 ice core, together with the full records of water stable isotopes, hydrogen peroxide, and trace ion records for MI0910. The stratigraphy study of the MI0910 ice core, and the calculation of the non sea salt sulphate record are also discussed.

2.2 Method

2.2.1 Ice core analysis

The Mill Island ice cores were processed and analysed in the glaciology laboratory at ACE CRC, Hobart, Australia. This section describes the analytical methods used, including the ice core processing, and measurements for hydrogen peroxide, water stable isotopes, and trace ion chemistry analysis.

Ice core processing

The Mill Island ice cores were processed in a clean freezer (−18℃) laboratory using similar techniques to those described by Curran and Palmer (2001). Ice core density calculations were carried out using the width, length, diameter and weight measurements for each core segment (∼1 m long). Visual observation was also completed for stratigraphy studies. The cores were then transversely divided into three sticks using a clean band-saw. The sticks were used for analyses, including hydrogen peroxide, stable water isotope, and trace ion chemistry measurements. The sticks for hydrogen peroxide and water stable isotope measurements were then cut into 4 cm samples and bagged for analysis. The chemistry sticks were cleaned to avoid contamination and sampled every 4 cm (i.e., approx. 25 samples per ∼ 1 m core segment). Cleaning was achieved by removing ∼ 3 mm of each surface with a microtome under a laminar airflow hood. Chemistry samples were stored in a Coulter cup and

melted in a refrigerator overnight to avoid MSA loss (Abram et al., 2008), then refrozen again. The refrozen samples were melted prior to analysis. All tools used for processing ice cores were carefully pre-cleaned with deionised ultra-clean Milli-Q water (resistivity $>$ 18 MΩ–cm), and polyethylene gloves were worn during the ice core processing, to minimise contamination.

Hydrogen peroxide (H_2O_2) measurement

Hydrogen peroxide (H_2O_2) is influenced by photochemical processes. This provides a strong seasonal variation, with a peak during summer when short-wave radiation fluxes are higher. Thus, it is useful for dating ice cores (Sigg and Neftel, 1988). Hydrogen peroxide measurements were carried out at ACE CRC, using a fluorescence detector as detailed by van Ommen and Morgan (1996). A 4 cm sample was analysed every 8 cm from the surface to a depth of 25 m, then every 12 cm for the rest of the core due to time constraints.

Water stable isotope measurement

The water stable isotope measurements (δD and δ^{18}O) were carried out at the ACE CRC/AAD isotope laboratory, Hobart, Australia, using a high-temperature elemental analyser (EA). The Eurovector EuroPyrOH-HT system was interfaced in continuous flow mode to an Isoprime isotope ratio mass spectrometer. Samples at 4 cm sample resolution were melted in a refrigerated unit prior to analysis. Liquid samples were sampled by a Eurovector liquid

auto-sampler (LAS EuroAS300). Analytical precision for δD is < 0.5 ‰ and for δ^{18}O is < 0.1 ‰, and values are expressed relative to the Vienna Standard Mean Ocean Water 2 (VSMOW2). D-ex was then calculated from the measured δD and δ^{18}O using the following equation

$$\text{D-ex} = \delta D - 8 \times \delta^{18} O \tag{2.1}$$

(Paterson, 1994).

Trace ion chemistry measurement

Trace ion chemical measurements were carried out using a suppressed ion chromatograph (IC) as detailed by Curran and Palmer (2001). Samples were melted overnight in a refrigerator prior to analysis. Due to the high sea salt concentration, the melted samples were diluted 50 times in autosampler polyvials using a micropipette within a laminar flow. Further dilutions (5 to 100 times) were completed according to the sea salt concentration from the result of the initial analysis.

Samples were then analysed using a Dionex AS18 ICS-3000 (2 mm) microbore ion chromatograph. Anions (i.e., MSA, Cl^-, SO_4^{2-}, and NO_3^-) were analysed using an IonPac AS18 separation column and AG18 guard column. Cation (i.e., Na^+, K^+, Mg^{2+}, and Ca^{2+}) analysis was performed using CS12A separation columns. The system performed anion and cation analysis simultaneously using dual isocratic pumps. The major ion species measured in this

study were $CH_3SO_3^-$ (MSA), Cl^-, NO_3^-, SO_4^{2-}, Na^+, K^+, Mg^{2+}, and Ca^{2+}. The $nssSO_4^{2-}$ record was then calculated using the formula

$$[nssSO_4^{2-}] = [SO_4^{2-}] - k_{Na} \times [Na^+] \tag{2.2}$$

where k_{Na} is sea salt ratio of SO_4^{2-} to Na^+, 0.120 (Mulvaney and Wolff, 1994). All trace ions were calibrated using diluted standards (Curran and Palmer, 2001) expressed in concentrations of microequivalents per litre ($\mu Eq/L$).

2.2.2 Dating

Accurate ice core dating is crucial for calibration and interpretation of ice core records. MI0910 was dated by counting annual layers of H_2O_2, water isotopes ($\delta^{18}O$, δD), and deuterium excess (D-ex) according to the methods presented in Plummer et al. (2012). The results of this dating method are presented in Section 2.3.2. The layer counting method using H_2O_2, $\delta^{18}O$, δD, and D-ex was subsequently confirmed by the non sea salt sulphate ($nssSO_4^{2-}$) record, which matches the timing of volcanic eruptions at Law Dome (LD) (Plummer et al., 2012) and at other ice core sites (Cole-Dai et al., 1997, 2000). The shallow cores MIp0910 and MI0809 were also dated using the layer counting technique to supplement the top of the MI0910 core (Table 2.1), and to verify the MI0910 dating.

Ice core	Lat	Lon	Depth (m)	Drill date
MI0910	65^o 33' 10" S	100^o 47' 06" E	120	2010-01-18
MIp0910	65^o 33' 10" S	100^o 47' 06" E	10.57	2010-01-15
MIp0809	65^o 33' 25" S	100^o 33' 26" E	16.69	2009-01-22

Table 2.1: Mill Island ice core information

2.2.3 Stratigraphy

Visual stratigraphy observation was achieved by counting and logging the crust layers. The crust layers were measured for thickness and counted manually during processing of the ice core. An example of the crust layers is given in Figure 2.13, and the results are presented in Figure 2.14.

2.3 Results and discussion

2.3.1 Measurement results

This section presents the full records of hydrogen peroxide (H_2O_2), water stable isotope ($\delta^{18}O$, δD), and trace ion chemistry. The top part of all records (depth 0 m to ∼2 m) was supplemented by the MIp0910 record.

H_2O_2 and water stable isotope records

Figure 2.1 presents the entire 120 m records of (a) H_2O_2, (b) $\delta^{18}O$, (c) δD, and (d) D-ex. The H_2O_2 record generally shows a strong annual cycle, except for

at depth $\sim$ 50 to 60 m and 80 to 90 m where there is an observed loss of H_2O_2 (Figure 2.1 a). Such a loss of H_2O_2 seasonality has previously been attributed to transient melt events (van Ommen and Morgan, 1996). However this is not necessarily the case at Mill Island. Further discussion of this loss of H_2O_2 is presented in Section 2.3.4. Because of the unambiguous peak distribution outside of these two regions (i.e., depth $\sim$ 50 to 60 m and 80 to 90 m), the H_2O_2 record was primarily used for dating MI0910 (Section 2.3.2). The H_2O_2 record shows a baseline drift below $\sim$ 100 m which is attributed to calibration problems. Despite this, the data show strong seasonal variations which are sufficient to assist annual layer counting throughout most of the record.

The water stable isotope (δ^{18}O, δD) and the deuterium excess (D-ex) records also show annual cycles throughout the core (Figures 2.1 b, c, and d respectively). Oxygen isotope (δ^{18}O) and deuterium (δD) show similar features.

Trace chemistry record

Ion chromatograph (IC) measurements of concentrations of a) Na^+, b) Cl^-, c) MSA, d) SO_4^{2-}, e) nssSO_4^{2-}, f) Mg^{2+}, g) Ca^{2+}, and h) NO_3^- for the Mill Island 120 m ice core are shown in Figure 2.2. Typically, these trace ion species show strong seasonal variations (e.g., Na^+ and Cl^- have a winter peak, MSA has a summer peak). Therefore, they are useful tools for annual ice core dating

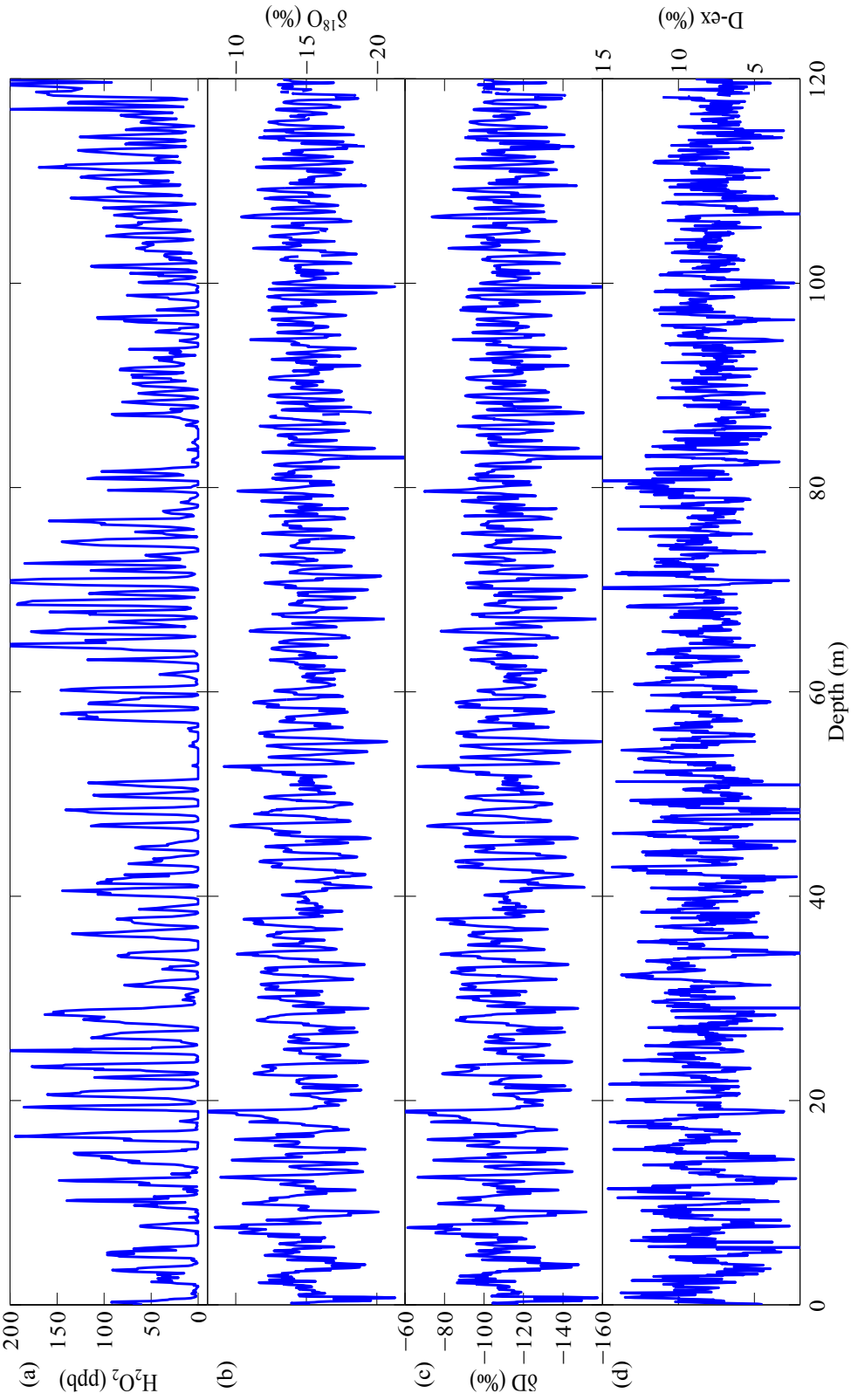

Figure 2.1: Mill Island 120 m ice core records of H_2O_2 (a), $\delta^{18}O$ (b), δD (c), and D-ex (d).

(Legrand and Mayewski, 1997). However the results for the trace ion chemistry at Mill Island show clear seasonality only in the top ~ 20 m of the ice core. The seasonality in trace chemistry either disappears, or shows incoherent peaks below ~ 20 m (Figure 2.2). The baselines of Na^+ and Cl^- are also higher from ~ 20 to ~ 100 m depth.

The mean concentration and standard deviation of each trace ion species is presented in Table 2.2. The standard deviation is higher than the mean concentration for all species. The mean concentration of all trace ion species (except nitrate) is higher at Mill Island than at LD (Curran et al., 1998). Further details and a comparison with other sites is provided in Figure 2.18 and Chapter 3.

The next section presents the dating of MI0910 using these records. Further discussion and interpretation of all records is given after the dating section.

2.3.2 Dating

Mill Island main ice core (MI0910)

Annual layers where seasonal variations occur in chemical and physical properties are typically used to mark year boundaries in ice cores that have sufficient and regular snow fall. The chemical signals at Mill Island are complicated (e.g., see Na^+ in Figure 2.2), and therefore a single parameter is insufficient

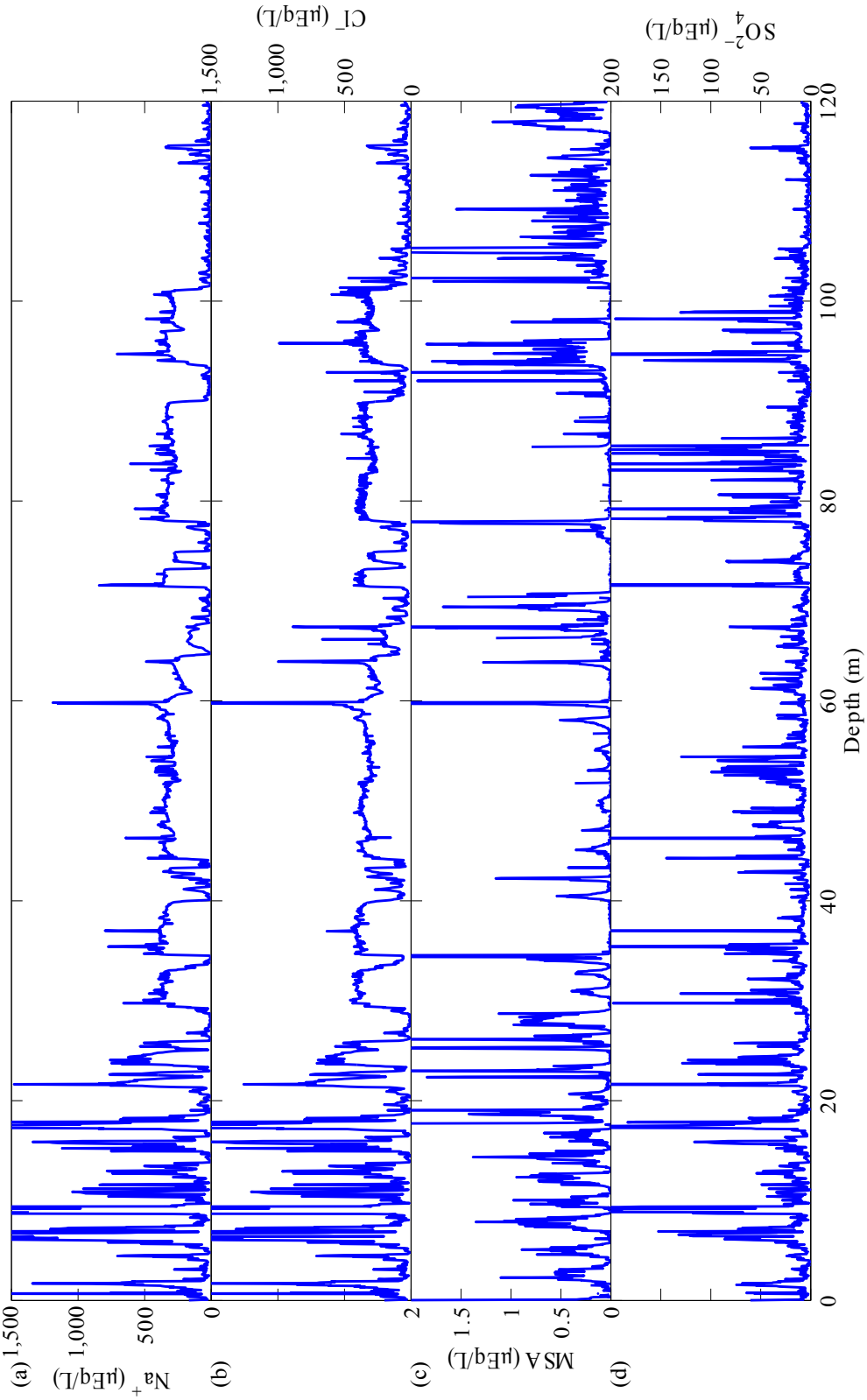

Figure 2.2: Mill Island 120 m ice core record of a) Na^+, b) Cl^-, c) MSA, and d) SO_4^{2-}.

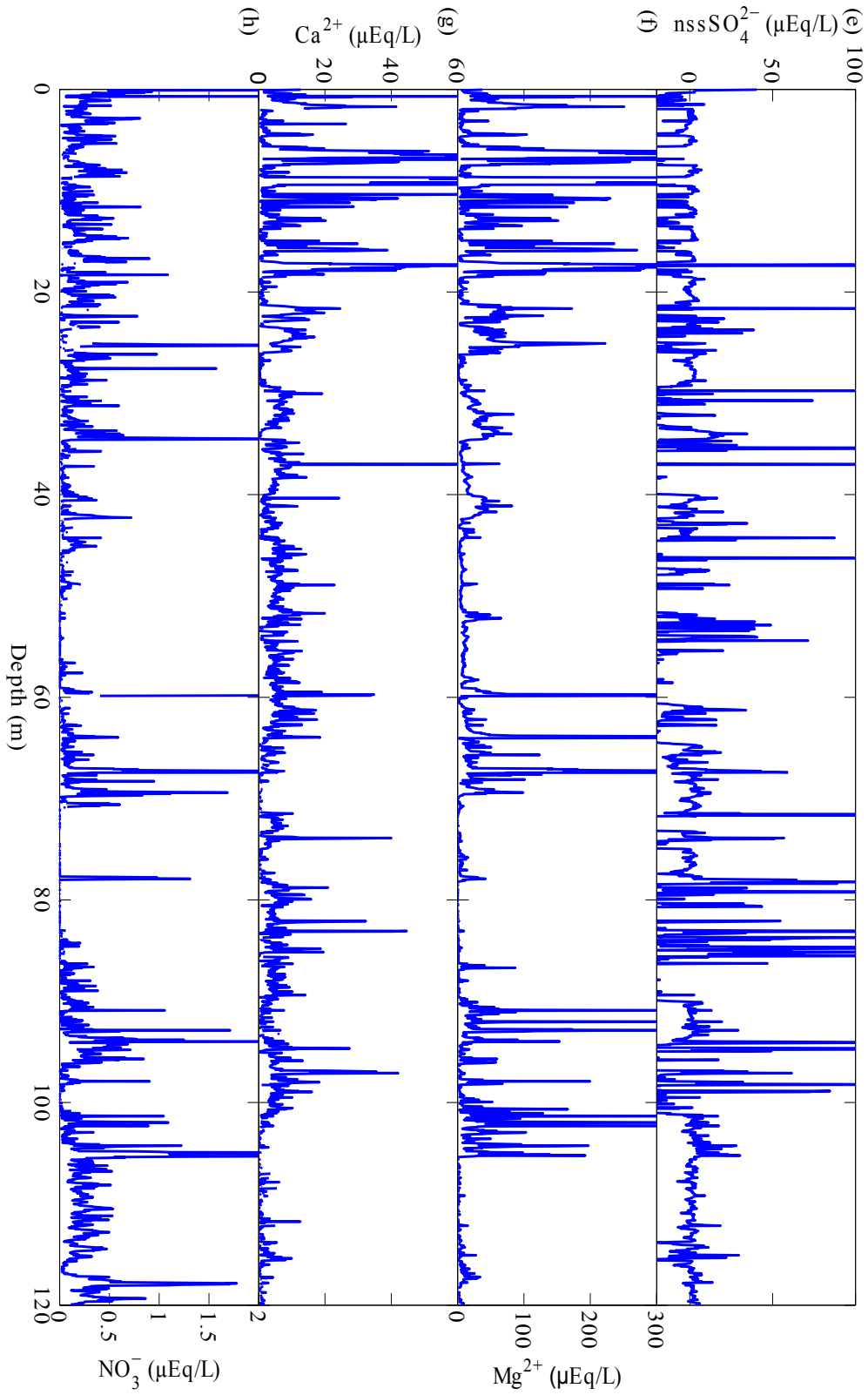

Figure 2.2: Mill Island 120 m ice core record of e) $nssSO_4^{2-}$, f) Mg, g) Ca, and h) NO_3.

Ion	Mean concentration ($\mu Eq/L$)	Standard deviation ($\mu Eq/L$)	Sample number	Standard error of the mean ($\mu Eq/L$)
Sodium	254.13	411.43	2913	7.62
Chloride	289.73	478.63	2912	8.87
MSA	0.21	0.54	2789	0.01
Sulphate	20.39	39.97	2913	0.74
nss-sulphate	-10.16	39.73	2913	0.74
Magnesium	32.20	90.51	2791	1.71
Calcium	6.50	15.02	2632	0.29
Nitrate	0.19	0.45	2489	0.01

Table 2.2: Mean concentration, standard deviation, sample number, and standard error of the mean of the trace ion species from the complete 120 m MI0910 ice core.

to determine annual layers at this site. H_2O_2 and $\delta^{18}O$ were primarily used to identify annual layers. Where there were ambiguities with these records, D-ex was also used. The trace chemistry record was not used to identify annual layers because seasonal variations are only present in the top $\sim$20 m of the record (see Section 2.3.1).

The oxygen isotope ratio ($\delta^{18}O$) peak was used as a marker of the beginning of the year. This is associated with temperature at the core site (Dansgaard, 1964; Paterson, 1994) and thus presents a maximum value during summer (e.g., at LD, van Ommen and Morgan (1997)). The Mill Island $\delta^{18}O$ record often shows multiple peaks throughout the year which makes it difficult to determine the maximum summer peak in some years. Therefore, the D-ex trough was used to guide the choice of the beginning of the year when required. D-ex commonly shows a summer trough. This feature is thought to be a consequence of open water nearby the site acting as a source of moisture (Delmotte et al., 2000).

Peak picking for the beginning of each year

Figure 2.3 shows an example of choosing a peak as a beginning of a year. Years 2001 and 1998 are relatively simple: There is one clear H_2O_2 and $\delta^{18}O$ peak, with a D-ex trough. Note that the year used in this thesis is A.D.

In 2000, the H_2O_2 peak indicates an annual layer marker at around

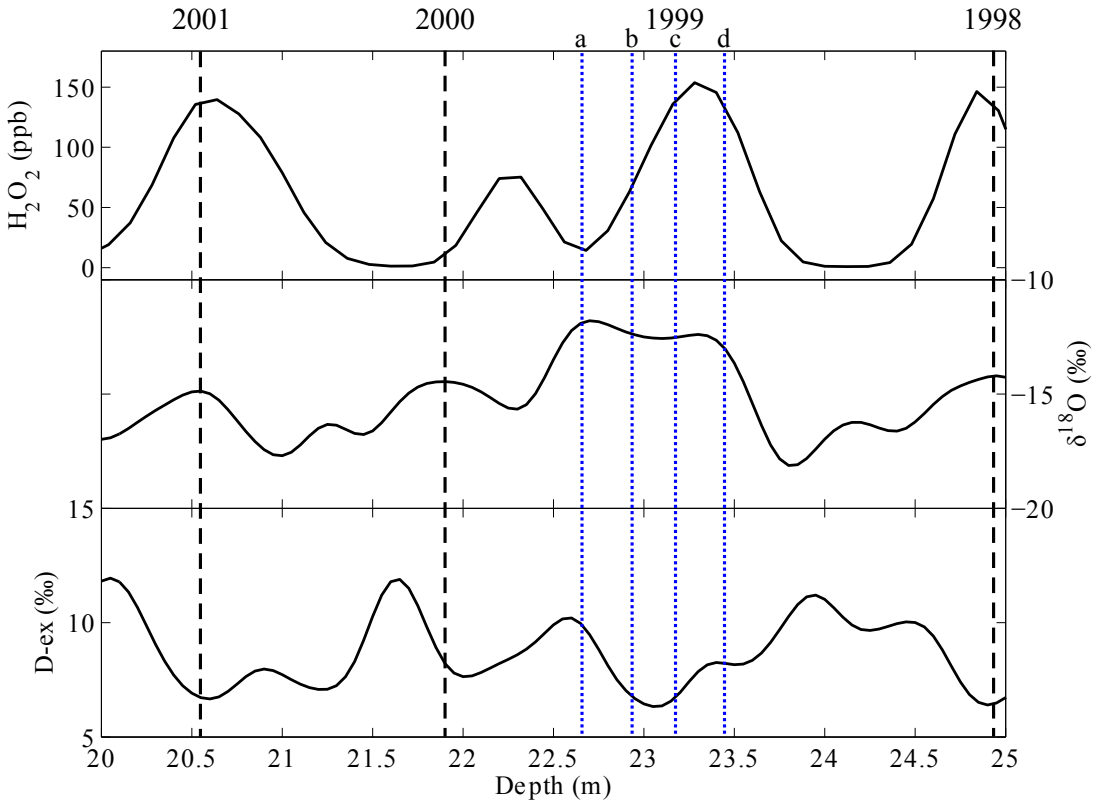

Figure 2.3: H_2O_2, δ^{18}O and D-ex records are shown, from depth 20 – 25 m. The black dashed vertical line represents the beginning of each year. The blue dotted lines, a, b, c, and d, demonstrate potential choices for the beginning of 1999. See the text for more details. Because the resolution of the H_2O_2 and isotope measurements is different (see Section 2.2.1), H_2O_2 data were re-sampled to a regular 12 cm grid, and smoothed with a Gaussian filter of width $\sigma = 1$ point; δ^{18}O and D-ex data were re-sampled to a regular 5 cm grid, and smoothed with a Gaussian of width $\sigma = 2.4$ points.

22.25 m depth. However $\delta^{18}O$ shows no peak and the D-ex shows no trough at this depth. The nearest peaks of $\delta^{18}O$, at depths of 21.9 m and 22.6 m (dotted blue line, a), are potential year markers. The peak at 21.9 m was chosen because of the D-ex trough at the same depth. The lack of a coincident H_2O_2 peak may arise from loss processes in warm, wet summer snow and/or reduced photochemical production.

The choice of the start of year 1999 was complicated. The clear H_2O_2 peak indicates an annual layer around 23.25 m depth. However $\delta^{18}O$ shows double peaks (dotted blue lines a and d). The D-ex trough does not match with the $\delta^{18}O$ peaks. Since $\delta^{18}O$ does not show a clear trough between the two peaks (dotted lines a and d), the potential year marker could be within the depth range of line a ($\sim$ 22.6 m) to line d ($\sim$ 23.5 m). Line c was eventually chosen as the 1999 year marker due to the concurrent H_2O_2 peak. Since the chemical signals are very complicated at Mill Island, there is no other record available to determine which peak should be picked as the year marker. These differences (dotted lines a to d) do not affect the total number of years which the MI0910 record covers. However it may affect subsequent interpretation of annual records.

Counting annual layers

There are eight such periods where the seasonality of H_2O_2 and/or $\delta^{18}O$ are ambiguous, which may contribute to dating errors (see Section 2.3.2).

These ambiguities were resolved by carefully cross-checking the seasonality of H_2O_2, $\delta^{18}O$, D-ex, and nssSO_4^{2-}. For example, Figure 2.4 shows an anomaly in

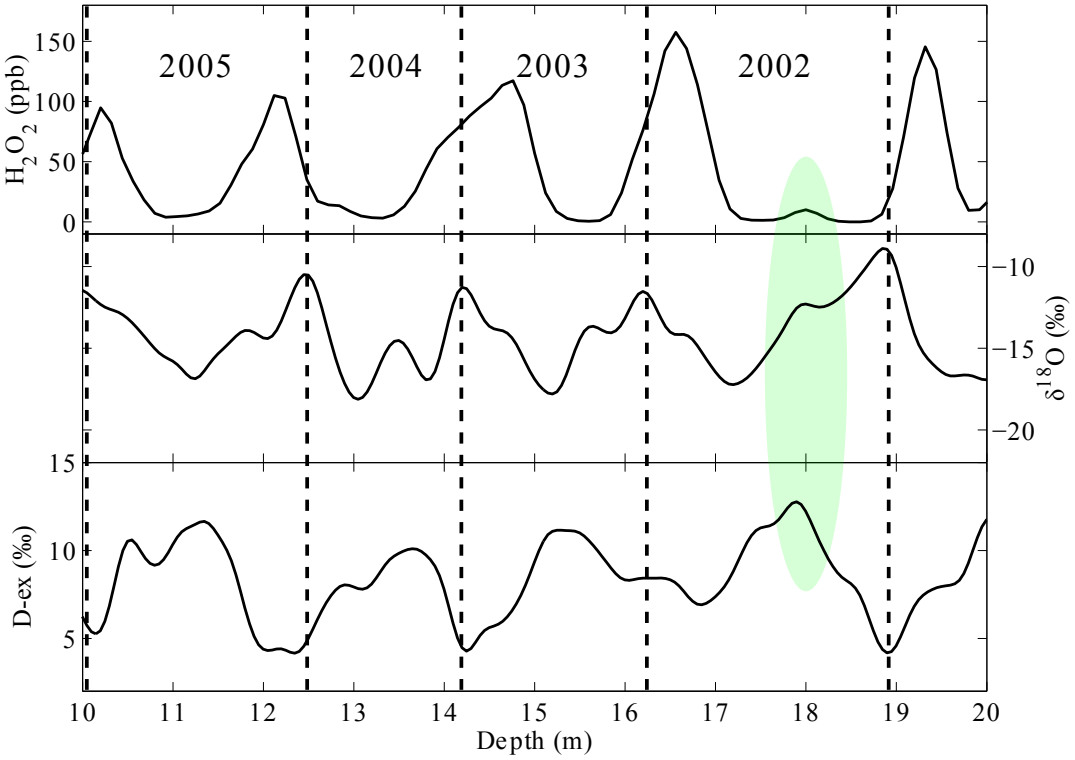

Figure 2.4: H_2O_2, $\delta^{18}O$ and D-ex records are shown, from depth 10 – 20 m. The dashed vertical line represents the beginning of each year. The green ellipse indicates the anomalous peak in H_2O_2 mentioned in the text. Because the resolution of the H_2O_2 and isotope measurements was different (see Section 2.2.1), H_2O_2 were re-sampled to a regular 12 cm grid, and smoothed with a Gaussian filter of width $\sigma = 1$ point; $\delta^{18}O$ and D-ex were re-sampled to a regular 5 cm grid, and smoothed with a Gaussian of width $\sigma = 2.4$ points.

H_2O_2 at 18 m (indicated by the green ellipse). However this was not counted as a new year marker because $\delta^{18}O$ does not show a clear peak, as expected at mid-summer. Thus the small H_2O_2 peak was assumed to be associated with a late summer or autumn deposition which contained low-level H_2O_2. The lack of D-ex trough also points to this being a non-summer feature. The highest

δ^{18}O in the peak area ($\sim$ 18.9 m) was chosen as the beginning of the year 2002. This is supported by the large D-ex trough at the same depth.

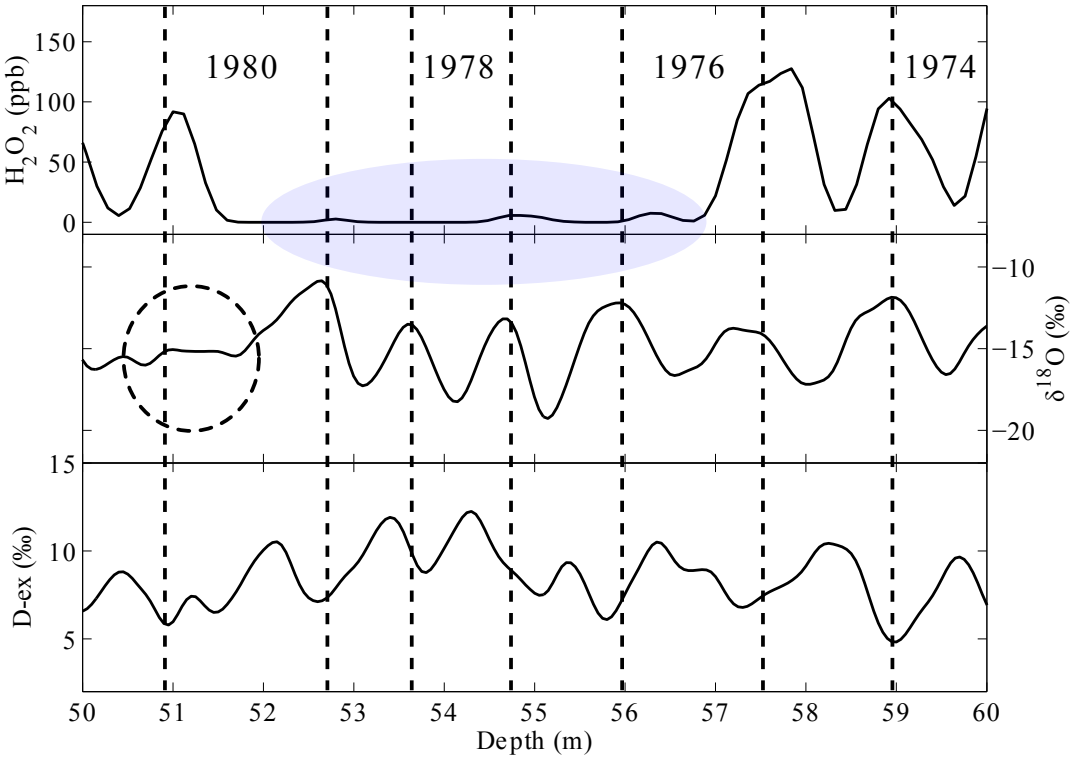

Figure 2.5: An example of the annual year dating process. H_2O_2, δ^{18}O and D-ex records are shown, from depth 50 – 60 m. The dashed vertical line represents the beginning of each year. The dashed circle indicates the anomaly in δ^{18}O, and the grey ellipse indicates the anomalous region of H_2O_2. See the text for more details. Due to the resolution of H_2O_2 and isotope measurement being different (see Section 2.2.1), H_2O_2 were re-sampled to a regular 12 cm grid, and smoothed with a Gaussian filter of width $\sigma = 1$ point; δ^{18}O and D-ex were re-sampled to a regular 5 cm grid, and smoothed with a Gaussian of width $\sigma = 2.4$ points.

Other examples are demonstrated in Figure 2.5. At a depth of $\sim$51 m, δ^{18}O does not show any obvious peak (within the dashed circle). However there is a clear H_2O_2 peak and D-ex trough. Thus this was counted as a new year marker. The depth between 52 and 57 m shows almost no H_2O_2

seasonality (within the grey ellipse). However $\delta^{18}O$ shows annual cycles, and corresponding D-ex troughs. Therefore, four years were counted in this section. Following this method, the MI0910 ice core was determined to cover 97 years i.e., the period from 1913 to 2009. For a complete discussion of all ambiguous dating events, please see Appendix A.

Shallow cores (MIp0910, MI0809)

MIp0910 was dated using the same methodology as MI0910. MIp0910 covers four years, from 2006 to 2009 (Figure 2.6 dashed green line). The MIp0910 record ($\delta^{18}O$, D-ex, Na^+, and SO_4^{2-}) agrees well with the MI0910 record for all species, and so the upper portion of MI0910 was supplemented with MIp0910 data. MI0809 was dated by counting annual layers of $\delta^{18}O$ and D-ex (H_2O_2 measurements are not available for MI0809). MI0809 covers 15 years, from 1994 to 2008 (Figure 2.6 dotted red line). The MI0809 record also agrees well with MI0910. These comparisons confirm the integrity of the MI0910 record. Moreover, the fact that these two individual nearby ice core records (10 km between MI0809 and MI0910 sites) acquired in different years and processed independently show similar records provides confidence in the ice core dating methodology used.

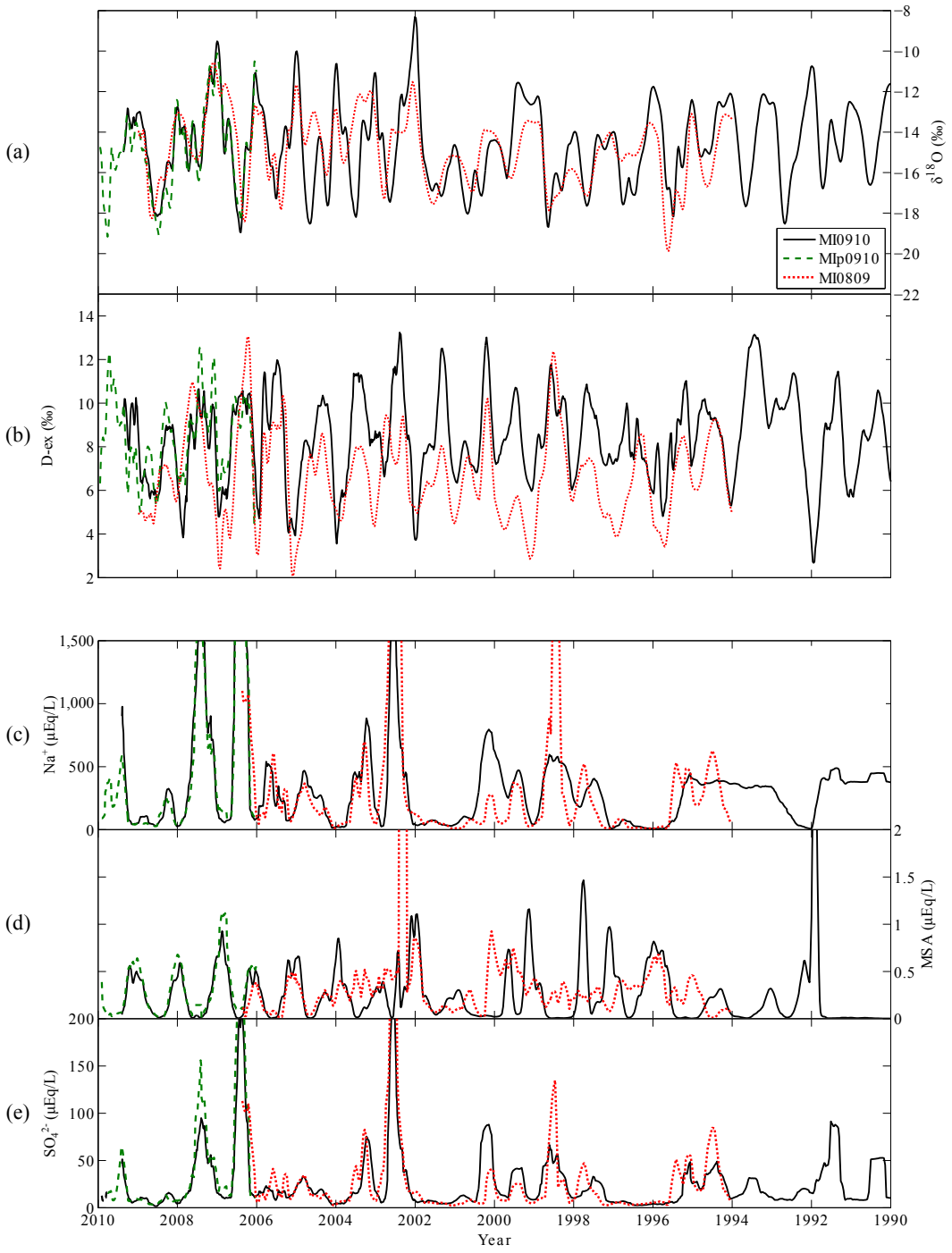

Figure 2.6: Comparison of (a) $\delta^{18}O$, (b) D-ex, (c) Na^+, (d) MSA, and (e) SO_4^{2-} records from MI0910 (black solid line), MIp0910 (green dashed line) and MI0809 (red dotted line).

Confirmation of the dating methodology

The trace chemistry record only shows clear seasonal variations throughout the upper ∼20 m (Section 2.3.1). The seasonality of sea salts (Na^+, Cl^-), and the ratio of sulphate to chloride (SO_4^{2-}/Cl^-) confirm the methodology of using H_2O_2, $\delta^{18}O$, and D-ex in the upper ∼20 m of the MI0910 ice core and provides confidence in dating of the remainder of MI0910. The layer counting chronology was confirmed by comparing the MI0910 nssSO_4^{2-} record with the dates of known volcanic events (Figure 2.7). The timing of large nssSO_4^{2-} peaks at MI0910 agrees well with the timing of volcanic eruptions recorded in the at LD ice core (Plummer et al., 2012, Table 2.3). The nssSO_4^{2-} peak at a depth of 35.5 m represents the Pinatubo eruption in the Philippines in 1991, at 46.3 m represents the El Chichon eruption in Mexico in 1982, and at 71.7 m represents the Agung eruption in Indonesia in 1963 (Palmer et al., 2001). The Mill Island ice core signal is generally slightly earlier than at LD. This is thought to be a consequence of differences in the timing of precipitation. The methodology used for layer counting together with identification of volcanic events confirms the chronology for MI0910.

Dating errors

The ambiguities in the seasonal cycles of H_2O_2 and $\delta^{18}O$ give rise to potential dating errors. For example, the feature in H_2O_2 at 18 m in Figure 2.4 was

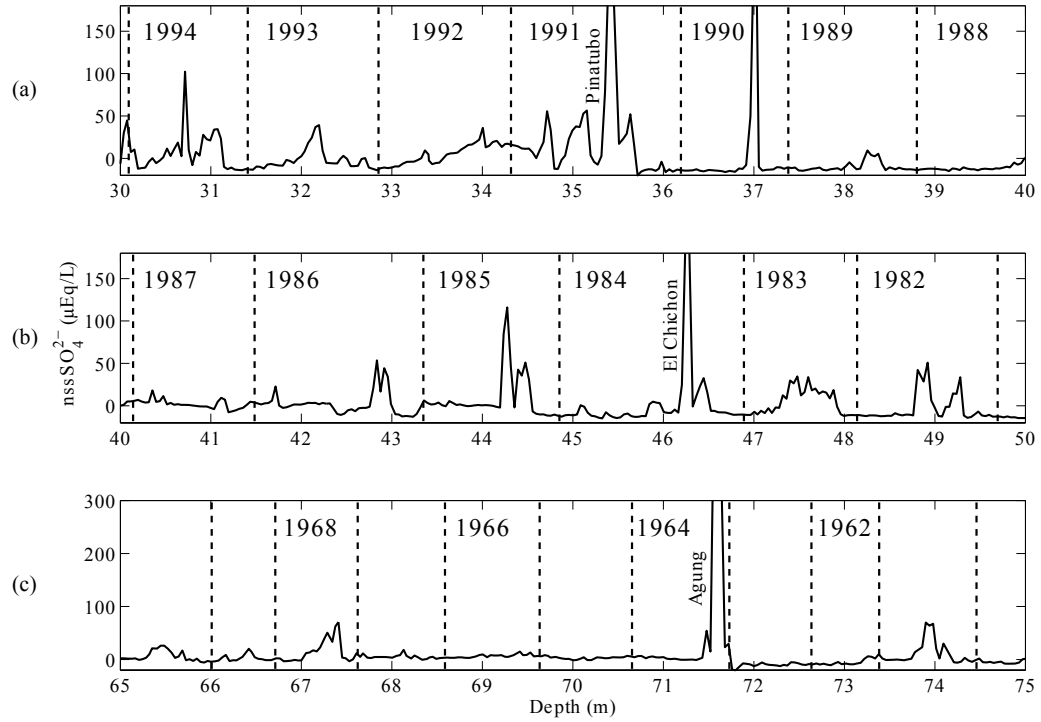

Figure 2.7: nssSO_4^{-2} records corresponding to major volcanic events (a) Pinatubo (1991), (b) El Chichon (1982) and (c) Agung (1963). The dashed vertical line represents the beginning of each year.

Volcano	Eruption year	MI ice date (year)	LD ice date (year)
Pinatubo	1991	1991.4	1991.7
El Chichon	1982	1984.3	1984.5
Agung	1963	1964.1	1964.1

Table 2.3: Volcanic eruption records as identified from nssSO_4^{2-} peaks in the Mill Island and LD ice cores during 1913 – 2009 (Palmer et al., 2001; Plummer et al., 2012). Years are reported as decimal fractions of a year.

not counted as a year and could result in a dating error of +1 year prior to 2003 (i.e., the year may be one year older at most). Another example is the irregular section of $\delta^{18}O$ and H_2O_2 as illustrated in Figure 2.5. This was counted as a period of five years and could result in a dating error of -5 years prior to 1981, although it is extremely unlikely that the error could be so large, because it would mean a ~ 5 m depth increment in a year where most neighbouring years are 1 - 2 m thick. Adding errors linearly, the total dating error of the MI0910 ice core is +4, -10 years. However, such errors are statistically independent, as the decision of counting a seasonal cycle as a year marker is not affected by other errors. Thus instead of adding each error linearly (Figure 2.8 dashed line), the errors can be combined in quadrature (e.g., error $= \sqrt{error1^2 + error2^2 + error3^2...}$ [Barlow (1989)], Figure 2.8 solid line). Because the dating is confirmed by the volcanic record, the errors are periodically set to zero at the timing of each major eruption year (e.g., 1991, 1984, and 1963, as indicated in Figure 2.8).

2.3.3 Glaciochemical timeseries and average seasonal cycles

Following this dating methodology, the MI0910 ice core was determined to cover 97 years i.e., the period from 1913 to 2009. The entire 97 year records of H_2O_2, water stable isotope, trace ion chemistry are presented in this section.

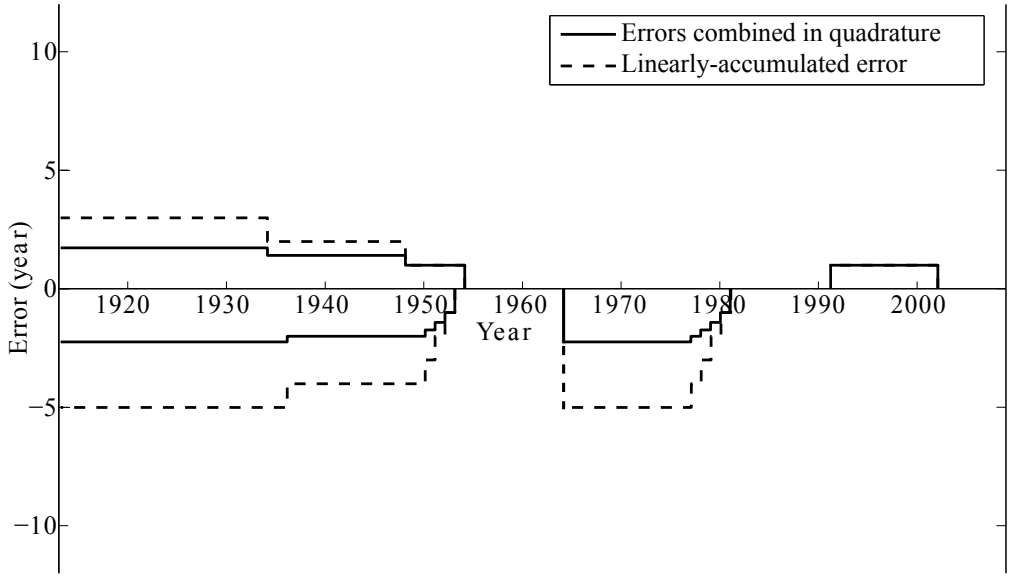

Figure 2.8: Figure showing the dating errors combined in quadrature (solid line) and linearly (dashed line). Negative error represents an ambiguous seasonal cycle counted as a year marker. Positive error represents an ambiguous seasonal cycle not counted as a year marker.

H_2O_2 and isotopes record

Figure 2.9 presents the entire 97 year records of (a) H_2O_2, (b) $\delta^{18}O$, (c) δD, and (d) D-ex. The observed loss of H_2O_2 at depth $\sim$ 50 to 60 m and 80 to 90 m (Figure 2.1 a) correspond to the late 1970s and early 1950s, respectively (Figure 2.9 a).

A water vapour diffusion correction was computed using the method adopted in van Ommen and Morgan (1997) and Sinclair et al. (2012), with specific Mill Island parameters (density profile, mean temperature, and atmospheric pressure). As a result, the diffusion length reached 6.7 cm at a depth of 43 m in the firn. With the high snow accumulation rate in the Mill Island ice core (1,312 kg/m^{2}yr, Roberts et al., 2013), this is small enough to ignore. Thus, the effects of water vapour diffusion were not considered in this thesis.

Figure 2.10 shows the average seasonal cycles of (a) H_2O_2, (b) $\delta^{18}O$, (c) δD, and (d) D-ex for the 97 yr MI0910 ice core record. The monthly mean was computed by linearly dividing each year into 12 portions. The average seasonal cycles are presented over two years to demonstrate the structure of both the summer and winter features.

The H_2O_2 average seasonal cycle shows a peak in summer with a maximum value in December, and a trough in winter with a minimum value in June (Fig 2.10 a). This timing coincides with the timing of the solstices, as

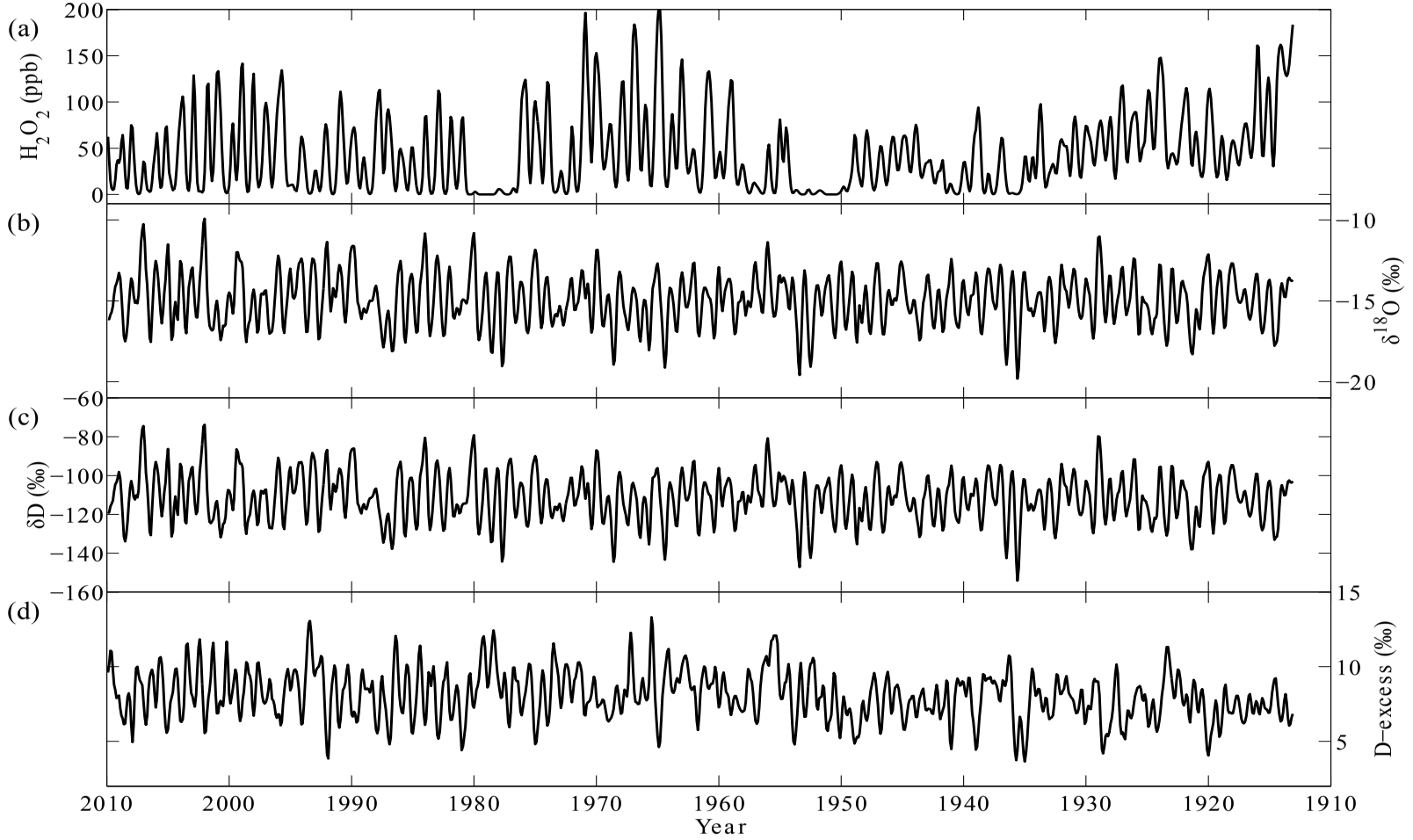

Figure 2.9: Ninety-seven year record of H_2O_2 (a), $\delta^{18}O$ (b), δD (c), and D-ex (d). All data were re-sampled to a 0.1 year grid and smoothed with a Gaussian filter of width σ=1 point.

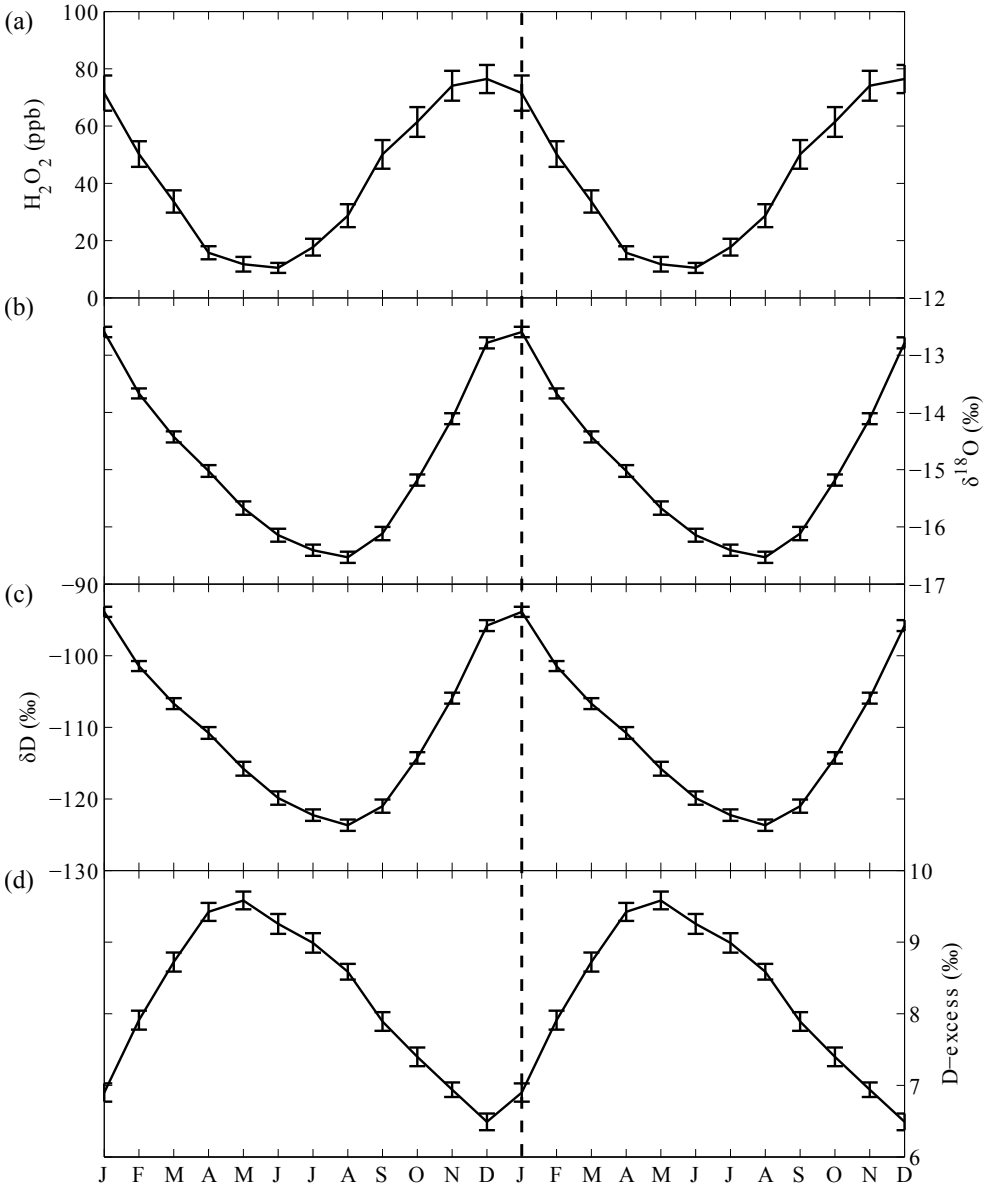

Figure 2.10: Average seasonal cycles of a) H_2O_2, b) δ^{18}O, c) δD, (d) D-ex for the entire MI0910 record. The error bars show the standard error of the mean.

expected, due to the requirement of sunlight for H_2O_2 production.

The average seasonal cycles of $\delta^{18}O$ and δD show a peak in summer and a trough in winter, with a maximum in January and a minimum in August (Fig 2.10 b and c, respectively). The $\delta^{18}O$ seasonal cycle was compared with the temperature record from the nearby (∼370 km) coastal Russian station, Mirny Station (66° 33' S, 93° 01' E) since no Automatic Weather Station (AWS) is installed in the region. The Mirny Station seasonal temperature record shows a maximum in January and a minimum in August. However the "coreless" winter pattern observed at Mirny Station, which is a broad temperature minimum during winter without trough, was not observed in the Mill Island isotopes record (Figure 2.10 b, and c). Further investigations and calibration of the oxygen isotope ratio as a proxy for the local temperature are further discussed in Chapter 4.

The D-ex seasonal cycle shows a minimum in summer (December), and a maximum in winter (May) (Fig 2.10 c). There is a four month lag in D-ex compared to $\delta^{18}O$. This is also reported by the LD ice core (Delmotte et al., 2000). The D-ex record is used as a proxy for the moisture source temperature and sea ice cover (Delmotte et al., 2000; Uemura et al., 2012). However D-ex is affected by the relative humidity of the oceanic source region as well as by sea surface and polar temperatures (Landais et al., 2008; Uemura et al., 2008). $\delta^{17}O$ measurement is required for proper interpretation of D-ex (Landais et al.,

2008; Winkler et al., 2012). However $\delta^{17}O$ was not measured for the Mill Island ice core due to laboratory limitations.

Trace chemistry record

Figure 2.11 shows concentrations of a) Na^+, b) Cl^-, c) MSA, d) SO_4^{2-}, e) $nssSO_4^{2-}$, f) Mg^{2+}, g) Ca^{2+}, and h) NO_3^- for the 97 year ice core (Figure 2.11). The Na^+ and Cl^- chemistry seasonality present from 2009 to 2001 disappears between $\sim$ 2000 and $\sim$ 1934, to be replaced by high baseline values. Prior to 1934 the seasonality is present again and values are lower than in the other period. These periods (2009 – 2001, 2000 – 1934, 1933 – 1913) are shown in Figure 2.11 and henceforth termed regimes A, B and C, respectively. Further discussion about this regime change are presented in Section 2.3.4.

Average seasonal cycles (1913 – 2009) of trace ion species are displayed in Figure 2.12. Despite the unclear seasonality prior to 2001 (Figure 2.11), the average seasonal cycles of Na^+ and Cl^- show clear seasonal variability with a peak in winter (May), and a trough in summer (December) (Figure 2.12, a and b, respectively).

The MSA average seasonal cycle shows low concentration during winter (May - October), then peaks in spring (November) and autumn (April) (Figure 2.12, c). However during summer (December - March), concentrations are relatively low. There is a reversed phase observed between Cl^- and MSA

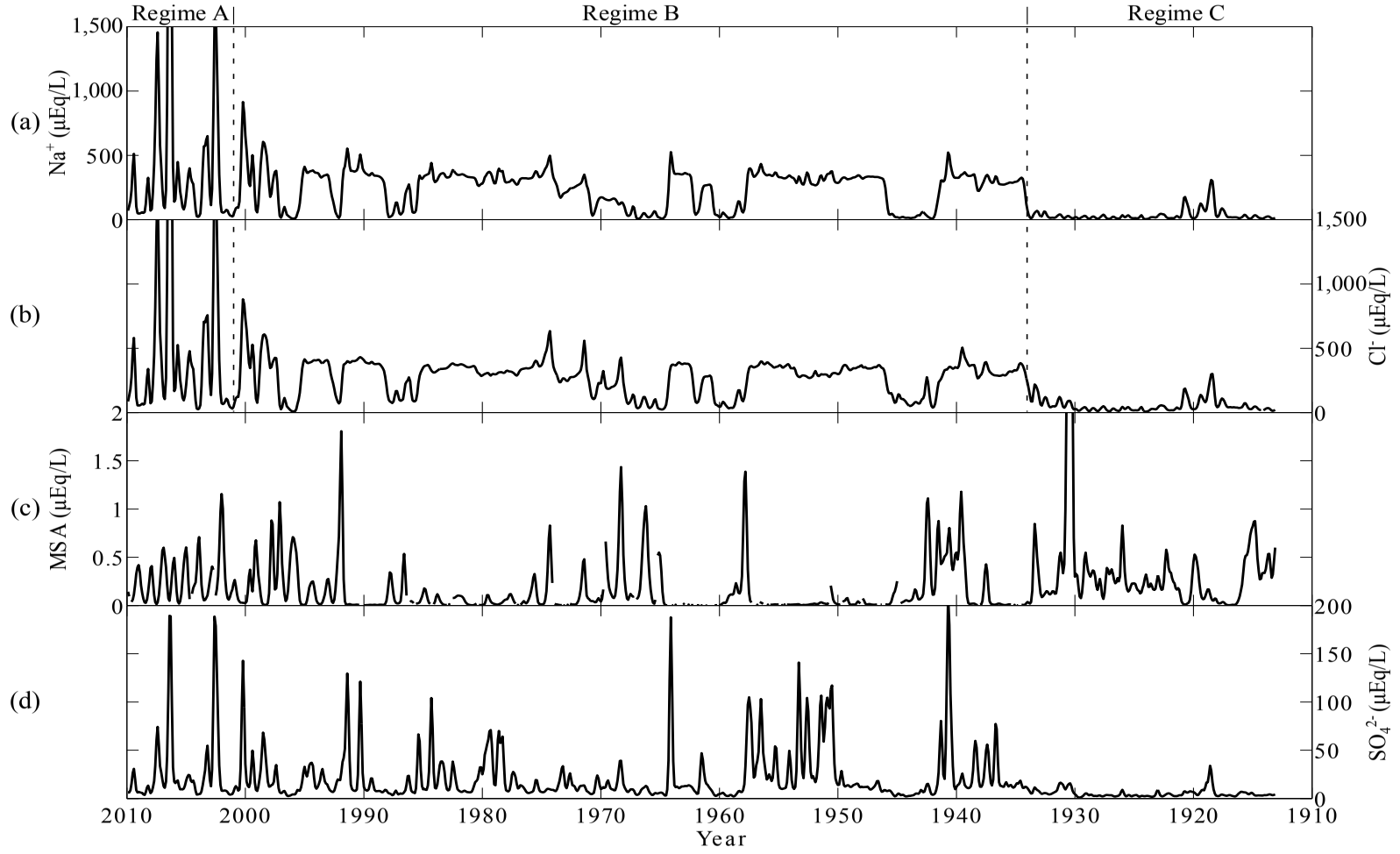

Figure 2.11: Trace ion chemistry data: a) Na^+, b) Cl^-, c) MSA, and d) SO_4^{2-}. All data were re-sampled to a 0.1 year grid and smoothed with a Gaussian filter of $\sigma = 1$ point. The Na^+ and Cl^- records can be partitioned into three regimes (Regime A, B, and C), as detailed in Chapter 3.

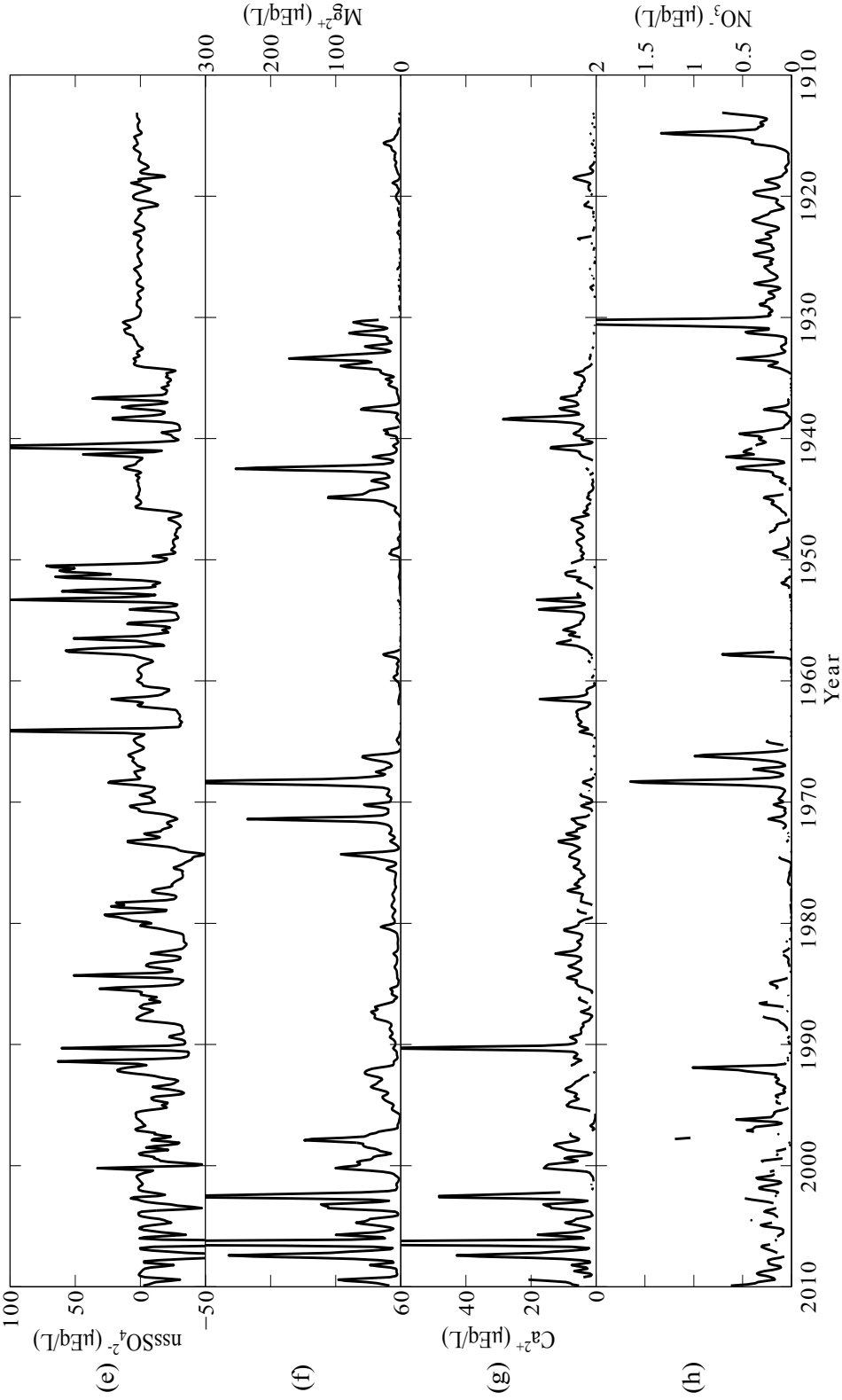

Figure 2.11: Trace ion chemistry data: e) nssSO_4^{2-}, f) Mg, g) Ca, and h) NO_3.

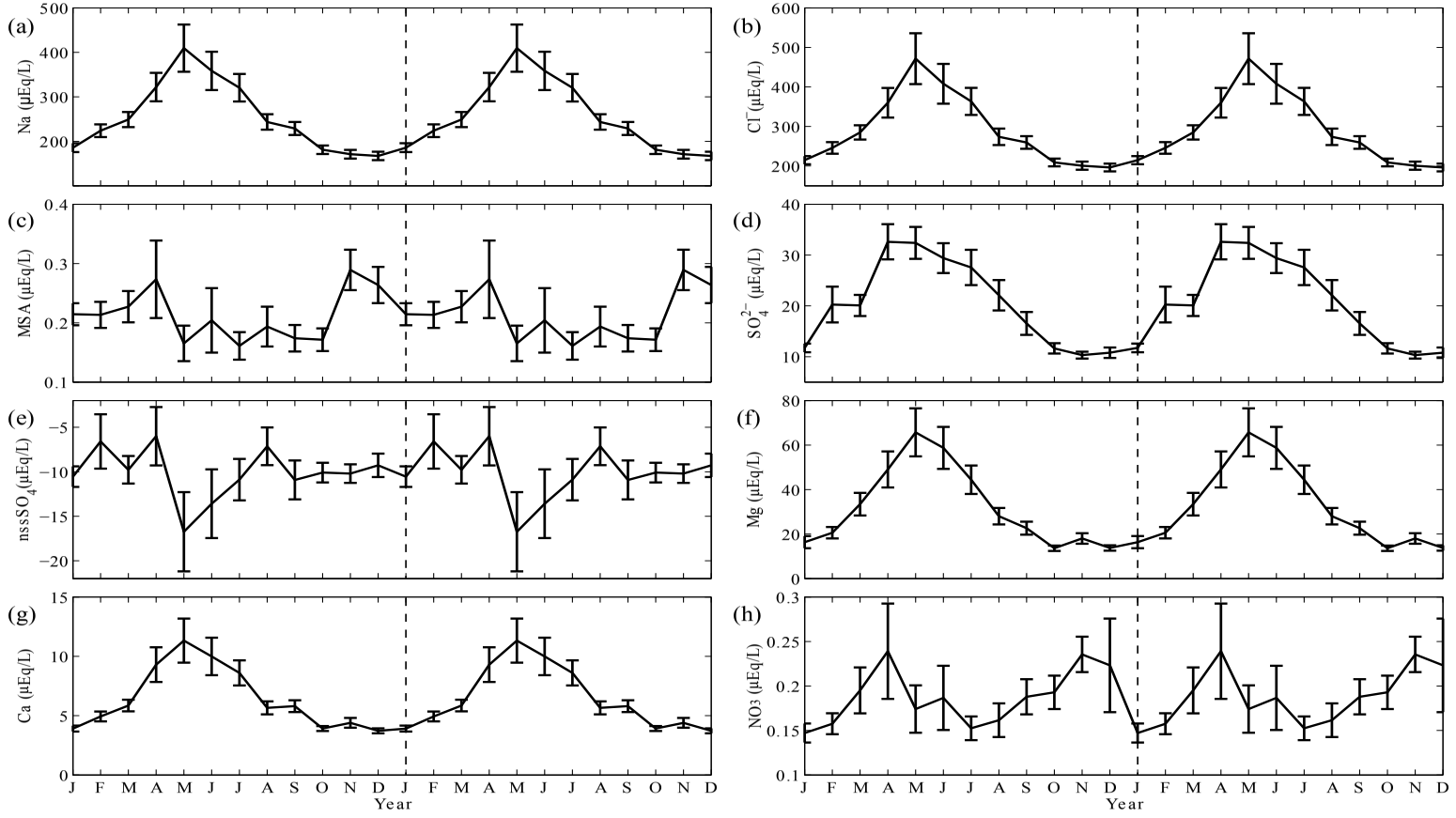

Figure 2.12: Average seasonal cycles of a) Na^+, b) Cl^-, c) MSA, d) SO_4^{2-}, e) $nssSO_4^{2-}$, f) Mg^+, g) Ca^+ and h) NO_3^-. The error bars show the standard error of the mean.

during the latest 10 years, however they are synchronised in older parts of the record (e.g., between ∼1965 to ∼1975). This is likely due to post-deposition MSA movement (Curran et al., 2002). Further details of post-depositional movement are discussed in Chapter 3.

Sulphate (SO_4^{2-}) also shows clear seasonal variability with a peak in April, and a trough in November (Figure 2.12, d). The winter time maximum in the SO_4^{2-} record indicates that sea salt is the dominant source of the SO_4^{2-} at this site.

The non sea salt sulphate ($nssSO_4^{2-}$) record was calculated using the formula 2.2. The mean concentration of $nssSO_4^{2-}$ is negative (Table 2.2) and the average seasonal cycle also shows a negative value throughout the year (Figure 2.12 e). This indicates that the $nssSO_4^{2-}$ at Mill Island is highly fractionated from sea-salt. Thus, a different k value is needed to correctly derive $nssSO_4^{2-}$. Investigation of the specific k value and sea salt fractionation are discussed in Section 2.3.5.

2.3.4 Sea salt regime changes and the stratigraphy of MI0910

The Na^+ record (Fig 2.11 a) can be divided into 3 regimes: A) Clear seasonality with high peak concentration (surface to ∼2001); B) no seasonality with generally high concentration (∼2000 to ∼1934); and C) seasonality with

relatively low peak concentration (∼1933 to bottom). The possible reasons for these features could be due to analytical error in measurement or methodology, snow/firn melt, or a true environmental signal.

Analytical error in measurement or methodology

Repeat trace ion chemistry analysis was completed using different dilutions and this yielded the same results, thus discounting the possibility of errors due to analytical measurement. Additionally, two shallow cores (MI0809, MIp0910) were analysed independently using the same instrument and method. These trace ion measurements from both shallow ice cores agree with the MI0910 record (see Section 2.3.2). Thus analytical error in measurement or methodology is not the cause of these features.

Snow/firn melt

Figure 2.13 presents an example of the crust layers observed in MI0910. This is a relatively thick crust layer at $\sim$ 5 mm. These layers are generally $\sim$ 1 to 5 mm thick, and sometimes consist of numerous thin layers within ∼20 mm thickness. From visual observation some layers have higher density and smaller grain size, while other layers have lower density and larger grain size, compared to the surrounding ice.

Figure 2.14 shows the distribution of crust layers observed in the ice core (blue vertical lines) along with the full records of H_2O_2, Na^+, and SO_4^{2-}. A

Figure 2.13: An example of the crust layers observed in MI0910.

total of 172 crust layers were recorded. The crust layers do not correspond with the periods of observed loss of H_2O_2 or reduced seasonality in the trace ion record. For example, the early 2000s (indicated with a grey ellipse labelled "a") includes multiple crust layers, but all three species (H_2O_2, Na^+, and SO_4^{2-}) show clear seasonality. Between late 1970s and early 1980s (grey ellipse "b") there is a loss of H_2O_2 seasonality, however, this period includes occurrences of both few crust layers (late 1970s) and many crust layers (early 1980s). Another period of observed loss of H_2O_2 seasonality occurs during the early 1950s (grey ellipse "c") yet this period shows only a few crust layers. In the trace ion record, grey ellipses "b" and "c" show similar characteristics for each

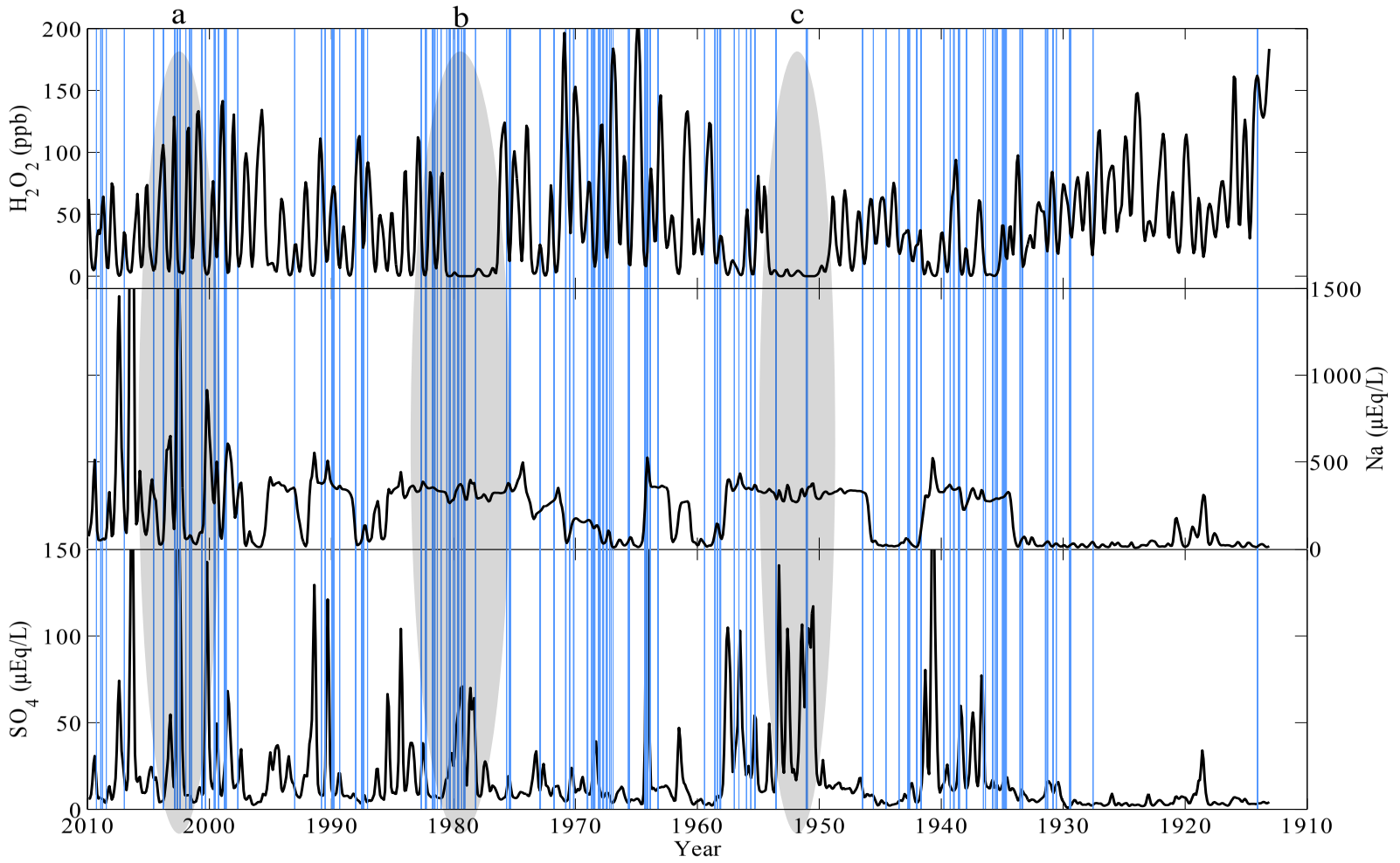

Figure 2.14: Crust layers recorded in MI0910 ice core (blue vertical lines) with 97 years of H_2O_2, Na^+, and SO_4^{2-} record. The thickness of the blue lines has been exaggerated, relative to the ice core thickness, in order to enhance visibility. Grey ellipses indicate regions discussed in the text. The firn/ice density is unrelated to the occurrence of crust layers.

species, whereby there is a high concentration of Na^+ with a muted seasonal cycle and a high concentration of SO_4^{2-} with peaks. However there is no relationship with crust occurrence frequency.

H_2O_2 loss may relate to SO_4^{2-} concentration. H_2O_2 is believed to be the most efficient oxidizing agent of SO_2, producing SO_4^{2-} (Laj et al., 1990). In the grey ellipses "b" and "c", large peaks of SO_4^{2-} are associated with the depletion of H_2O_2. However, not all SO_4^{2-} peaks are associated with H_2O_2 loss. Nitrogen oxides also tend to reduce the concentration of peroxide (Sigg and Neftel, 1991). However, there are no associated nitrate features observed in the record (see Figure 2.11). The reason for the absence of the H_2O_2 peaks in these two regions is unknown.

In the polar snowpack percolation zone, melt events occur generally during summer (Langway, 1970). Assuming that all summer crust layers are caused by melt events, there is an implication that these events are associated with temperature (hence $\delta^{18}O$). The crust layers during the summer period (October – March) and summer mean $\delta^{18}O$ were compared and presented in Figure 2.15. Thirty-four summers out of the 97 year record had crust layers, and the data points were not normally distributed (Figure 2.15), thus a Spearman's rank correlation was used to asses the correlation. There was no significant correlation between the number of melt layers and the associated summer mean $\delta^{18}O$ ($\rho = -0.08$, p = 0.62, n = 34). This indicates that these

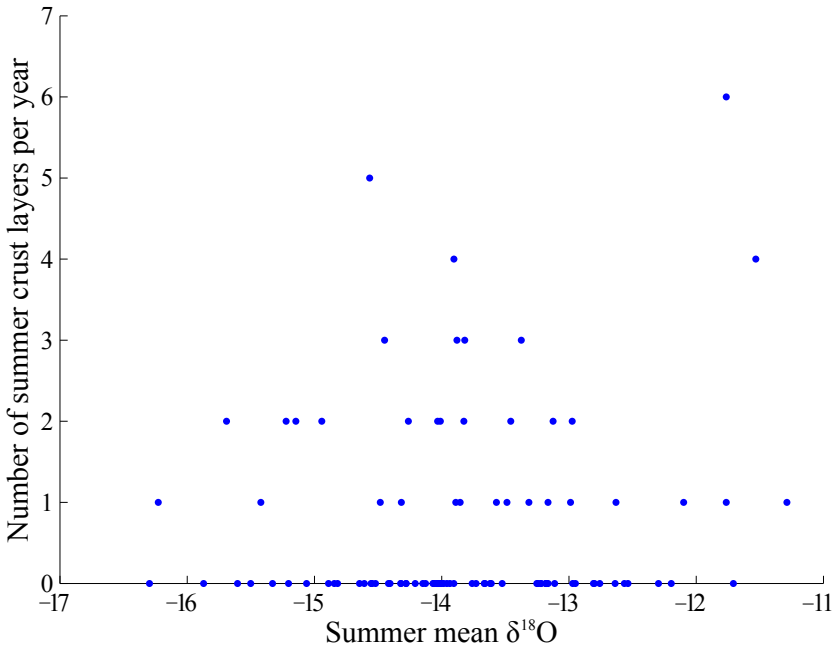

Figure 2.15: The number of summer (October – March) crust layers per year and summer mean δ^{18}O.

crust layers are likely not melt layers.

Figure 2.16 shows monthly bins of crust layers, mean temperature, mean number of six-hourly wind speed data which exceed 15 m/s (i.e., high wind periods), and mean number of six-hourly wind speed data which are less than 5 m/s (i.e., low wind periods). The wind and temperature data were derived from National Centers for Environmental Prediction (NCEP) Climate Forecast System Reanalysis (CFSR) (Environmental Modeling Center, 2010) due to no long term observation records being available on Mill Island. CFSR provides high resolution data ($\sim$ 0.313 degree $\times$ 0.312 degree, 6 hourly). The closest grid point to Mill Island is at 65° 24' 42.84" S, 100° 56' 15" E, which is 17 km

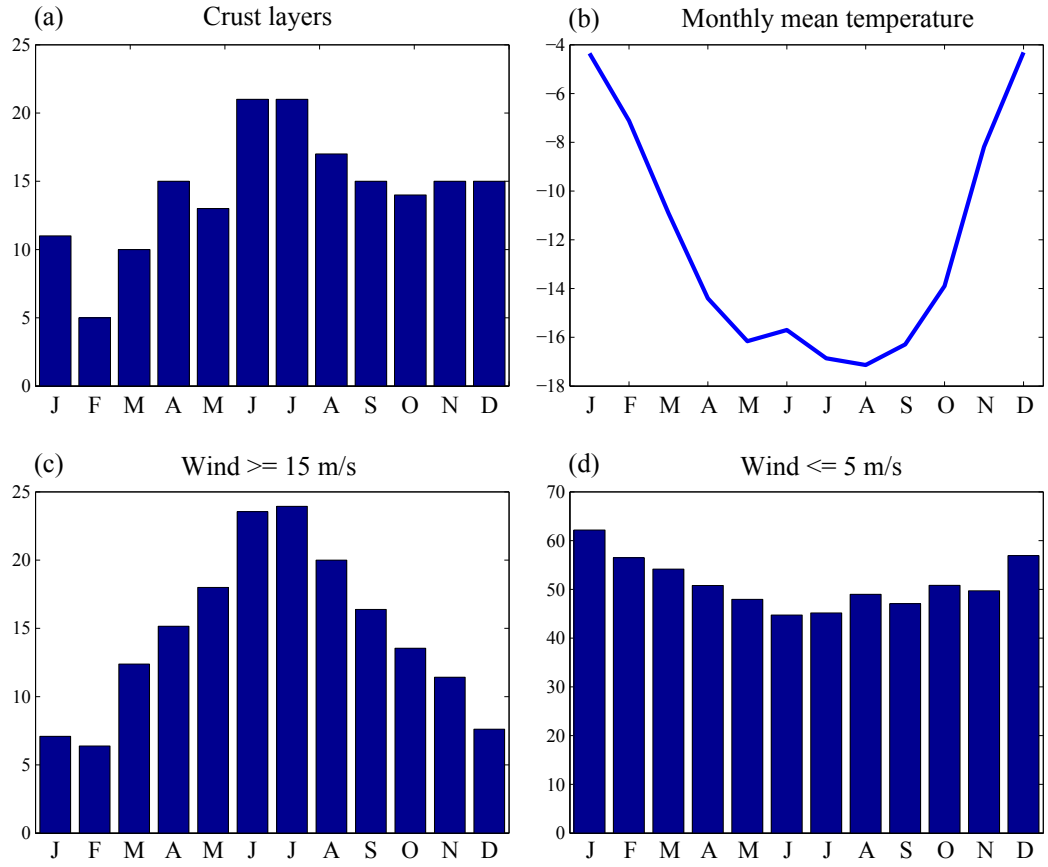

Figure 2.16: Figures of a) monthly total crust layers, b) Monthly mean temperature, c) monthly mean number of wind exceed 15 m/s data from six hourly data, d) same as c, but wind speed is less than 5 m/s.

east of the exact drilling point of MI0910. This point was chosen for this analysis. The data period for analysis is between 1979 and 2009. Generally, there is higher wind speed during winter. Both the number of crust layers and the number of high wind periods peaks in June and July. This indicates that the crust layers identified during winter are likely formed by strong wind events (Alley et al., 1997). The maximum monthly mean temperature is −4.3 ℃ and there were four data points exceeding 0 ℃ during the CFSR data period. In addition, Alley et al. (1990, 1997) reported that the Sun can warm the snow surface by as much as four to five K compared to surface air temperature under fair weather conditions. These conditions often result in depth hoar, as is observed in Greenland (Alley et al., 1990). Hence, the summertime maximum monthly mean temperature of −4.3 ℃, together with low wind speed may provide ideal conditions for melt or/and depth hoar formation in the summer, especially during December and January.

Additionally, fog events could be a cause of the crust layers. Fog and rime accretion associated with the fog events were observed during the field season at Mill Island (M. Curran, personal communication 2014). This rime deposition may appear as low-density crust layers (Alley et al., 1997). However fog events are difficult to study from atmospheric model output data. An AWS instrumented with a relative humidity sensor and shortwave and longwave radiometers (in addition to standard components, wind speed/direction/mean

sea level pressure/precipitation) would provide an ideal tool to assess the occurrence of fog events at the Mill Island site. Fine resolution (1 cm sample resolution) isotope measurements from the Mill Island shallow core show no apparent influence of crust layers on the record (A. Moy, personal communication, 2015). Thus the crust layers probably have a minimal impact on the chemical interpretation of the Mill Island ice core records.

The possibility of true environmental signals causing crust layers

Since both analytical errors in measurement or methodology and snow/firn melt were discounted as the cause of the ambiguous sea salt seasonality, the three different regimes identified may indicate the recording of different environmental signals at Mill Island. The influence of true environmental signals on the chemistry record at Mill Island is explored in Chapter 3.

2.3.5 Non sea salt sulphate and fractionation

The presence of negative nssSO_4^{2-} values in the Mill Island ice core record indicates the occurrence of sea salt fractionation (i.e., a depletion of sulphate relative to sodium (Wagenbach et al., 1998a)). Thus, the calculation of nssSO_4^{2-} is not accurate when using the k value from typical seawater composition. A new k value, k', for the sulphate to sodium ratio in fractionated sea salt is required for the nssSO_4^{2-} calculation at this location. Following the Hall and Wolff (1998) study, k' was acquired by calculating the linear regression slope

of nssSO_4^{2-} versus Na^+.

nssSO_4^{2-} (calculated using the sea water ratio of Na^+ to SO_4^{2-}) versus Na^+ data are shown in Figure 2.17a. Negative nssSO_4^{2-} concentrations extend down to $\sim -600\ \mu Eq/L$. The new, corrected k value, k', is obtained by subtracting the regression slope, r from k, i.e., $k' = k - r$. As a result, $k' = 0.049$. The negative nssSO_4^{2-} values from the 97 year ice core record were used for the regression line calculation, rather than only using winter data (Hall and Wolff, 1998). This methodology is due to the ambiguous seasonality in the Mill Island ice core record. The nssSO_4^{2-} record during known volcanic eruption years (1991, 1984, and 1964) was excluded.

To verify this result, k' was obtained independently by minimising the correlation coefficient between nssSO_4^{2-} (calculated using a k' range from 0.01 to 0.12 in steps of 0.001) and the associated Na^+ value (Wagenbach et al., 1998a). The correlation coefficient r is a function of k'. The k' value for a correlation coefficient of $r \cong 0$ is at $k' = 0.049$, confirming the simple linear regression method (Figure 2.17b). The zero correlation indicates that the sea salt influence on SO_4^{2-} is removed.

Using this linear regression method, k' was calculated for each sea salt regime (see Section 2.3.4 for a definition). Table 2.4 presents k', percentage of fractionation, and mean SO_4^{2-} at Mill Island. The percentage of fractionation is given by $100 \times 0.12/$*regression slope* (i.e., if the slope is 0.12, the SO_4^{2-} is

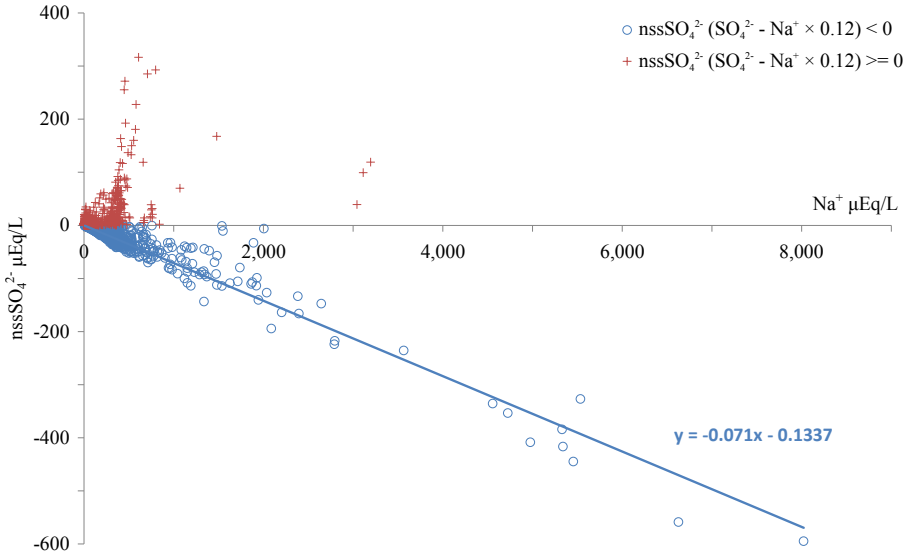

(a) Scatter plot of nssSO_4^{2-} (calculated using the seawater ratio of sulphate to sodium, 0.12) versus Na^+. The linear regression line was computed with negative nssSO_4^{2-} values only.

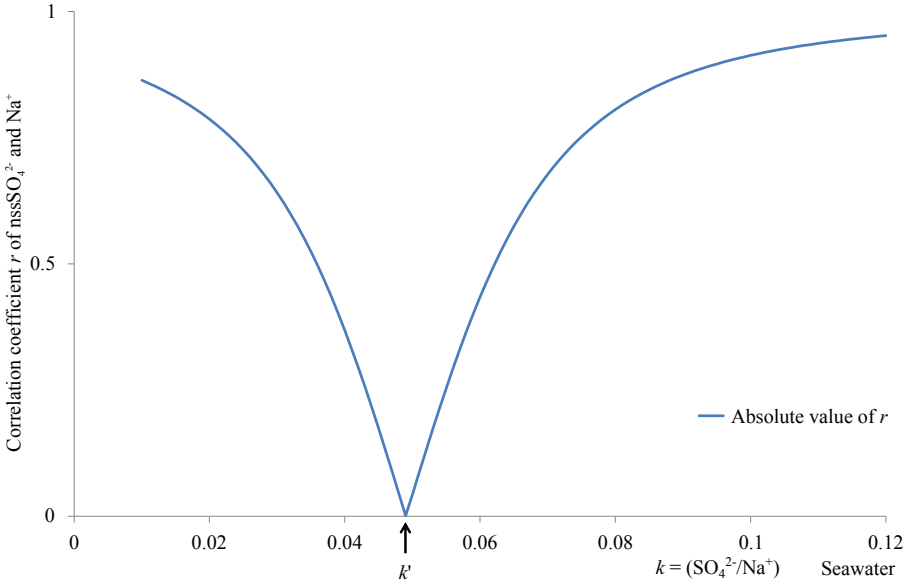

(b) Absolute value of the correlation coefficient between nssSO_4^{2-} and Na^+, varying the seawater reference ratio k used to calculate the nssSO_4^{2-} values.

Figure 2.17: Investigating k': a) linear regression slope, b) correlation coefficient.

100% fractionated). The SO_4^{2-} was most fractionated in regime B (67.5% depleted). Comparing with the LD *k'* value of 0.087 (Palmer et al., 2002; Plummer et al., 2012), the Mill Island ice core is more fractionated at all times. The highly fractionated sulphate record indicates that frost flowers are likely to be an important sea salt source at Mill Island. Frost flowers have a sea salt concentration three times higher than sea water (Perovich and Richter-Menge, 1994; Wolff et al., 2003; Kaleschke et al., 2004). Hence frost flower-originated aerosols contain a higher concentration of sea salt than aerosols originated from sea water. This may explain the high sea salt concentration at Mill Island.

Site	Regression slope	*k'*	Fractionation (%)	mean nssSO_4^{2-} ($\mu Eq/L$)
Mill Is (97 yrs)	0.071	0.049	59.2	7.26
Mill Is (Regime A)	0.073	0.047	60.8	8.13
Mill Is (Regime B)	0.081	0.039	67.5	7.79
Mill Is (Regime C)	0.068	0.052	56.7	3.98

Table 2.4: The corrected *k* value and mean nssSO_4^{2-} concentration in each regime.

Sea salt fractionation and mean concentration of Na^+ from several ice core sites in East Antarctica are shown in Figure 2.18 and Table 2.5. As the distance from coast increases, the sea salt fractionation and Na^+ concentration both decrease. The ice core taken from B09B iceberg was only 5 km away from the iceberg edge and was highly fractionated (65.3%). Both the Mill

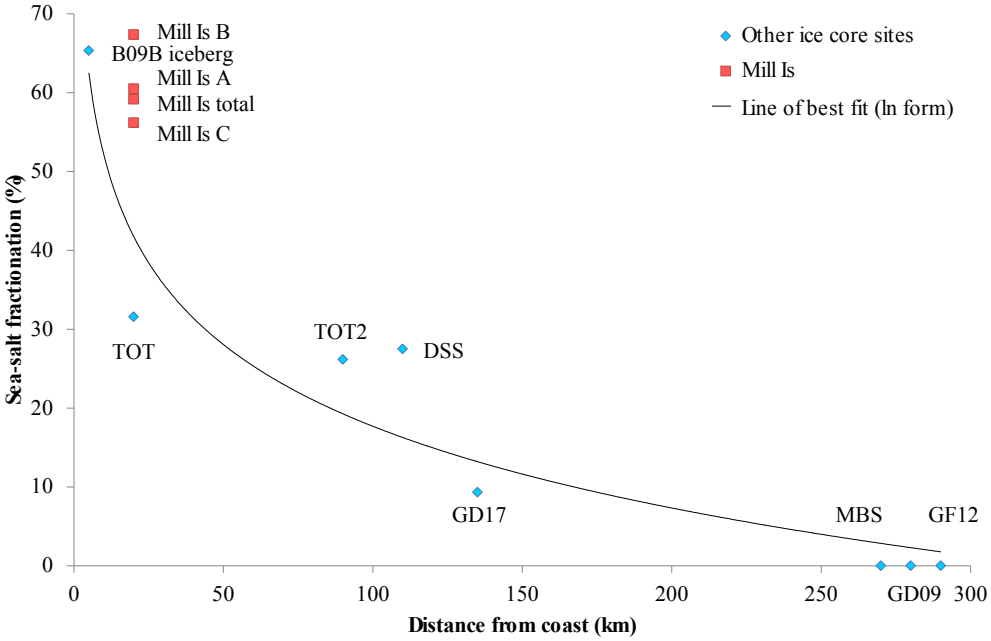

(a) Scatter plot of sea salt fractionation vs distance from coast.

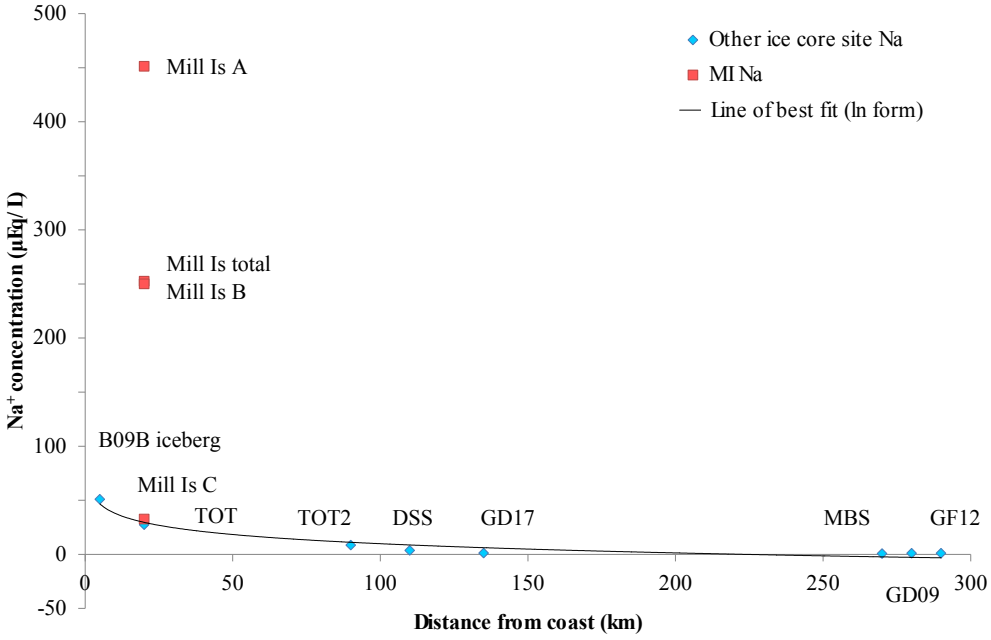

(b) Scatter plot of mean Na^+ concentration vs distance from coast.

Figure 2.18: Comparison of distance from coast and a) sea salt fractionation, b) mean sodium concentration at several East Antarctica ice core sites. See Table 2.5 for further infomation of other sites.

Island ice core and the Totten Glacier (TOT) ice core were 20 km away from the coast. The TOT ice core was less fractionated (31.6%) compared to the Mill Island ice core 97 yr record (59.2%) and all regimes (A: 60.8%, B: 67.5%, C:56.7%). This may be because the Totten Glacier is more strongly influenced by katabatic winds. When the distance from the coast is over 250 km, no sea salt fractionation is observed (MBS, GD09, and GF12). Mill Island fits well within the fractionation trend (Figure 2.18a). However, the sodium concentration from Mill Island (in regimes A and B) is much higher than at any other ice core site (Figure 2.18b). This indicates that inclusion of frost flower-originated aerosols is not the only reason for the high sea salt concentration at Mill Island. If frost flower aerosol inclusion is the major contributor for the observed high Na^+ concentration, then Na^+ concentration from iceberg B09B should be even higher than that from Mill Island.

The Na^+ concentration from regime C is similar to the TOT ice core, and fits well within the sea salt concentration trend. However in regime B, Na^+ concentration became five times higher than in regime C. This suggests that a significant change to the ice-scape surrounding Mill Island may have occured between regimes B and C, i.e., in the mid-1930s.

Further comparison of the mean Na^+ concentration and other sites is presented in Figure 2.19. Typically, Na^+ concentrations decrease quickly with increasing distance from the coast (Figure 2.19). Mill Island Na^+ concentra-

Site name/region	Ice core	Lat	Long	Reference
Iceberg B09B	B09B	67^o14' S	148^o26' E	(Long, 2004)
Totten Glacier	TOT	66^o59' S	116^o00' E	Unpublished
Totten Glacier 2	TOT2	67^o26' S	113^o32' E	Unpublished
Law Dome	DSS	66^o46' S	112^o48' E	(Curran et al., 1998)
Wilkes Land	GD17	67^o51' S	127^o03' E	(Wong, 2007)
Mt. Brown South	MBS	69^o7' S	85^o59' E	Unpublished
Wilkes Land	GD09	69^o39' S	123^o3' E	Unpublished
Wilkes Land	GF12	68^o29' S	97^o11' E	Unpublished

Table 2.5: Site information of the other ice core sites in Figure 2.18. Data were derived from Wong (2007); Long (2004) and M. Curran (Personal communication, 2014).

tions show elevated concentrations like those recorded at Dronning Maud Land (DML, $\sim 70^o$S, 4^oE) snow pit snow samples (Gjessing, 1989). The DML mean Na^+ concentration was 360 $\mu Eq/L$ at 0.01 km from the ice edge, and decreased to 124 $\mu Eq/L$ at 8 km, and decreased further to 2.90 $\mu Eq/L$ at 200 km. No other coastal ice core or snow sample from the Antarctic ice sheet shows as high Na^+ concentrations as recorded at DML or Mill Island. The Mill Island Na^+ concentration in regime C (average 32.62 $\mu Eq/L$) is only $\sim$7 % compared to regime A (average 451.24 $\mu Eq/L$), and yet the Na^+ concentration during regime C is still higher than most values at other sites. Further investigation and discussion about these regimes is given in Section 3.3.1.

The average seasonal cycle of nssSO_4^{2-} was calculated using $k' = 0.049$

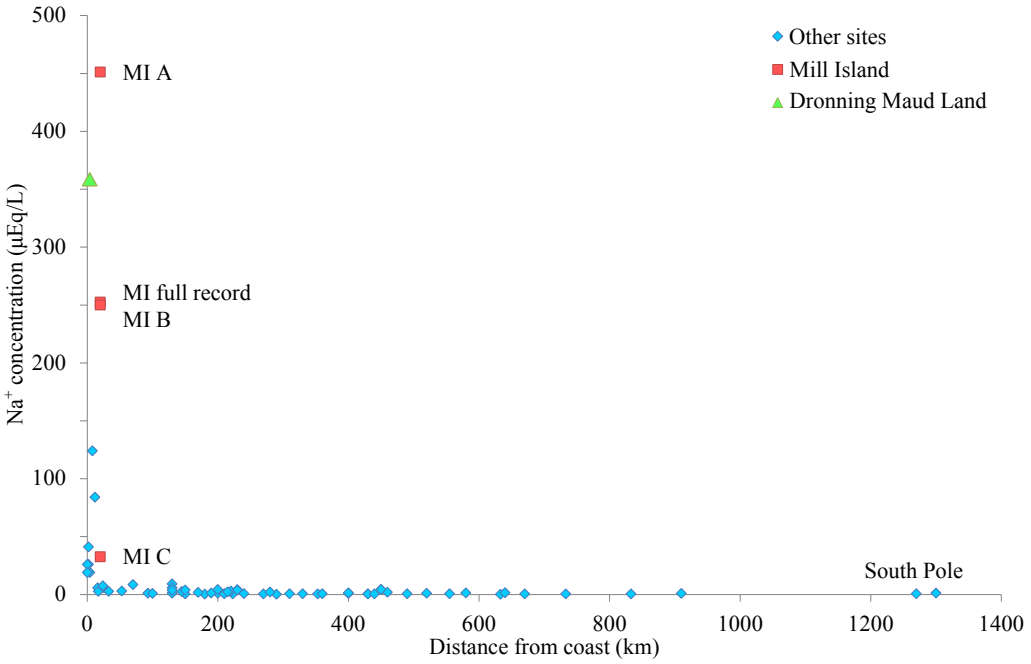

Figure 2.19: Mean Na^+ concentrations at Antarctic ice core and snow pit sites. Na^+ concentration is $\mu Eq/L$ and distance is the distance in kilometres from the coast. Figure adapted from Table 1 of Mulvaney and Wolff (1994). Mill Island values are shown as averages during Regime A, B, and C (see the text for details) and averaged for the 97 year Mill Island record.

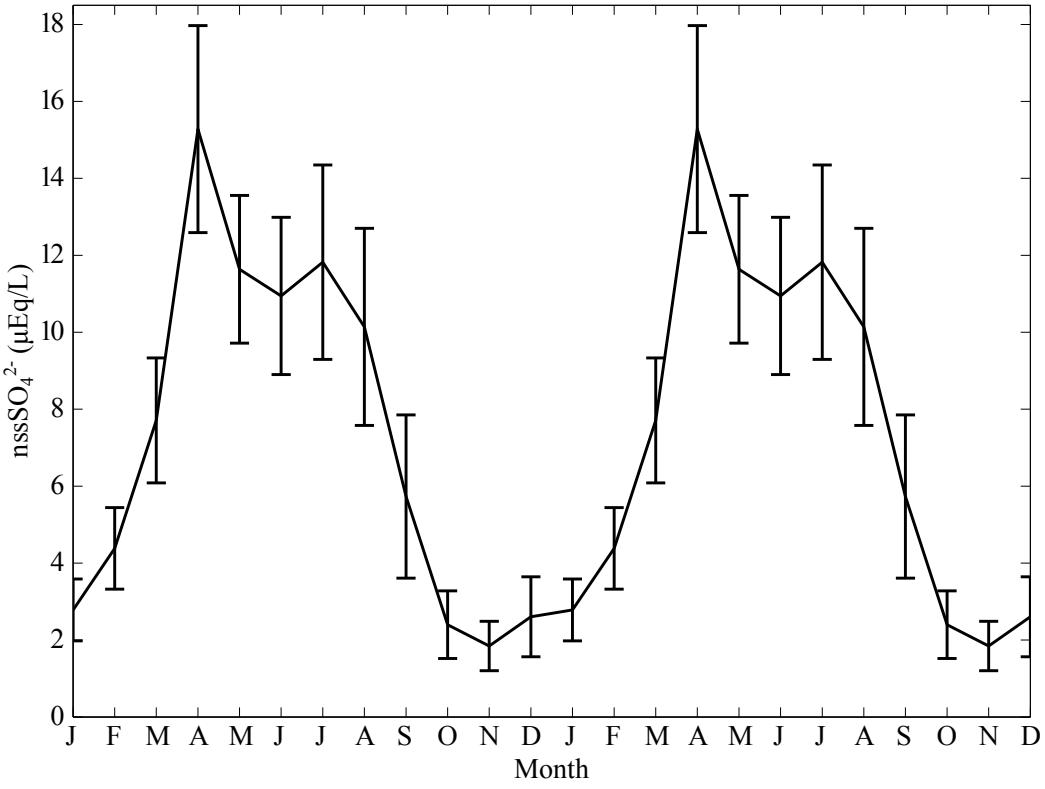

Figure 2.20: Average seasonal cycle of nssSO_4^{2-} calculated with the corrected value of *k'*. The error bars show the standard error of the mean. Note: volcanic eruption years were excluded from this calculation.

(Figure 2.20). It shows a broad peak during autumn – winter with a maximum value in April. However, considering that the main source of nssSO_4^{2-} is from biological activity, it is expected to peak during summer. One possible reason for this may be that the irregular seasonality in the sea salt record precludes the simple regression method from accurately calculating nssSO_4^{2-} at Mill Island.

Regime B (1934 – 2000) shows a high concentration baseline in the Na^+ record (Figure 2.11). This masks the seasonal cycle, and may adversely affect the calculation of nssSO_4^{2-} in equation 2.2. However, upon closer inspection

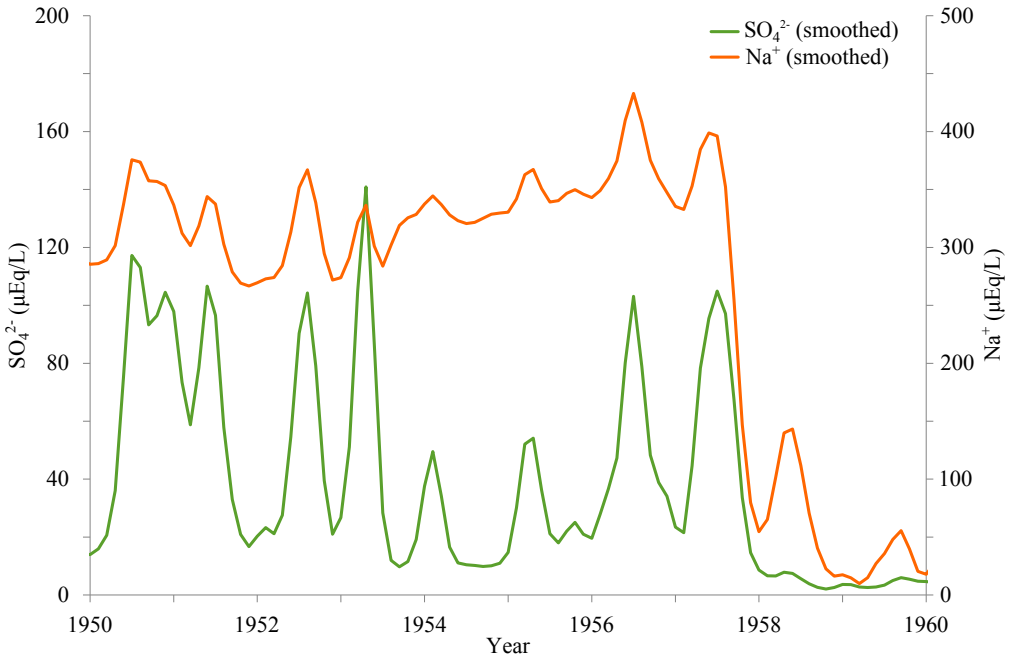

Figure 2.21: Sodium and sulphate records between 1950 and 1960. Data were smoothed as in Figure 2.9.

(see Figure 2.21), Na^+ and SO_4^{2-} show concurrent peaks. For example, the Na^+ peak timing matches the SO_4^{2-} peak timing between 1950 and 1960. This indicates that these peaks most likely represent sea salt deposition. Furthermore, these peaks are observed during winter, i.e., the time of maximum sea salt concentration in ice cores, which explains why the average seasonal cycle of Na^+ shows a winter maximum (Figure 2.12). The high concentration baseline of the sodium leads to errors in equation 2.2 because it leads to an overcorrection, i.e., subtracting too much sea salt sulphate from total sulphate during the summer period. This may be the reason for the winter maximum in Figure 2.20. Using *k'* derived from the entire record may be useful for studies

of the overall features of sea salt fractionation, and to compare with other sites. However it may not be suitable for reliable calculations of nssSO_4^{2-} at Mill Island.

2.4 Conclusion

A high resolution, well-dated record of water stable isotopes and trace ion chemistry from Mill Island was presented in this chapter. The Mill Island main ice core (MI0910) has been dated by counting annual layers of H_2O_2, $\delta^{18}O$, and D-ex. The ice core contains ∼97 years of climate record (from 1913 to 2009). The record has maximum dating uncertainties of +2.4, -3.5 years. The stratigraphy shows crust layers throughout the ice core. The cause of the crust layers is likely wind-related, and there is no evidence that the crust layers are caused by melt events. Furthermore the record shows that these layers are not the cause of the ambiguous trace ion seasonality.

The results of H_2O_2, $\delta^{18}O$, δD, D-ex, and trace ion chemistry are also presented. The H_2O_2, $\delta^{18}O$, δD, and D-ex records generally show strong seasonality. The temperature calibration of the $\delta^{18}O$ record is presented in Chapter 4. The chemistry record shows unique regime structure, including periods of clear seasonality with high concentration, periods of ambiguous seasonality with high mean concentration, and periods of clear seasonality with low mean concentration. The mean concentration of major ion species are generally

much higher than in other nearby ice core records. SO_4^{2-} most likely originated from sea salt, and is highly depleted relative to Na^+. The appropriate ratio of SO_4^{2-}:Na^+, $k' = 0.049$, was calculated to derive nssSO_4^{2-}.

Further details of the Na^+ and SO_4^{2-} records, especially the regime changes, and comparison with other environmental data, e.g., wind and sea ice concentration, are discussed in Chapter 3. $\delta^{18}O$ is further investigated to produce a temperature proxy for Mill Island in Chapter 4.

Chapter 3

Investigating the high sea salt concentration at Mill Island

3.1 Introduction

The origin of sea salt on the Antarctic Ice Sheet and its interpretation as an environmental proxy have been previously discussed (see Section 1.4.3 for further details). However, it is summarised here to aid clarity. Early ice core studies attributed the main source of sea salts to sea spray from the open ocean, transported by strong winds associated with storm events (e.g., Legrand and Mayewski, 1997; Curran et al., 1998; Wagenbach et al., 1998a). Thus these findings concluded that sea salt represents storminess and the onshore wind component (Wagenbach, 1996). More recently, Rankin et al. (2002) reported the importance of frost flowers (sea salt crystals formed on new sea-ice) as a sea salt source, and Yang et al. (2008) suggested the sublimation of salty blowing snow on sea ice as a potential sea salt source. It is likely that different sea salt sources dominate and contribute to the sea salt records at different sites (Abram et al., 2011).

The sea ice-covered ocean, where frost flowers are created, is an important sea salt source (Rankin et al., 2002; Kaleschke et al., 2004). Since the Mill Island ice core record is highly depleted in SO_4^{2-} relative to sea salt, frost flowers are thought to be an important sea salt source at Mill Island (see further details in Section 2.3.5). The high sea salt concentration at Mill Island (as shown in Section 2.3) is the highest sea salt record observed in Antarctica (see Figure 2.18b and Figure 2.19). Unfractionated sea salt-enriched blowing snow from nearby sea ice-covered regions also could be an important sea salt source (Yang et al., 2008).

Another prominent feature of the Mill Island sea salt record is the apparent regime changes. The sea salt record can be divided into three regimes based on the sodium (Na^+) record: A) Clear seasonality with high peak concentration (2009 to ∼2001); B) ambiguous seasonality with high concentration base line (∼2000 to ∼1934); and C) seasonality with low peak concentration (∼1933 to 1913).

The aim of this chapter is to investigate the seasonal and interannual variability of sea salts, in order to reveal the climate factors that influence the Mill Island ice core record. This will be done by investigating the characteristics and the differences of the trace chemistry record in each regime, and by examining the environmental factors that influence and contribute to the regimes, e.g., wind speed and direction, sea ice configuration, and deposition

processes. Na^+ and sulphate (SO_4^{2-}) records will be examined and used as representatives of sea salt at Mill Island. Additionally, observed post-depositional movement of chloride (Cl^-), Na^+, magnesium (Mg^{2+}), and methanesulphonic acid (MSA) will be discussed.

3.2 Datasets

Hydrogen peroxide (H_2O_2), water stable isotopes ($\delta^{18}O$, δD, and D-ex), and trace ion chemistry ($CH_3SO_3^-$ (MSA), Cl^-, NO_3^-, SO_4^{2-}, Na^+, K^+, Mg^{2+}, Ca^{2+}, and $nssSO_4^{2-}$) records from the Mill Island 120 m main ice core datasets were presented in Chapter 2. The time series of Na^+, SO_4^{2-}, $\delta^{18}O$, and D-ex from Chapter 2 are used for further analysis in this chapter. Other datasets used in this chapter are described in this section.

3.2.1 Wind direction and wind speed

Due to no long term in-situ meteorological observation data available at Mill Island, atmospheric model outputs were used to investigate the differences between regimes. Wind data were derived from National Centers for Environmental Prediction (NCEP) Climate Forecast System Reanalysis (CFSR) (Environmental Modeling Center, 2010). CFSR provides high resolution data ($\sim$ 0.313 degree $\times$ 0.312 degree). The closest grid point to Mill Island was chosen for this analysis (65° 24' 42.84" S, 100° 56' 15" E, $\sim$ 17 km east of the

exact MI0190 drilling site). CFSR data are available from 1979.

3.2.2 Sea ice concentration

Satellite observation data were also used for investigation of sea ice conditions. Sea ice concentration data were provided by the National Snow & Ice Data Center (NSIDC). Bootstrap sea ice concentrations were derived from the Scanning Multichannel Microwave Radiometer (SMMR) on the Nimbus-7 satellite, and from the Special Sensor Microwave/Imager (SSM/I) sensors on the Defense Meteorological Satellite Program's (DMSP) -F8, -F11, and -F13 satellites. Measurements from the Special Sensor Microwave Imager/Sounder (SSMIS) aboard DMSP-F17 are also included. The data are provided at a monthly time step and have a spatial resolution of 25 km (Comiso, 2000. Updated 2014). The datasets are available since 1979.

3.3 Results and discussion

3.3.1 Sea salt regimes at Mill Island

Time series of Na^+, SO_4^{2-}, $\delta^{18}O$, and D-ex are shown over the period from 1913 to 2009 (Figure 3.1, Table 3.1). Na^+ shows clear differences between the regimes. The Na^+ winter (April to October) peak during regime A is not present in regime B. Instead, Na^+ in regime B shows lengthy "plateau" or "maxima" periods, which are broad periods of high concentration ($\sim$ 300

$\mu Eq/L$), and "valley" or "minima" periods, which have a relatively low concentration ($< 100\ \mu Eq/L$). Na^+ in regime C shows lower concentrations ($\sim 30\ \mu Eq/L$) with observable seasonality (except for 1917 – 1920).

The SO_4^{2-} record shows peaks in winter during regime A, and seasonally-random high concentration peaks ($> \sim 40\ \mu Eq/L$) in regime B. Regime C, however, differs to regimes A and B, with low concentrations of SO_4^{2-} ($\sim 5\ \mu Eq/L$). In regime B, SO_4^{2-} shows occasional winter peaks, e.g., between 1934 and 1940; 1950 and 1957; and 1977 and 1987. The winter peaks in SO_4^{2-} in regime B suggest that the main source of SO_4^{2-} is sea salt. When the SO_4^{2-} record shows a high winter concentration ($> \sim 40\ \mu Eq/L$), the Na^+ record plateaus.

For the $\delta^{18}O$ ratio, other than higher values during summer (December – January) after 2000, there appears to be little difference between regimes. D-ex also does not show any differences associated with the regimes. Although, lower values are observed during winter before 1950 than after 1950. It appears that the regime shifts are only evident in the sea salt trace ion record. Note that chloride (Cl^-) also shows features similar to the Na^+ record, i.e., clear seasonality in regime A, mix of "plateau" and "valley" regions in regime B, and lower concentrations with observable seasonality in regime C (Figure 2.11 b).

Table 3.1 shows the mean concentrations of Na^+ and SO_4^{2-}, and the

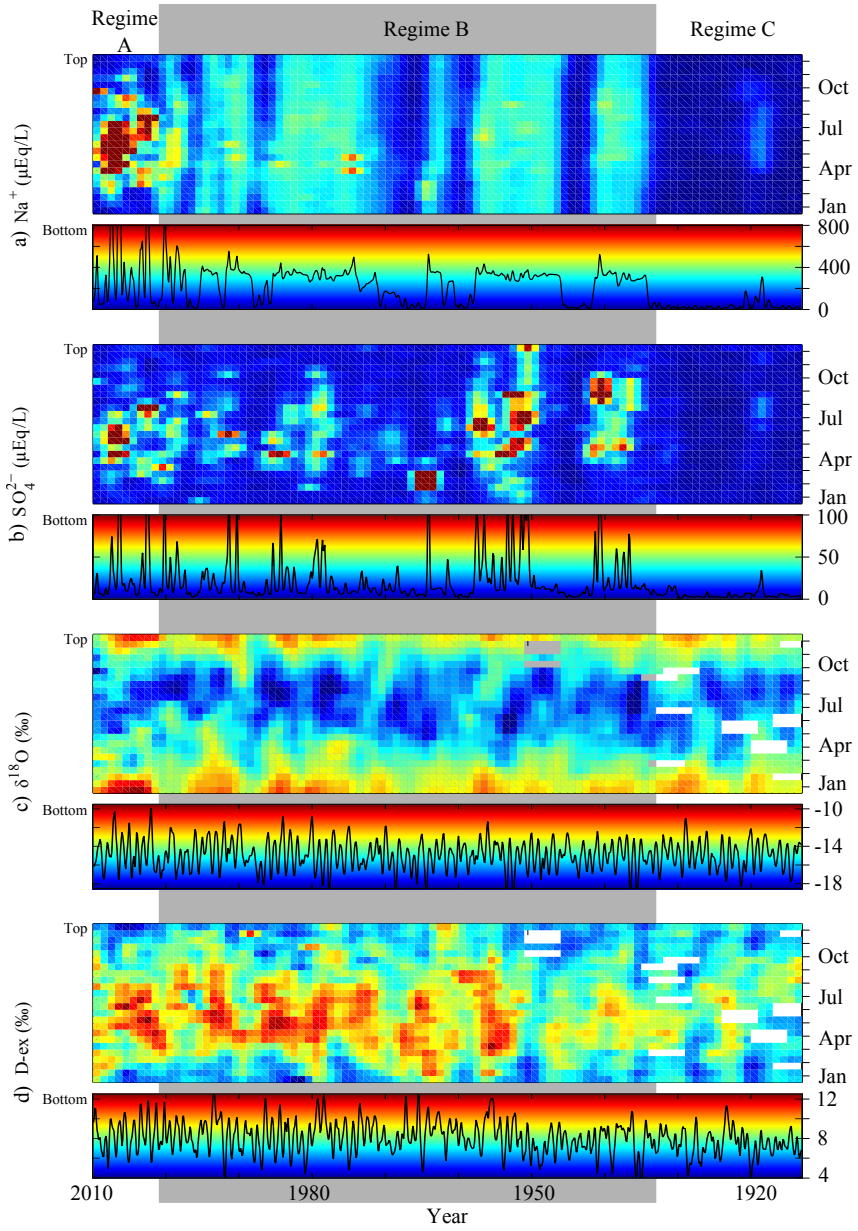

Figure 3.1: Time series of a) Na^+, b) SO_4^{2-} concentrations, and the ratio of c) $\delta^{18}O$, and d) D-ex records over the period from 1913 to 2009. Each top panel: Data were interpolated to 24 points per year, then smoothed with a Gaussian filter of width $\sigma = 1$ point. The x-axis is year, the y axis is month, and color scale is shown in each bottom panel. Each bottom panel: Time series of each species as in Figure 2.9 and Figure 2.11. The background color indicates as color bar of the top panel. Y axis is the concentration/ratio. Regimes A (2009 – 2001), B (2000 – 1934), and C (1933 – 1913) were partitioned using a grey panel.

mean ratios of δ^{18}O and D-ex for each regime. Again, Na^+ and SO_4^{2-} show clear differences between regimes, with the highest values in regime A (451.24 $\mu Eq/L$ and 30.24 $\mu Eq/L$, respectively). Both species show the lowest value in regime C (32.62 $\mu Eq/L$ and 5.58 $\mu Eq/L$, respectively). The values in regime C are only 7.23% and 18.45% of the values in regime A, respectively. In all cases for Na^+ and SO_4^{2-}, the standard deviation is greater than the mean values (except Na^+ in regime B). This indicates high variability throughout the whole record.

Average seasonal cycles of Na^+, SO_4^{2-}, δ^{18}O, and D-ex for each regime are shown in Figure 3.2. Na^+ and SO_4^{2-} both show seasonality with a winter peak in regimes A (blue line) and B (green line). The variability of the Na^+ concentration is less in regime B (minimum 214 $\mu Eq/L$ in November, maximum 293 $\mu Eq/L$ in April) compared with regime A (minimum 92 $\mu Eq/L$ in December, maximum 1,222 $\mu Eq/L$ in May), and the seasonality is not as clear (Figure 3.2 a). The Na^+ variation and concentration was lowest during regime C (minimum 17 $\mu Eq/L$ in January, maximum 55 $\mu Eq/L$ in July), and seasonality is still evident, with a peak in winter. However SO_4^{2-} seasonality is not evident in regime C.

δ^{18}O shows enriched values (~ -11 ‰) during summer in regime A compared to regimes B and C (Figure 3.2 c). This suggests that the controlling influence on δ^{18}O (e.g.,temperature) at the coring site increased during summer in recent decades. Further investigation of the δ^{18}O record is given in

		A (2001 – 2009)	B (1934 – 2000)	C (1913 – 1933)
Na^+ ($\mu Eq/L$)	mean	451	254	32.47
	std	900	156	49.97
	min	1.09	0.18	0.18
	max	8,023	1,480	343
SO_4^{2-} ($\mu Eq/L$)	mean	30.24	21.22	5.59
	std	55.78	38.61	6.30
	min	0.45	0.00	0.20
	max	502	563	60.40
$\delta^{18}O$ (‰)	mean	-14.50	-14.95	-14.94
	std	2.43	2.01	1.85
	min	-21.30	-22.56	-19.22
	max	-7.48	-9.15	-10.38
D-ex (‰)	mean	8.33	8.31	7.48
	std	2.54	2.21	1.67
	min	1.81	-0.53	0.98
	max	14.65	16.89	11.64

Table 3.1: Mean concentrations, standard deviation, minimum and maximum values of the Na^+, SO_4^{2-}, $\delta^{18}O$, and D-ex in each regime.

Chapter 4. The D-ex seasonal cycle shows the most depleted values (~ 5 ‰) during summer in regime A. In regime C, the D-ex variability within a year is smaller than other regimes (Figure 3.2 d). This may indicate that the moisture source has changed, or some changes have happened in the moisture source region since regime C (or since 1950, according to Figure 3.1).

In summary,

Regime A: Clear seasonality with a winter peak is observed for Na^+ and SO_4^{2-}. The mean concentrations of Na^+ and SO_4^{2-} are highest among the three regimes (451 $\mu Eq/L$ and 30.2 $\mu Eq/L$, respectively) (Figure 3.1, 3.2).

Regime B: Na^+ shows "plateaus" of ~ 300 $\mu Eq/L$ and "valleys" (short periods of low concentration, < 100 $\mu Eq/L$). SO_4^{2-} shows seasonally-unaligned peaks ($> \sim 40$ $\mu Eq/L$) during which Na^+ "plateau" periods (Figure 3.1).

Regime C: The concentrations of Na^+ and SO_4^{2-} are low (32.5 $\mu Eq/L$ and 5.6 $\mu Eq/L$, respectively). Na^+ shows a peak during winter, but no seasonality is observed in the SO_4^{2-} record (Figure 3.1, 3.2).

Note: The regime changes seem to influence only the trace ion record: $\delta^{18}O$ shows higher values in summer after 2001, and D-ex shows lower values prior to 1950.

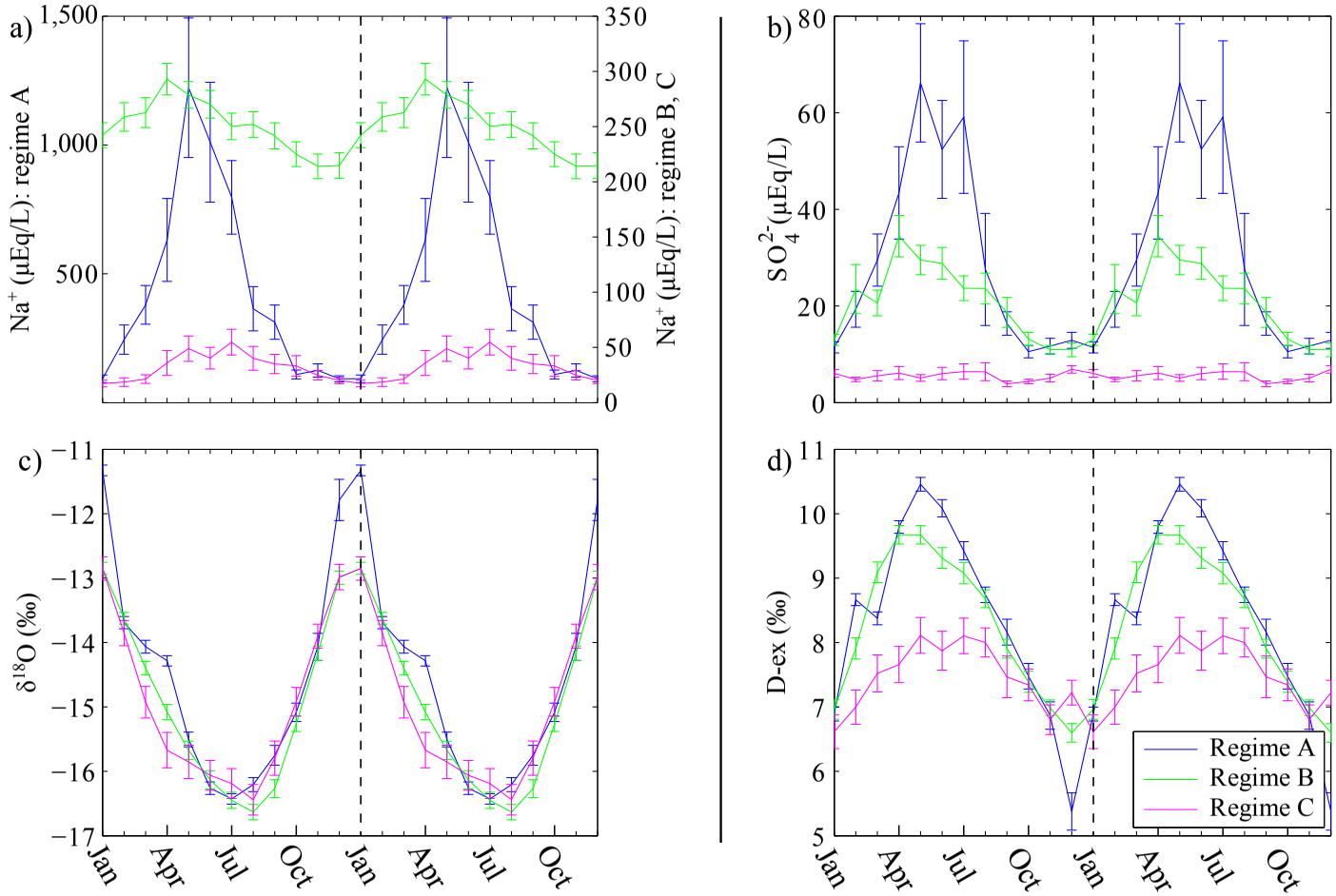

Figure 3.2: Average seasonal cycles of a) Na^+, b) SO_4^{2-}, c) $\delta^{18}O$, and d) D-ex for each regime. Regime A: 2001 – 2009 (blue), Regime B: 1934 – 2000 (green), Regime C: 1913 – 1933 (magenta). The x axis shows the month, y axis shows the concentration/ratio. Note that the Na^+ concentration is shown with a different scale for regime A (left y axis) and regimes B and C (right y axis).

Both sea ice and atmospheric reanalysis data are available only since 1979. Thus only regimes A and B (after 1979) are investigated in the next section.

3.3.2 Wind direction and wind speed at Mill Island

Many ice core studies suggest that sea salt is a proxy for wind and storminess (e.g., Wagenbach, 1996; Legrand and Mayewski, 1997; Curran et al., 1998), because salt is transported by air mass movement, i.e., wind. Thus, wind direction and speed are investigated in this section to determine the origin of sea salt at Mill Island.

The wind rose climatology, which represents the 6-hourly wind speed and direction data at Mill Island, was generated using data from 1979 to 2009. A wind rose is an effective way to present the long-term wind conditions. It displays the frequency of wind blowing from a range of directions in several speed bins over the specified period. The direction of each spoke shows the direction which the wind has come from (i.e., the spoke towards to east indicates an easterly, or westward, wind), while the color shows the wind speed (i.e., dark blue indicates a wind speed between 0 m/s and 5 m/s). The length of each spoke segment shows the relative frequency of wind from that direction. At Mill Island, the wind direction is predominantly from the east, and the mean wind speed over the period is 7.6 m/s (see Figure 3.3).

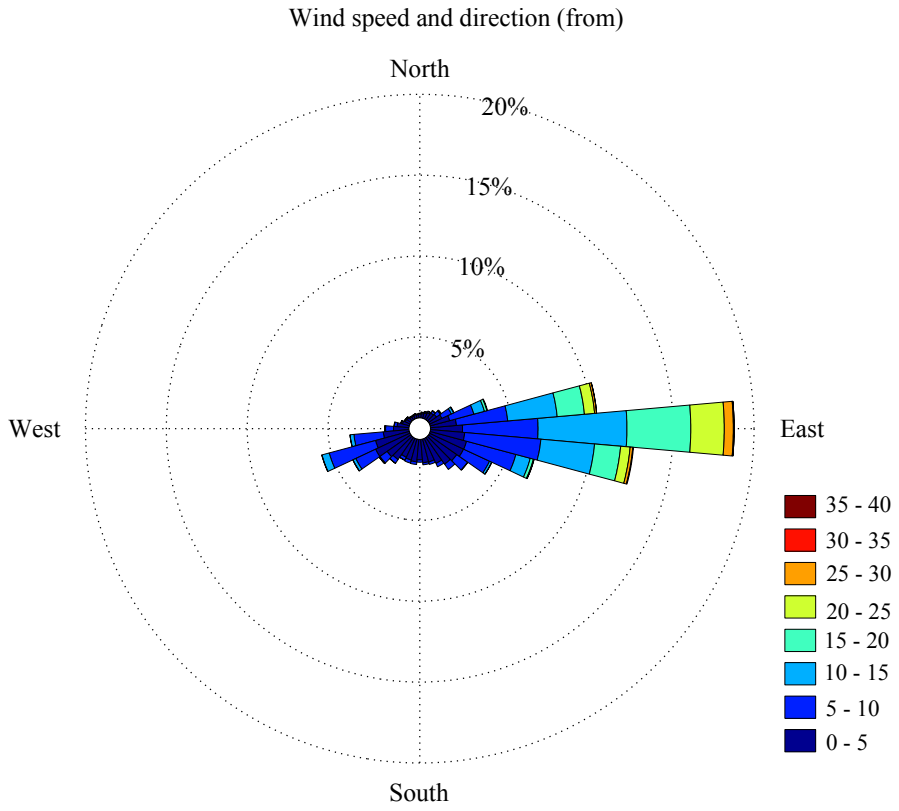

Figure 3.3: Wind rose climatology near Mill Island (grid point: 65.4119° S, 100.9375° E) from 1979 to 2009. The wind data were derived from the NCEP CFSR reanalysis model (Environmental Modeling Center, 2010).

The relationship between wind speed and Na^+ and SO_4^{2-} concentration was investigated by correlating annual, summer (October – March) and winter (April – September) means of Na^+ and SO_4^{2-} concentration against the number of data points where the wind speed was < 5 m/s, 5 – 15 m/s, and > 15 m/s in the associated period (see Table 3.2). There are no significant correlations between annual mean Na^+ concentration and annual mean wind speed. The number of data points per year where the wind exceeds 15 m/s, or less than 5 m/s also show no significant correlations with annual mean Na^+ concentration. There is a significant negative correlation between Na^+ concentration and number of data between wind speed 5 m/s – 15 m/s per year ($r = -0.51$, $p < 0.01$). However this correlation is strongly influenced by two data point outliers in 2006 and 2007 where the Na^+ concentration is extremely high. The regression slope of the Na^+ concentration versus medium wind speed is low, indicating that this correlation displays little predictive power. This negative correlation between Na^+ and wind speed 5 m/s – 15 m/s is likely coincidental and thus disregarded. To confirm that this relation is coincidental, the number of data points per year with wind speed less than or more than 7 m/s also shows no correlation with Na^+ concentration. Similarly, the significant correlation between the data points and wind speed 5 m/s, 5 – 15 m/s, and > 15 m/s during winter is thought to be due to outlying data points in the winters of 2002, 2006, and 2007. Thus, the wind speed is unlikely related

to the Mill Island sea salt regime changes, at least post-1979. Correlations between SO_4^{2-} concentration and wind speeds show almost the same results, except the outliers occur in years 2002 and 2006.

Wind speed	Na^+			SO_4^{2-}		
(m/s)	annual	summer	winter	annual	summer	winter
< 5	0.22	0.11	− 0.01	0.15	0.33	− 0.09
5 – 15	**− 0.51**	− 0.14	**− 0.48**	**− 0.42**	− 0.32	**− 0.36**
> 15	0.18	0.01	**0.41**	0.18	− 0.09	**0.42**

Table 3.2: Correlations between CFSR wind speed at Mill Island and concentration of Na^+ and SO_4^{2-} during winter and summer and for the annual average. Bold values indicate $p < 0.05$.

Sixty percent of the wind at Mill Island comes from the easterly quadrant (wind direction between 45 and 135 degrees). Only 3 % of wind comes from the north (315 – 45 degrees), 19 % from the west (225 – 315 degrees) and 15 % from the south (135 – 225 degrees). More than half of the westerly, southerly and northerly winds have speed less than 5 m/s, and 99 % of wind speed greater than 15 m/s wind blows from east. Slopes with an aspect facing toward the prevailing wind have higher snow accumulation (Goodwin et al., 2003). This result matches with the east-west snow accumulation gradient observed between two shallow ice cores MIp0809 and MIp0910 (Section 1.3.2) (Domensino, 2010).

The sea salt source at Mill Island is predominantly from the east of Mill Island. Therefore, the next section focuses on the environment to the east of

Mill Island.

3.3.3 Relationship between sea ice concentration and sea salt

Section 3.3.2 confirms that the dominant wind direction is from the east of Mill Island. Bowman Island (65° 12' S, 103° 00' E) is located ∼100 km east of Mill Island (Figure 3.4). During the observation record, the ocean between Mill Island and Bowman Island is typically free of ice during summer, and covered with sea ice during winter. The sea ice cover in this area could possibly influence the sea salt record.

Monthly sea ice concentration (SIC) was investigated for the region between Mill Island and Bowman Island for the period between January 1979 and December 2009. Sea ice concentration data indicates what fraction of each pixel is covered by sea ice. There are five SIC pixels between Mill Island and Bowman Island (see Figure 3.4 for coordinates). Annual mean sea ice concentration in these pixels was compared with annual mean concentrations of Na^+ and SO_4^{2-}.

Table 3.3 shows the correlation coefficient between annual mean sea ice concentration and annual mean concentrations of Na^+ and SO_4^{2-}. Annual mean sea ice concentration is negatively correlated at a statistically significant level with mean annual Na^+ concentration except for SIC-W ($r = -0.28$, $p =$

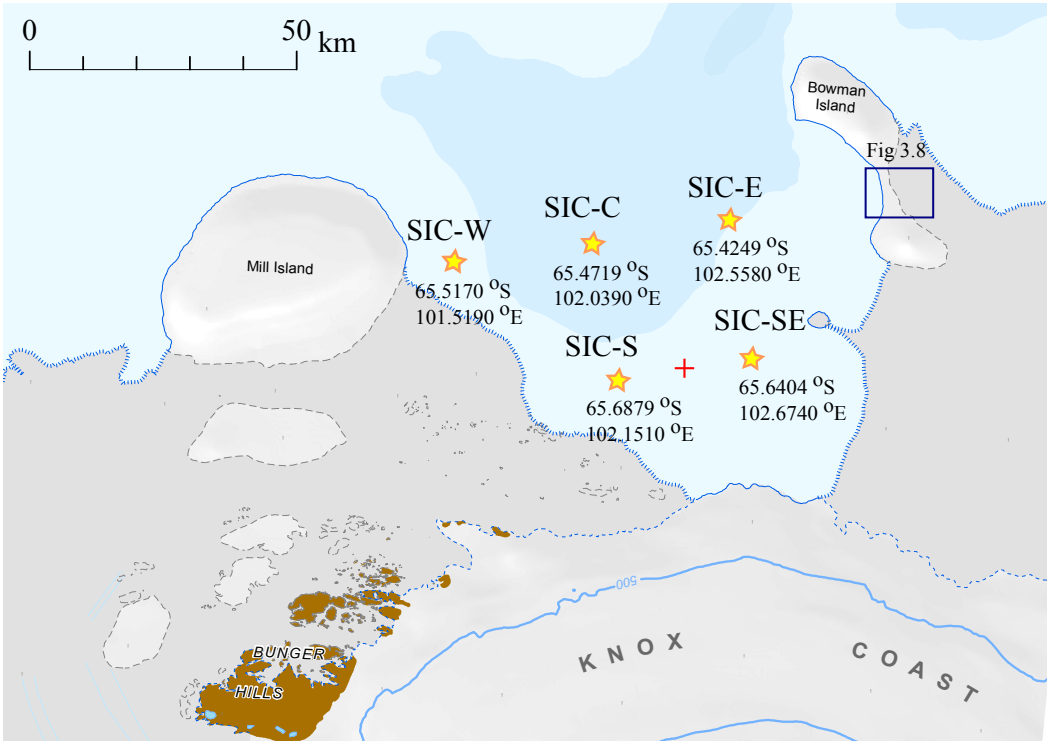

Figure 3.4: The coordinates and names of the five sea ice concentration data pixels. The red plus symbol indicates the centroid position of the derived time series SIC-m, formed by averaging SIC-S and SIC-SE. The dark blue rectangle indicates the location of the photograph shown in Figure 3.8. Map courtesy of the Australian Antarctic Division, © Commonwealth of Australia, 2012.

0.13). The highest correlation with Na^+ is at SIC-SE ($r = -0.57$, $p < 0.01$). The annual mean concentration of SO_4^{2-} is also significantly anti-correlated with annual mean sea ice concentration at the five SIC pixels. SIC-S shows the highest negative correlation ($r = -0.58$, $p < 0.01$). Thus, sea ice concentration values from SIC-S and SIC-SE were averaged to form a single record, termed SIC-m.

	Na^+	SO_4^{2-}
SIC-W	− 0.28	**− 0.49**
SIC-C	**− 0.47**	**− 0.52**
SIC-E	**− 0.53**	**− 0.55**
SIC-S	**− 0.53**	**− 0.58**
SIC-SE	**− 0.57**	**− 0.57**

Table 3.3: Correlation coefficients between annual mean sea ice concentration at each pixel and the annual mean concentration of Na^+ and SO_4^{2-}. Bold numbers indicate $p < 0.01$.

Table 3.4 shows the correlation coefficient between annual mean sea ice concentration at SIC-m and annual mean concentrations of Na^+ and SO_4^{2-} between 1979 and 2009. Sea ice concentration is significantly anti-correlated with both Na^+, and SO_4^{2-} in all three periods. Note that regime C is before the satellite era, thus there are no sea ice concentration observation data available.

Figure 3.5 shows time series of annual mean concentration of SIC-m, Na^+, and SO_4^{2-} for the period between 1979 and 2009, covering all of regime

	Na^+	SO_4^{2-}
SIC-m_{AB}	**− 0.56**	**− 0.58**
SIC-m_A	**− 0.76**	**− 0.80**
SIC-m_B	**− 0.52**	**− 0.47**

Table 3.4: Correlation coefficients between annual mean sea ice concentration at SIC-m and the annual mean concentrations of Na^+ and SO_4^{2-} during the periods of 1979 – 2009 (SIC-m_{AB}), regime A (2001 – 2009, SIC-m_A), and regime B (1979 – 2000, SIC-m_B). Bold numbers indicate $p < 0.03$.

A and approximately one third of regime B. This figure clearly shows the negative correlation between SIC-m and Na^+, SO_4^{2-} (note that the y axis for SIC, the left y axis, is reversed).

Given that the Mill Island site shows high sea salt concentrations, the prevailing wind is from the east and the sea ice to the east frequently shows low concentration, a mechanism to explain these relationship between wind direction, sea ice concentration, and high sea salt concentration is proposed here.

1. Lower concentration sea ice coverage in the SIC-m area (i.e., SIC-S and SIC-SE) leads to formation of new sea ice.

2. Frost flowers are produced on newly formed sea ice, then fragments are transported to Mill Island by the prevailing easterly wind (Hall and Wolff, 1998); and/or sea salt enriched brine migrate upwards through sea ice to the snow on sea ice. Then the salty snow is blown to Mill

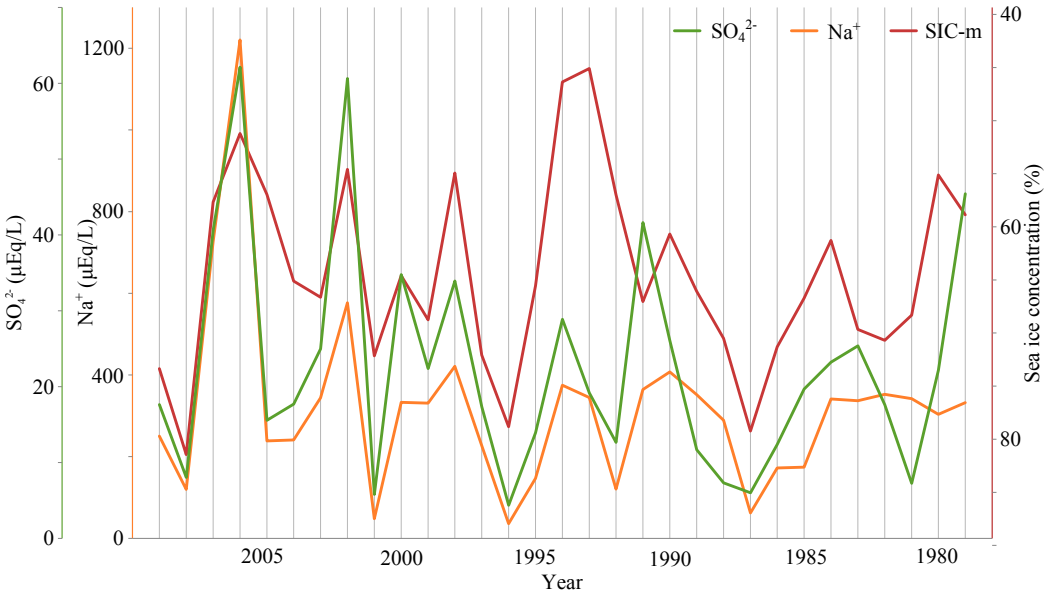

Figure 3.5: Time series of annual mean SIC-m (red, right y axis), Na^+ (orange, left y axis), and SO_4^{2-}(green, left y axis) over the period from 1979 to 2009. Sea ice concentration data were derived from NSIDC (see text). Note that the right y axis is reversed to highlight the high degree of anti-correlation.

Island by the prevailing easterly wind.

3. Southerly katabatic-driven wind at sea level advects this new sea ice export from the region between Mill Island and Bowman Island. Hence the SIC-m area is cleared and new sea ice can form again (i.e., a coastal polynya forms in the lee of Bowman Island (Nihashi and Ohshima, 2015)).

4. The process of sea ice formation and advection repeats.

However, SIC-m does not show particularly low concentration in 2002, 2006, and 2007 when Na^+ and SO_4^{2-} are high. The lowest SIC-m years are in 1993 and 1994 (45.1 % and 46.4 %, respectively). In these years, Na^+ and SO_4^{2-} show a mid-range concentration (weak anti-correlation between SIC and Na^+, SO_4^{2-}).

Differences between 1993 – 1994 and 2006 – 2007 are found in SIC-W. Figure 3.6 is the same as Figure 3.5, but with the addition of SIC-W concentration (blue). The horizontal dashed blue line indicates the mean sea ice concentration in SIC-W, and dotted blue lines indicate the 1σ standard deviation of SIC-W. In 2006 – 2007, SIC-W concentration is within 1σ of the mean sea ice concentration (73.9 % in 2006 and 69.6 % in 2007), whereas in 1993 – 1994, sea ice concentration is more than 1σ below the mean (58.0 % and 62.2 % respectively). This implies that sea ice concentration in the SIC-W

area may affect the sea salt transport process. Though in 2002, the high levels of Na^+ are not clearly explained with this hypothesis alone.

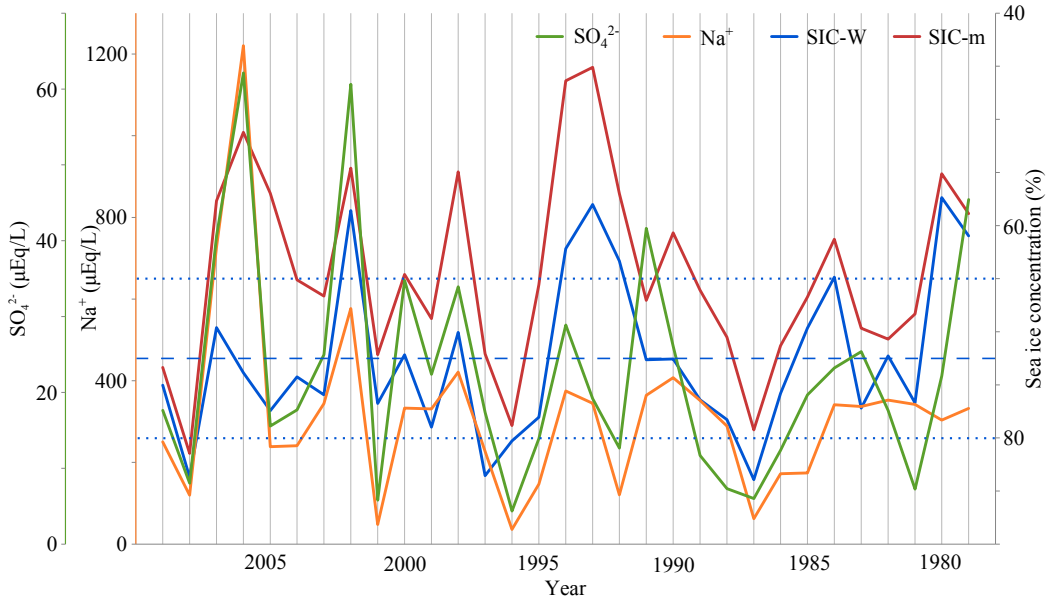

Figure 3.6: Time series of annual mean SIC-m (red, right y axis), SIC-W (blue, right y axis), Na^+ (orange, left y axis), and SO_4^{2-} (green, left y axis) over the period from 1979 to 2009. The horizontal dashed blue line indicates the mean sea ice concentration in SIC-W, dotted blue lines indicate the 1σ standard deviation of the sea ice concentration in SIC-W. Sea ice concentration data were derived from NSIDC (see the text for details). Note that the right y axis is reversed to highlight the high degree of anti-correlation.

Figure 3.7 shows a schematic diagram of a hypothetical sea salt transport mechanism. The edge of large ice-covered islands such as Mill Island typically exhibits a vertical discontinuity on the order of > 10 m, which likely blocks the transport of direct sea spray and sea water aerosol particles onto the island (Figure 3.7 a). If stable land-fast sea ice cover exists, it facilitates formation of a snow ramp, which effectively bridges the vertical gap between the land-

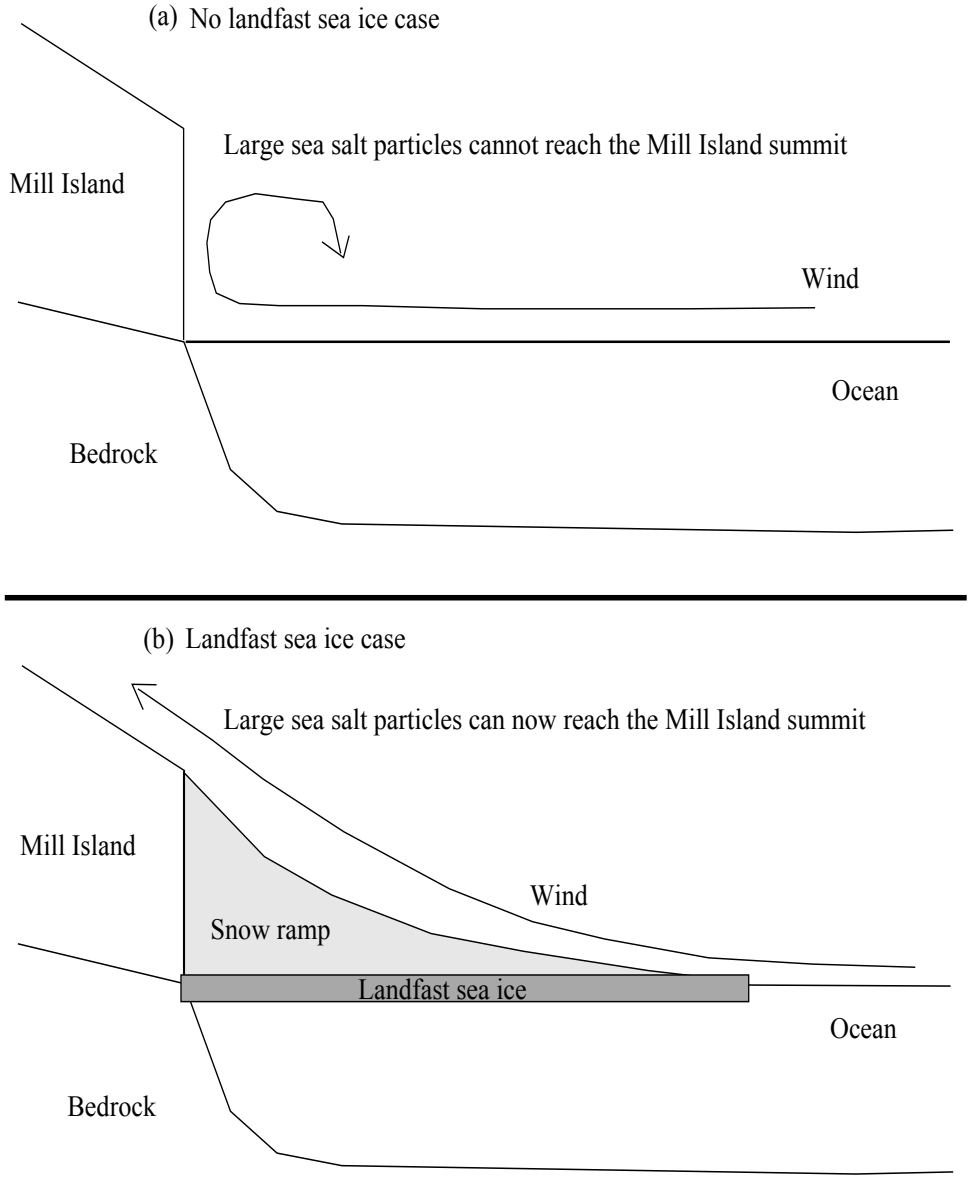

Figure 3.7: Schematic diagram of a hypothetical sea-salt transport mechanism at Mill Island, including formation of a snow ramp.

fast sea ice and the ice sheet (Figure 3.7 b). For example, when SIC-m is low and SIC-W is high (2006), Mill Island records extremely high sea salt concentrations, because of an abundance of available sea salt as frost flowers in SIC-m area and as salty brine snow in SIC-m and SIC-W areas, as well as an effective mechanism to transport sea salt to Mill Island. When both SIC-m and SIC-W are relatively low (2002), Mill Island records still high Na^+ but not as high as the first case, because although there is an abundance of sea salt, the pathway (i.e., snow ramp formation) is not present. When both SIC-m and SIC-W are high (2001, 1996, 1987), Mill Island records low sea salt concentrations, suggesting that frost flowers are more important sea salt source than the salty brine snow. This hypothesis is strengthened by noting that the ratio of SO_4^{2-} to Na^+ in 2001 (0.121) and 1996 (0.122) is close to the sea water ratio of 0.12 (except in 1987 when it is 0.097). When both sea ice concentration at SIC-m and SIC-W, and sea salt are high (e.g., 1991), the source of sea salt could be the salty brine snow on sea ice and/or nearby open water with storm events (the ratio of SO_4^{2-} to Na^+ in 1991 is 0.114). This is, however, not always the case. In 2005, the sea ice concentration is similar to 2006 but sea salt concentration is much lower. The snow ramp theory works well for the vast majority of years.

Figure 3.8 shows an example of an ice-capped island edge, adjacent to landfast sea ice, covered with a well-formed snow ramp. The photo was taken

on the 11^{th} of February, 1947 over Bowman Island. The circle (a) shows an example of the vertical discontinuity from sea level to the ice cap. The circle (b) demonstrates a well-formed snow ramp. The same feature is expected to form at Mill Island. Fraser et al. (2012) demonstrated the presence (and, at times, absence) of multi-year landfast ice to the east of Mill Island, which would facilitate snow ramp formation.

Figure 3.9 shows annual variations of SIC-m, SIC-W, Na^+ and SO_4^{2-} concentrations for the period between 1979 and 2009. Both SIC-m and SIC-W are generally high in early summer (December and January), and low in late summer (February and March). The negative correlation between SIC-m and trace ions can be seen on a monthly basis here. For example, SIC-m in early 1995 shows low concentrations ($< \sim 60$ %) then becomes higher ($> \sim 70$ %) later in the year. Na^+ shows high concentration ($> \sim 300\ \mu Eq/L$) in early 1995, then low concentration ($< \sim 100\ \mu Eq/L$) later in the year. Similar features are also seen in 2000. A case showing high SIC-m and SIC-W but low sea salt is observed from 1985 – 1987. Some years show high sea ice coverage in SIC-W throughout the period, which suggests the existence of multi-year land-fast ice (e.g., 1986 – 1991, 1995 – 1997, and 2003 – 2006).

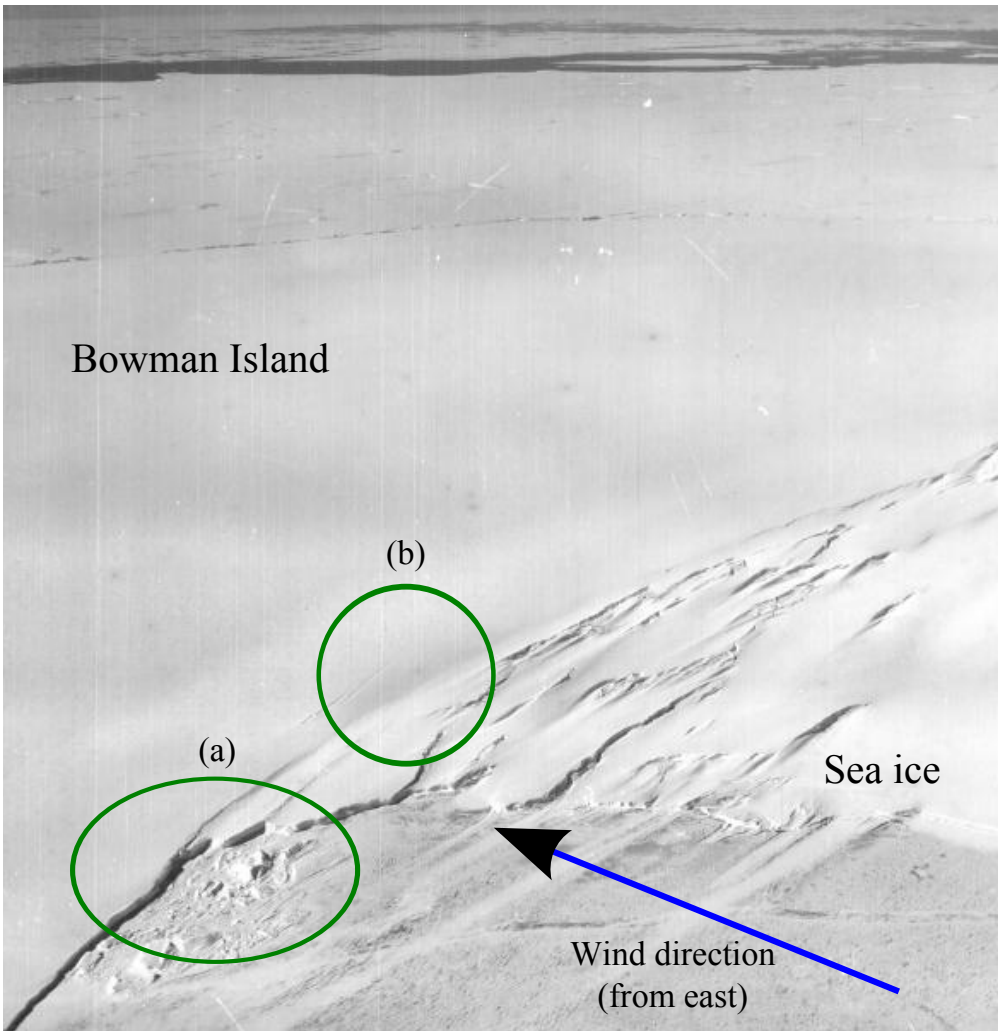

Figure 3.8: An aerial photo over Bowman Island on 11^{th} February, 1947. The circle (a) shows an example of the vertical discontinuity from sea level to the ice cap. The circle (b) demonstrates a clear snow ramp. Some scale is provided by cross-referencing with the rectangle in Figure 3.4. Photo courtesy of the Australian Antarctic Division, © Commonwealth of Australia, 2015.

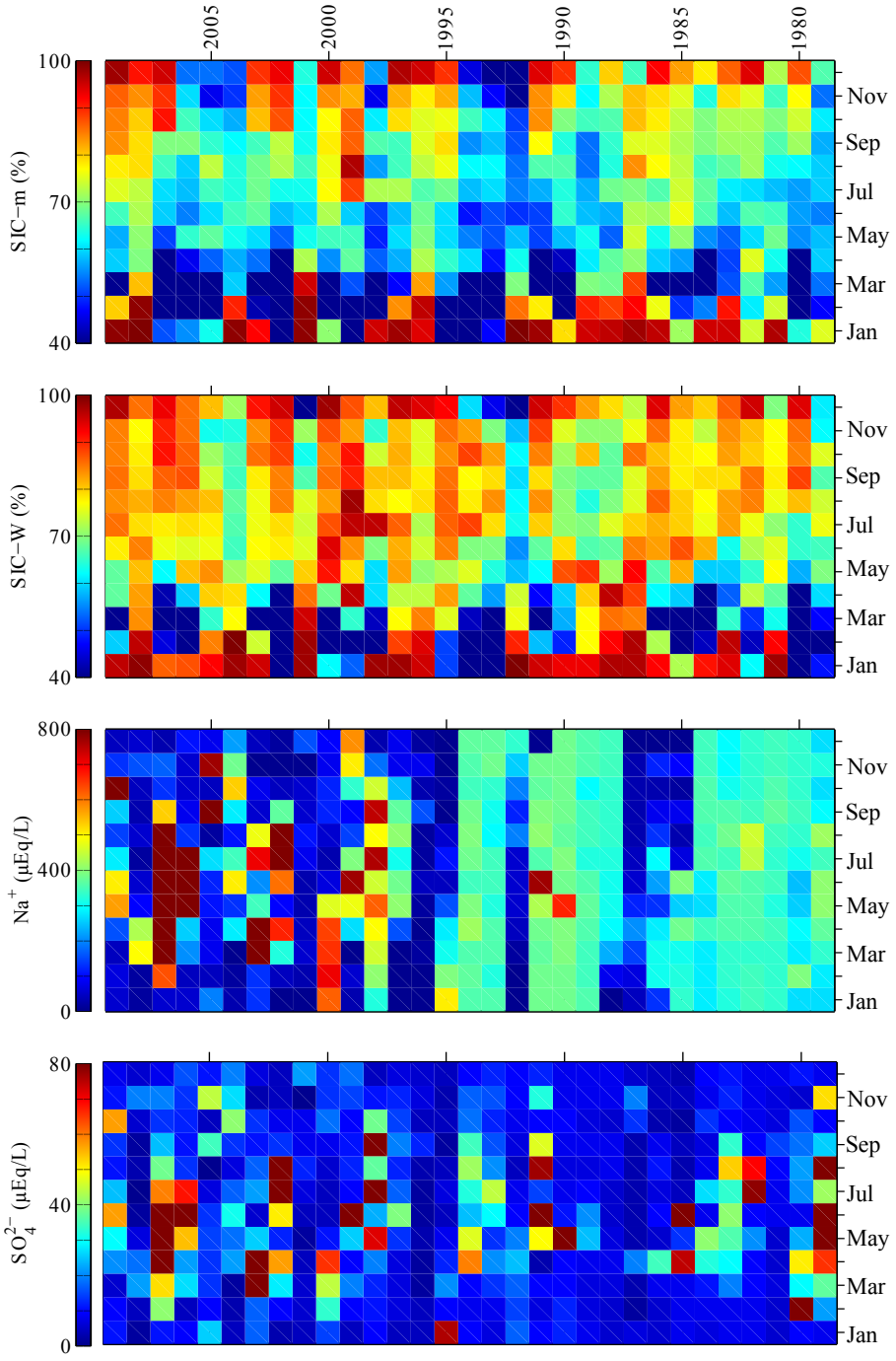

Figure 3.9: Annual variations in SIC-m, SIC-W, Na^+, and SO_4^{2-} over the period from 1979 to 2009. The x axis is year, y axis is month, and the color shows sea ice/trace ion concentration. Each pixel shows the monthly mean concentration of associated species. Chemical data were interpolated to 12 data points per year. No filtering was used.

3.3.4 Local ice shelf variability

The local sea ice concentration changes mentioned in Section 3.3.3 may be related to corresponding changes in the local ice shelf configuration (Massom et al., 2010). Using NASA Moderate Resolution Imaging Spectroradiometer (MODIS) satellite imagery, two major configuration changes were observed between 2000 and 2009 (Figures 3.10 and 3.11).

The first event was the calving of the Scott Glacier in 2002 between Chungunov Island and Mill Island (Figure 3.10b, red dashed line). The event formed an iceberg named C20 (not shown), which drifted westward and continued to break up (Evers et al., 2013). This change occurred entirely to the west of Mill Island (i.e., downstream both oceanographically and atmospherically), thus is unlikely to have influenced the Mill Island record.

The next event was the export of Pobeda Ice Island (C5) from the north-north-west of Mill Island in 2003 or 2004 (Figure 3.11). In the image from the 6^{th} of Mar, 2003 (Fig 3.11a), a large tabular iceberg, Pobeda Ice Island, is grounded to the north-west of Mill Island. This iceberg is not present in the 15^{th} of Sep, 2004 image (Fig 3.11b). Periodic grounding/ungrounding of such icebergs (forming the Pobeda Ice Island) is a regular event in this region. The Denman Glacier calves periodically, and the calved iceberg becomes grounded in this area for up to a few decades (Young and Gibson, submitted, 2013).

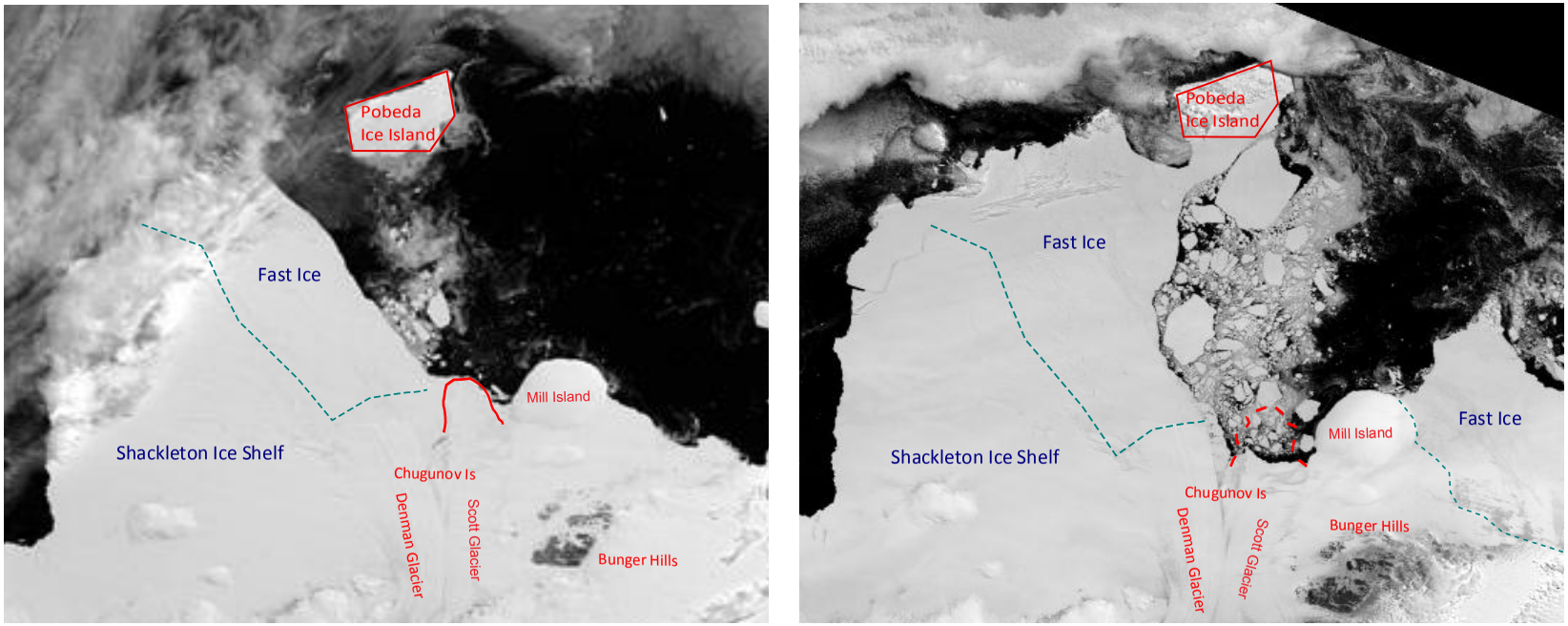

(a) 14^{th} Feb 2002

(b) 29^{th} Dec 2002

Figure 3.10: MODIS images of the Shackleton Ice Shelf and Mill Island area. Green dashed line divides fast ice and ice shelf.

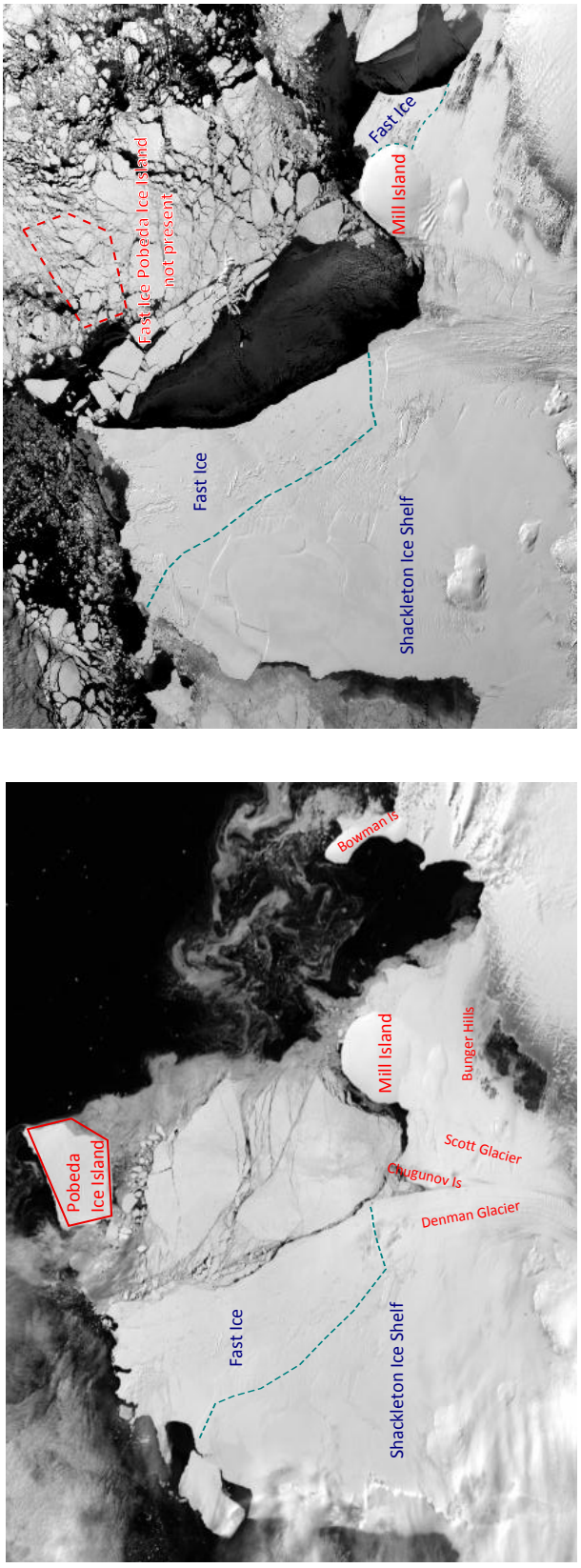

(a) 6^{th} Mar 2003 (b) 15^{th} Sep 2004

Figure 3.11: MODIS images of the Shackleton Ice Shelf and Mill Island area.

According to the Young and Gibson (submitted, 2013) study, the Denman Glacier calved sometime between February, 1947 and February, 1956. Pobeda Ice Island formed subsequently, then remained in place until it was exported in the mid-1970s. The Denman Glacier calved again in late 1984, and the resulting iceberg also grounded to form the Island, until again it was exported in 2004. The presence of such an ice island presents a strong dynamical barrier to mobile pack ice being advected westward in the coastal current, leading to higher pack ice concentration to the east of this barrier (Fraser et al., 2012).

Young and Gibson (submitted, 2013) also studied the historical record of the Shackleton Ice Shelf reported by the early expeditioners: Charles Wilkes observed the Shackleton Ice Shelf during his 1838-1842 voyage. The position of the ice shelf calving front was located further north than Mill Island. Sir Douglas Mawson, polar explorer, observed the Termination Ice Tongue in 1911 - 1914. This ice tongue, a possible hyper-extension of the Denman Glacier tongue, disappeared by 1931. These changes all occurred to the north or west of Mill Island. Considering that the Shackleton Ice Shelf, Pobeda Ice Island and Scott Glacier are all downstream of Mill Island, changes in these ice-scape elements are unlikely to have any strong influence on the Mill Island record, which, as the wind rose climatology shows (see Figure 3.3), is likely more strongly influenced by ice-scape changes to the east (i.e., upstream). Whereas ice shelf configuration to the immediate west of Mill Island varies on decadal

(or longer) timescales, the immediate east (i.e., the region of ocean between Mill Island and Bowman Island) likely varies on much shorter timescales due to inter-annual variations in sea ice concentration (see Section 3.3.3).

3.3.5 Post-depositional sea salt migration

Comparing the Na^+ and SO_4^{2-} records in Figure 3.9, it is evident that the Na^+ concentration becomes progressively smoother with increasing depth/time. The smoothing process is clearly visible in the Na^+ record prior to 2000. For the pre-2000 years with high SO_4^{2-} concentration in winter, Na^+ shows a broad high concentration throughout each year, e.g., 1998 – 2000 (Figure 3.9). The mean concentration of Na^+ in regime A (post 2000, 451.24 $\mu Eq/L$) becomes close to that in regime B (1934 – 2000, 254.06 $\mu Eq/L$), if the anomalously high concentration years, 2006 and 2007, are excluded (the Na^+ mean concentration of 2001 – 2005 and 2008 – 2009: 277.86 $\mu Eq/L$). This is evidence of progressive Na^+ smoothing. With this in mind, it is useful to reconsider the three regime structure of the ice core into a two-pattern structure:

> Pattern α: High sea salt deposition during winter. The Na^+ record becomes progressively smoothed after deposition (e.g., 1979 – 1985 and 1988 – 1991). The SO_4^{2-} record does not become smoothed. Mean Na^+ concentration is 328.83 $\mu Eq/L$.
>
> Pattern β: Low sea salt deposition, no, or less, diffusion (e.g., 1986 – 1987

and Regime C [1913 – 1933]). Mean Na^+ concentration is 50.41 $\mu Eq/L$

A question here is why SO_4^{2-} does not show the smoothing evident in the Na^+ record. Both species most likely originated from sea salt, as suggested by concurrent timing of the Na^+ and SO_4^{2-} peaks in Figure 2.21. Thus it is reasonable to expect to see similar patterns in both records.

Ionic species migration within ice cores has been reported in many ice core studies. Species observed to migrate include MSA (Mulvaney et al., 1992; Wolff, 1996; Pasteur and Mulvaney, 2000; Curran et al., 2002) and Mg^{2+} (Wolff, 1996; Kreutz et al., 1998). According to Wolff (1996), sea salt cations such as Na^+ and Mg^{2+} are considered highly conservative species making reaction impossible, and diffusion very slow. No post-depositional Na^+ migration has been reported in the literature so far, however Mg^{2+} migration has been observed from the relatively high sea salt concentration sites at Dolleman Island, Antarctic Peninsula (70°35' S, 60°56' W, $Na^+ = \sim 12.6 \mu Eq/L$, Mulvaney et al. (1992)) and Siple Dome, West Antarctica (81°39' S, 148°48' W, $Na^+ = \sim 7.1 \mu Eq/L$, Kreutz et al. (1998)).

Wolff (1996) reported Mg^{2+} migration relative to Na^+ at Dolleman Island. The Na^+ and Mg^{2+} records were synchronised near the surface, because they were deposited at the same time as the sea salt. At greater depths, however, Mg^{2+} diffused and formed new peaks on the shoulders of the original Na^+ peak. The Mill Island Mg^{2+} record also exhibits this phenomenon. Figure 3.12

shows Mg^{2+}, Na^{+} and MSA concentration for 2005 – 2009 (depth: ∼13 m to surface), and 1925 – 1929 (depth: ∼110 to 105 m). Near the surface (Figure 3.12a), Na^{+} and Mg^{2+} are very highly correlated, as expected, because they are both sea salt species. From ∼2001 (a depth of ∼20 m, not shown), the Mg^{2+} peaks start smoothing and migrating to form new peaks in regions of lower Na^{+} concentration. Figure 3.12b clearly demonstrates that Mg^{2+} forms a peak on either side of the coincident Na^{+} peak.

The mechanism proposed by Wolff (1996) to explain Mg^{2+} migration is briefly summarised here, along with potential applications to Na^{+} and Cl^{-} in the Mill Island ice core. Wolff (1996) proposed that there is limited space for cations, either within each snow grain/ice crystal, or at the grain boundaries. Initially, sea salts are likely to deposit as a particle, then slowly dissolve in the ice with time. When the sea salts dissolve, Cl^{-} is incorporated into the lattice up to its solubility limit, but Na^{+} and Mg^{2+} stay at the grain boundaries. The grain boundary surface area decreases as grain size grows with depth. This limits space for cations. Preferentially, Na^{+} may stay locked with an anion, i.e., Cl^{-} (Livingston and George, 2002). As Na^{+} occupies the space in the grain boundary, Mg^{2+} moves to other available spaces with lower Na^{+} concentration and this forms new peaks either side of the Na^{+} peak. At Mill Island, sea salt concentration is extremely high (Na^{+} = 328.83 $\mu Eq/L$, Cl^{-} = ∼364.38$\mu Eq/L$ for pattern α), such that Cl^{-} concentration exceeds the

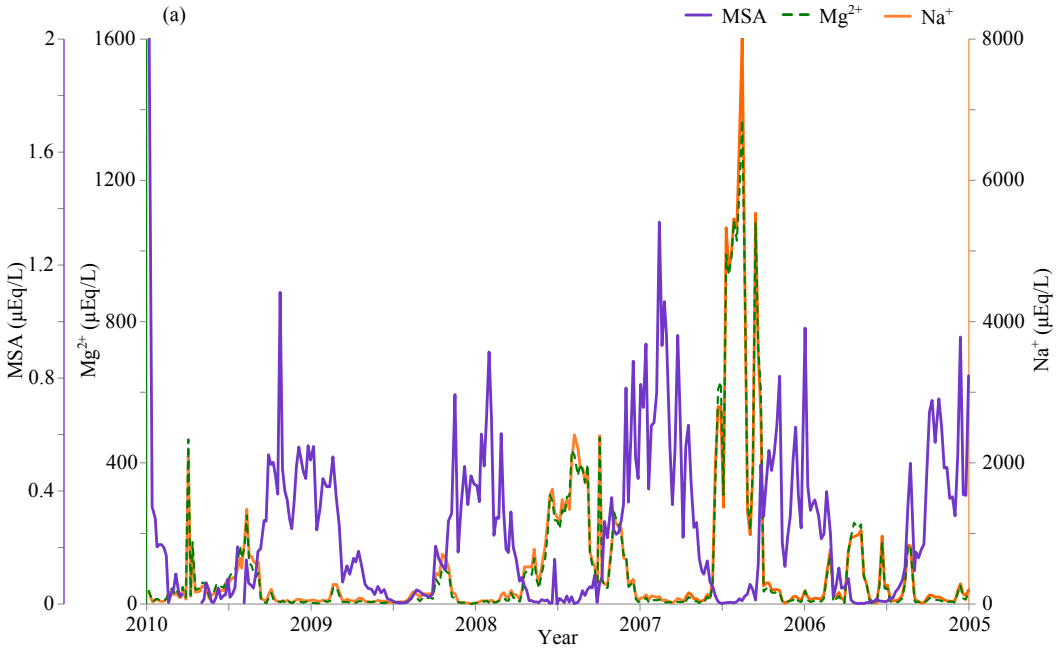

(a) Concentration of Na^+, Mg^{2+} and MSA between 2005 and 2009

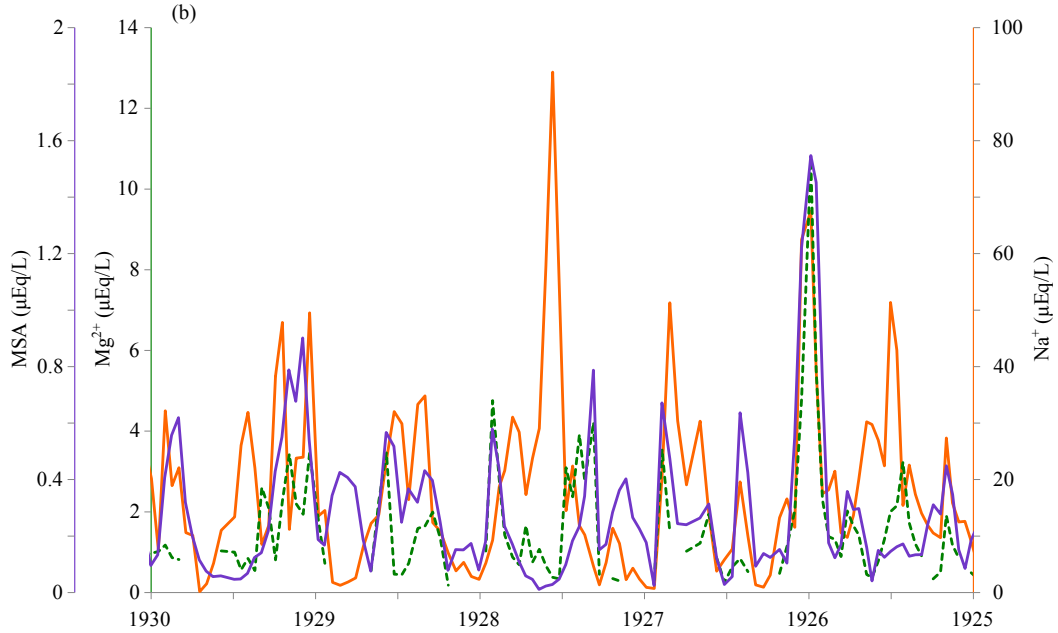

(b) Concentration of Na^+, Mg^{2+} and MSA between 1925 and 1929

Figure 3.12: Concentrations of Na^+ (red solid line), Mg^{2+} (green dashed line) and MSA (purple solid line) for (a) 2005 – 2010, (b) 1925 – 1930. No data smoothing was performed.

solubility limit. The Cl^- solubility limit was found to be 100 – 200 $\mu Eq/L$ in laboratory-grown ice, but could be up to 300 – 400 $\mu Eq/L$ in natural ice because laboratory grown ice does not experience the recrystallization process which occurs in natural polar ice sheets, and so has only one lattice-building opportunity for impurities to be incorporated. (Moore et al., 1994; Wolff, 1996). Cl^- exceeding the solubility limit is segregated and becomes mobile. This mechanism can well explain the observed Cl^- signal in the "plateau" area (see Figure 2.11 b, 1934 – 2000) which was categorised as regime B in Section 3.3.1. The mean Cl^- concentration in regime B is 283 $\mu Eq/L$, and in the "plateau" region is 364 $\mu Eq/L$, which is within the apparent solubility limit of Cl^-. The higher the bulk concentrations, the greater the proportion of grain boundaries, which are coated with impurities. The impurities will increase the connectivity between grain boundaries displaying liquid-like properties due to impurity coating (Barnes and Wolff, 2004). Cl^- exceeding the solubility limit may coat grain boundaries as Na^+Cl^- (Barnes and Wolff, 2004). This can explain the high correlation of Na^+ with the Cl^- in pattern α. In 1925 – 1930, the Mill Island core Cl^- concentration does not reach the solubility limit. Thus no Cl^- migration occurs, so Na^+ remains in place. But there is still sufficient sea salt concentration to enable migration of Mg^{2+}. Na^+ and Cl^- migration have never been reported in any other ice core record.

MSA post depositional migration has been reported at several sites (Mulvaney et al., 1992; Kreutz et al., 1998; Pasteur and Mulvaney, 2000; Curran et al., 2002). MSA is deposited during summer, because it is produced as a consequence of marine organic activity (Curran et al., 2002). In near-surface snow, MSA peaks generally occur in summer (Curran et al., 1998). MSA then migrates towards winter layers and reforms a peak in the winter layer with increasing depth (Pasteur and Mulvaney, 2000; Curran et al., 2002). The migration mechanism has been investigated, but is not yet fully understood. Pasteur and Mulvaney (2000) suggested that the migration of MSA may be related to impurity concentrations in the firn and the accumulation rate at the site.

Pasteur and Mulvaney (2000) also suggested a mechanism involving initial diffusion in the vapor or liquid phase, then entrapment by sea salt cations to form soluble MSA salts in the winter layer. MSA migration observed in the Mill Island record may support this hypothesis: MSA in the Mill Island core shows a clear summer peak at the surface but an unpredictable peak with increasing depth (see Figure 2.11 c). MSA does not show a winter peak with depth because this is probably a loss of the winter peak in sea salt cations due to Na^+ and Cl^- migration as a consequence of sea salt concentration exceeding the solubility limit. This indicates that MSA migration is probably related to impurity concentrations. In Figure 3.12, Mg^{2+} correlates with

MSA significantly between the years 1925 and 1929 (correlation coefficient of $r = 0.73$, $p < 0.01$, $n = 116$), but not as much between 2005 and 2009 ($r = -0.27$, $p < 0.01$, $n = 303$). This indicates the presence of magnesium methanesulphonate ($(CH_3SO_3)_2Mg\cdot 12H_2O$) at this depth. This provides evidence of trapping of MSA by sea salt cations to form soluble MSA salts in the winter layer. Mg^{2+} does not show a winter peak during this period due to the high Na^+ concentration as explained above, indicating that MSA was trapped by Mg^{2+} here and formed new peaks. Magnesium methanesulphonate salt was observed in the Dome Fuji ice core in Last Glacial Maximum (LGM) ice (Sakurai et al., 2010). This study reported temperatures of -5.0 ± 0.5 ℃ for the eutectic point of $(CH_3SO_3)_2Mg\cdot 12H_2O$, which is warmer than in Mill Island ice, ~ -14 ℃ (Roberts et al., 2013). Thus the existence of $(CH_3SO_3)_2Mg\cdot 12H_2O$ may be possible. However, Mg^{2+} and MSA is highly correlated only during this short period.

To summarise, in pattern α, the extremely high sea salt concentration exceeds the Cl^- solubility limit, leading to post depositional migration of Na^+ and Cl^-. Na^+ follows Cl^- migration and occupies limited space at grain boundaries, leading to Mg^{2+} migration. In pattern β, sea salt concentration is within the Cl^- solubility limit, so there is no obvious Cl^- or Na^+ migration. Yet, the concentration is still high enough to enable migration of Mg^{2+} as indicated by new peaks associated with Na^+ peaks. In addition, at some

depth Mg^{2+} may form $(CH_3SO_3)_2Mg\cdot 12H_2O$ with MSA.

The abrupt change observed in the sea salt concentration record in 1934 may indicate significant changes in the ice-scape of the Mill Island area. Given the magnitude of the observed regime shift, this ice-scape shift is likely the result of changes to the configuration of the eastern part of the Shackleton Ice shelf. Although there is no reported historical information about the east side of Shackleton Ice Shelf (see Section 3.3.4), a large calving event or disintegration may have happened on the east side of Shackleton Ice shelf in the mid-1930s.

In the cases of Dolleman Island (Wolff, 1996) and Siple Dome (Kreutz et al., 1998), Mg^{2+} appears to migrate to the shoulders of Na^+ peaks (i.e., migration occurs within an annual cycle). Therefore it is expected that Mg^{2+} migration will not affect interpretations based on more than annual resolution data (Kreutz et al., 1998). At Mill Island, however, Na^+ (and Cl^-) likely migrate across annual markers, and therefore eliminate seasonality. Hence, it will require special attention to interpret trace ion records in the Mill Island ice core.

On the other hand, the Mill Island ice core offers an ideal natural laboratory for studying the behaviour of impurities in firn and ice. Further studies are needed with continued snow sample collections and in laboratory experiments to fully understand the interactions of chemical species and ice as suggested

by Kreutz et al. (1998), Pasteur and Mulvaney (2000), and this study.

3.3.6 Fog and rime formation

It appears that understanding the mechanism behind the observed high sea salt concentration is the key to further interpretation of the Mill Island record. Wind speed does not strongly relate to the sea salt record here (as shown in Section 3.3.2). Furthermore, proximity to the coast and frost flower particle transport and deposition provide insufficient explanation for the observed extremely high levels of sea salt (Section 2.3.5).

Another factor contributing to the observed high sea salt levels may be rime accretion associated with fog events. During the Mill Island drilling in the 2009/10 field season, the expedition team observed many fog events at the summit of Mill Island (M. Curran, personal communication, 2014). When supercooled fog droplets deposit onto a surface, it forms rime, a form of deposited ice. Rime deposits generally have greater concentrations of all trace elements than fresh snow samples (Ferrier et al., 1995). Figure 3.13 shows an example of accumulated rime. This photo was taken on 23^{rd} October, 2011, at Roosevelt Island (79°25' S, 162°00' W), within the Ross Ice Shelf. Roosevelt Island is the ice core drilling site of the Roosevelt Island Climate Evolution (RICE) project, which is an international collaboration project led by New Zealand. Roosevelt Island has a similar geographical setting to Mill Island,

i.e., the distance from coast is ∼20 km and the altitude of the summit is ∼560 m. The field team found ∼0.5 m of rime ice on the Automatic Weather Station (AWS) when they returned to the site after an interval of one year (Figure 3.13). The team experienced frequent fog, and growth of rime ice associated with the fog. The team also collected and analysed surface snow precipitation samples from the site. They found complex chemical signals such as multiple peaks of most measured trace elements within a single annual layer (A. Tuohy, personal communication, 2015).

Figure 3.13: A photo of an Automatic Weather Station covered by thick rime ice at Roosevelt Island (79°25' S, 162°00' W), 23^{rd} October, 2011. Photo provided by N. Bertler.

With this in mind, the hypothetical snow ramp scenario proposed earlier, which explains the extremely high observed sea salt concentration, is developed further here:

1. New sea ice forms between Mill Island and Bowman Island.
2. Frost flowers grow on the new sea ice, upwards migration of sea salt enriched brine through sea ice produces salty snow on the sea ice, and are advected west in the prevailing easterly wind.
3. Easterly winds also create a coastal polynya in the lee of Bowman Island, allowing formation of new sea ice on the open water.
4. The easterly wind advects the frost flowers, salty snow, and sea ice towards Mill Island.
5. The process of formation and advection repeats.
6. Meanwhile, immediately east of Mill Island, sea ice accumulates and forms stable land-fast ice.
7. Precipitation and drifting snow create a snow ramp which bridges the vertical discontinuity between the land-fast ice and ice-cap at the edge of Mill Island.
8. Frost flower particles and sublimed salty snow can easily be transported to the summit of Mill Island via the snow ramp.

9. At the Mill Island summit, many fog events lead to rime accretion.

Given the lack of in-situ chemical and physical observations at the eastern base of Mill Island, it is difficult to prove this hypothesis. For further study, a high resolution snow pit study and contemporaneous in-situ weather observation data (i.e., AWS data including a relative humidity sensor, and shortwave and longwave radiometers) will be crucial to verify this hypothesis.

3.4 Conclusion

Trace ions of sea salt species (particularly Na^+, SO_4^{2-}, and Mg^{2+}) were investigated in this chapter. Also, in order to investigate the high sea salt concentration with three regimes found in Chapter 2, wind direction/speed, sea ice concentration, and historical changes of ice-scape were studied.

It was found that the dominant wind direction is from the east, but wind speed was unlikely to influence the Na^+ and SO_4^{2-} records at Mill Island. Instead, the Na^+ and SO_4^{2-} records were found to correlate well with sea ice concentration between Mill Island and Bowman Island. Based on current knowledge, no remarkable historical ice configuration changes have been noted that might affect the Mill Island ice core record. However the abrupt change in the sea salt record in 1934 may indicate a significant, unknown ice configuration change east of Mill Island.

Na^+, Cl^-, Mg^{2+}, and MSA migration were observed prior to ∼2001. The likely mechanism, migration due to extremely high sea salt concentrations, has been elucidated in this chapter. Also, the evidence of magnesium methanesulphonate existence observed between 1925 and 1930 may indicate the MSA migration mechanism. Yet, further studies are required to prove and fully understand these mechanisms.

Two patterns were found in the Mill Island sea salt record instead of three regimes: Pattern α) extremely high sea salt concentration (mean $Na^+ = \sim 328\ \mu Eq/L$) with post depositional movement in chloride, Na^+, Mg^{2+}, and MSA; and pattern β) lower sea salt concentration than pattern α, yet still relatively high (mean $Na^+ = \sim 50\ \mu Eq/L$). Mg^{2+} and MSA migration were observed here but not Cl^- or Na^+ migration.

A hypothetical mechanism for high sea salt concentration deposition was proposed, including sea ice concentration, snow ramp formation, and rime (associated with fog) deposition. Further studies, including installation of AWS at Mill Island and a high resolution snow pit study are required to prove this hypothesis and to reveal the post-depositional sea salt movement mechanism.

It appears that the Mill Island trace ion record is difficult to interpret due to its high sea salt concentration, ambiguous seasonality and post-depositional migration. However these feature changes observed in trace ion records do not

affect water stable isotopes. Interpretation of the water stable isotope record is presented in Chapter 4

Chapter 4

Mill Island snow accumulation and δ^{18}O record: regional comparisons and δ^{18}O as temperature proxy

4.1 Introduction

This chapter performs a regional comparison of δ^{18}O and snow accumulation rate with nearby existing temperature and precipitation records, respectively, from ice cores, observational stations, and atmospheric models, in order to seek the optimal method for temperature reconstruction using the Mill Island ice core record. With its high snow accumulation (1,312 kg/m^{2}yr, Roberts et al., 2013), the Mill Island δ^{18}O record has the potential to act as a temperature proxy at a sub-annual resolution.

The oxygen isotope ratio, δ^{18}O, in ice cores is typically empirically related to temperature at the site by a linear relationship, given by the equation

$$\delta^{18}O = \alpha T + \beta \tag{4.1}$$

where T is the site temperature and the parameters $\alpha = \mathrm{d}\delta\ /\mathrm{dT}$ and β are the calibration constants for the isotope thermometer (see Section 1.4.2 for

further information). Typically, decadal (or longer) time-scales are required for a good signal-to-noise ratio in the isotopic signal (van Ommen and Morgan, 1997).

The lack of a long term validation temperature record at Mill Island combined with suspected small changes in the surface air temperature (Roberts et al., 2013) makes it difficult to calibrate the δ^{18}O palaeothermometer at Mill Island. Previous sub-annual/seasonal variability ice core studies have assumed that the snowfall is consistent through each year (e.g., van Ommen and Morgan, 1997; Vance et al., 2015). However this simplification is generally inaccurate: Precipitation climatologies generally suggest a higher snowfall rate in winter (e.g., Ligtenberg et al., 2012). Differences in precipitation timing are likely to influence sub-annual ice core record interpretation, including δ^{18}O (Charles et al., 1995; van Ommen and Morgan, 1997; Krinner and Werner, 2003; Persson et al., 2011). Snowfall timing may thus impact a sub-annual δ^{18}O temperature reconstruction.

In order to compute a sub-annual temperature proxy from δ^{18}O, it is required to assess the most representative precipitation and temperature datasets for Mill Island, since there are no long term observational climate data available at Mill Island. Firstly, the annual snow accumulation were compared with several atmospheric model precipitation data close to Mill Island in order to assess which model output is the most representative of Mill

Island. Together with the most representative model output, precipitation and snow accumulation records from other nearby sites e.g., Mirny Station, Casey Station, and Law Dome (LD) were compared with the Mill Island snow accumulation record to seek the most representative dataset for Mill Island.

The snow accumulation record from ice cores is a proxy for the net precipitation record (i.e., precipitation minus losses from evaporation and wind transport). By extension, the accumulation record provides a record of synoptic scale storm events, not only at the ice core site but also in the wider area (Cohen and Dean, 2013). Ice core records are also important for investigating surface mass balance changes, which have the potential to contribute to sea level rise (Monaghan et al., 2006). Snow accumulation processes involve not only precipitation, but are also complicated by factors including wind redistribution, ablation and sublimation (Cohen and Dean, 2013). Since Mill Island experiences high accumulation but relatively low wind speeds (7.6 m/s), and limited summer melt (see Section 2.3.4 for more detail), these complicated factors are expected to be minor and thus are neglected here (as with van Ommen and Morgan, 2010, at LD).

The annual δ^{18}O record was also compared with temperature and δ^{18}O records from nearby sites in order to evaluate the spatial temperature variability, and to verify that the most representative precipitation dataset is also representative of temperature. With the most representative precipitation and

temperature records, the δ^{18}O record was investigated in order to explore the use of the Mill Island δ^{18}O record as a temperature proxy.

4.2 Method

4.2.1 Datasets

Section 4.2.1 describes the datasets used for analysis in this chapter. Ice core records from two sites (Mill Island and LD), three observational atmospheric records (Casey Station, Mirny Station and an Automatic Weather Station [AWS] in the broader region), and four atmospheric model datasets were used for the analysis. These datasets were used for finding the most representative records of Mill Island precipitation and temperature, in order to produce a sub-annual climate proxy.

Mill Island ice core snow accumulation record

Mill Island δ^{18}O data are described earlier in this thesis (Chapter 2.3). This section describes Mill Island annual snow accumulation.

The Mill Island annual snow accumulation record was obtained from the thickness of annual layers after ice core dating was completed. The firn layer displays a depth-dependent density relationship. Thus, the thickness of annual layers needs to be corrected using the density profile. The thickness of annual layers is also affected by ice flow thinning. Assuming that ice thinning

is only caused by vertical strain (as may be expected at the summit of a dome such as Mill Island), the effect of ice flow thinning can be calculated from the vertical strain rate. According to the method and density profile in Roberts et al. (2013), the vertical strain rate was estimated by least squares fitting from the density-corrected thickness of each annual layer. The flow correction is broadly consistent with the estimated ice thickness and a uniform vertical strain rate.

Law Dome Summit South ice core record

LD is a coastal ice cap, and a well established ice core drilling site located east of Casey Station. The Dome Summit South (DSS) ice core is located to the south of the LD summit (66° 42' S, 112° 42' E, 1,395 m elevation). The DSS site is located ∼120 km from the coast, and 620 km east of Mill Island. DSS is a high accumulation site (0.7 m ice equivalent per year) with relatively low winds (mean wind speed 8.3 m/s), and is free from summer melt (mean annual temperature is − 21.8 ℃, Morgan et al. 1997). A series of ice cores was obtained from DSS and has been studied over recent decades (Morgan, 1985; Morgan et al., 1997; Curran et al., 1998; van Ommen and Morgan, 2010; Roberts et al., 2015). DSS snow accumulation data (Roberts et al., 2015) and δ^{18}O data (PAGES 2k Consortium et al., 2013) were used to compare with the Mill Island snow accumulation record.

Casey Station

Observational weather data from the permanently occupied Casey Station (66° 16' 48" S, 110° 31' 12" E, 42 m elevation) are used for comparison with Mill Island data. Casey Station is located ∼500 km east of Mill Island (see Figure 1.1). The weather at Casey Station is strongly influenced by LD. Unlike other coastal stations which are strongly influenced by katabatic wind, Casey generally experiences light wind, weak katabatic flow and little precipitation. Precipitation events here are generally associated with the passage of synoptic-scale low pressure systems. The monthly mean temperature is below zero Celsius throughout the year, with a maximum in January and a minimum in May (Turner and Pendlebury, 2004). Monthly precipitation data are available from March 1977 to present, and monthly mean temperature data are available from 1959 to present. Observational precipitation data are less reliable due to surface drift (S. Carpentier, personal communication, 2015). However, this dataset was explored briefly to indicate the characteristics of precipitation at Casey Station. These data were provided by the Australian Bureau of Meteorology.

Mirny Station

Mirny Station (66° 33' S, 93° 01' E, 35 m elevation) is a Russian station which has been operational since February 1956. It is located ∼350 km west of Mill

Island, on the coast of Queen Mary Land (see Figure 1.1). The station experiences frequent blizzards, especially during winter, and strong katabatic winds. The average monthly temperature is below zero throughout the year with a maximum in January. Mirny displays a typical "coreless" winter temperature climatology, i.e., a broad, long winter without a well-defined minimum (Turner and Pendlebury, 2004). Observational data are available from February 1956 to June 2014, and were obtained from the Russian Antarctic Expedition website.

Automatic Weather Station - GF08

The closest AWS to Mill Island is named GF08 (68° 29' 36" S, 102° 10' 32" E, 2,123 m elevation). GF08 is located ∼350 km inland of Mill Island. Surface temperature data are available from October 1986 to September 1998, and from January 2000 to December 2007 (Roberts et al., 2013). Snow accumulation data are only valid for approximately two and a half years from Jan 2000, so these data were excluded from this analysis and only the temperature data were used.

Atmospheric reanalysis model records

Since there is no AWS installed at Mill Island and the closest observational data are 350 km away, atmospheric model output data were used to represent the Mill Island climate record. To obtain the most representative model for

Mill Island, four atmospheric reanalysis models were compared. ERA-interim is a global atmospheric reanalysis product provided by the European Centre for Medium-Range Weather Forecasts (ECMWF), with grid spacing of 1.5 degree (∼167 × 70 km at 65° S) (Dee et al., 2011). The National Centers for Environmental Prediction (NCEP) Climate Forecast System Reanalysis (CFSR) provides higher resolution data (∼ 0.313 degree × 0.312 degree [∼37 × 15 km at 65° S]) from 1979 to present (Environmental Modeling Center, 2010). The Regional Atmospheric Climate Model (RACMO) has 27 km grid spacing from 1979 to present (Lenaerts et al., 2012). The Antarctic Mesoscale Prediction System (AMPS) model has 20 km grid spacing prior to October 2008, and 15 km thereafter, but data are only available back to 2007 (Powers et al., 2012). Table 4.1 shows the grid spacing and data period for each dataset.

Model	Grid spacing	Data period
ERA-interim	1.5 degree (∼167 × 70 km at 65° S)	1979 to present
CFSR	0.313 × 0.312 degree (∼37 × 15 km at 65° S)	1979 to present
RACMO	27 km	1979 to present
AMPS	20 km	Mar 2007 to Sep 2008
AMPS	15 km	Oct 2008 to Jan 2012

Table 4.1: The atmospheric model datasets assessed in this chapter. Note that ERA-interim data were obtained only from 1983 to 2009 for trial analyses.

4.2.2 Intercomparison of snow accumulation and temperature datasets

Mill Island snow accumulation data were compared with the other precipitation and snow accumulation records described in Section 4.2.1, in order to find the most representative monthly snow record. First, all atmospheric model precipitation outputs were compared to determine most representative reanalysis model for Mill Island. Next, the most representative model output was compared with other observational precipitation or snow accumulation datasets to find whether the most representative climate data for Mill Island are from observational data or reanalysis model outputs. It is worth bearing in mind that measuring precipitation in polar areas is difficult, and some measurements are not completely reliable. In order to verify that the most representative precipitation dataset is also representative of temperature, Mill Island annual mean δ^{18}O record were also compared with the other δ^{18}O record and temperature records described in Section 4.2.1. As an aside, the two longest time series records, DSS and Mirny Station, were compared to the Mill Island record on an annual basis to investigate decadal/multi-decadal regional precipitation co-variability.

4.2.3 Monthly ice core dating techniques

This section proposes a monthly dating method using precipitation data from atmospheric reanalysis models. Three different monthly ice core dating methods are presented and compared: Linear monthly dating; precipitation-weighted monthly dating using the precipitation time series; and precipitation-weighted monthly dating using the precipitation climatology.

Linear monthly dating

Linear monthly dating requires only an annually-dated ice core with sub-annual resolution. After annual dating has been completed (see Section 2.3.2 for details), all samples for each year are divided into 12 based on the fraction of a year corresponding to the sample depth. Monthly sample values are then averaged to obtain the monthly mean δ^{18}O. For example, Figure 4.1 shows the δ^{18}O time series (dashed line) and monthly mean δ^{18}O (solid line) for 2009. The x-axis shows the fraction of the year. In the case of 2009, the end of the year lies at the snow-air interface and the beginning of the year lies at a depth of 1.46 mIE. The vertical lines partition one year equally into 12 monthly portions.

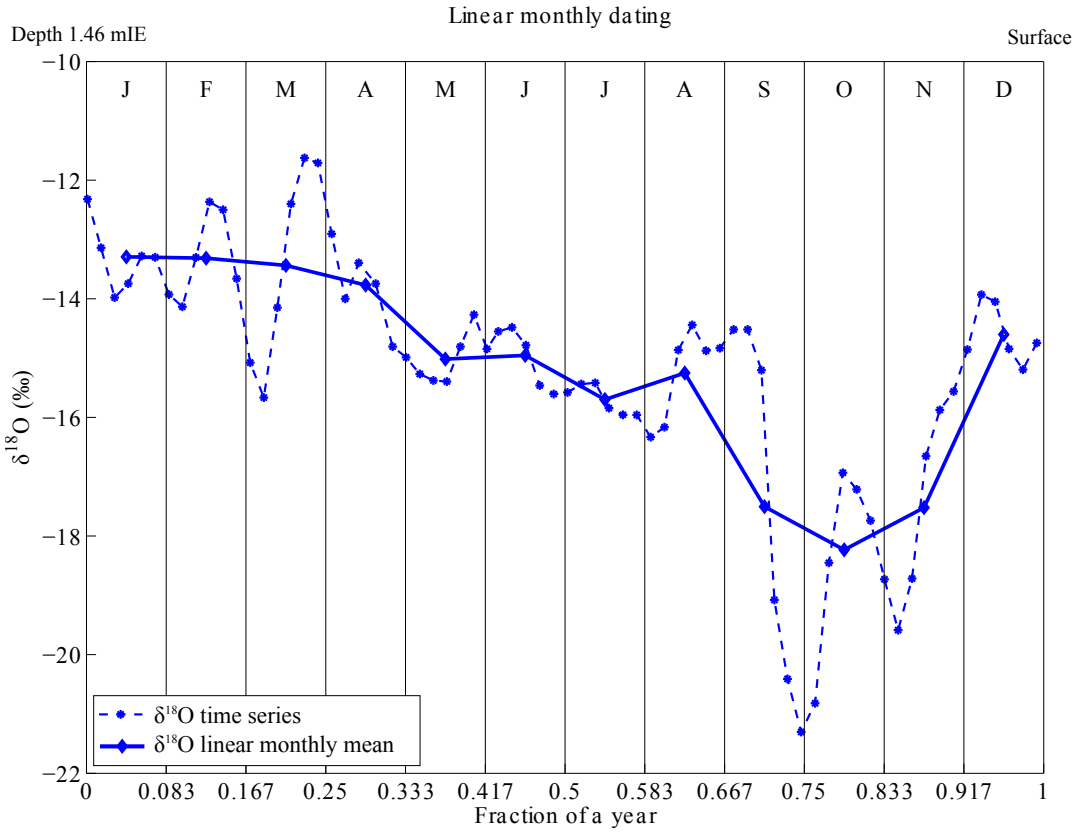

Figure 4.1: An example of the linear monthly dating process for 2009. The dashed line shows the δ^{18}O ratio time series, and the solid line shows the monthly mean δ^{18}O ratio. The vertical lines partition a year equally into 12 portions. The uncertainty of the δ^{18}O measurements is < 0.1 ‰.

Precipitation-weighted monthly dating

Precipitation-weighted monthly dating requires a time series of monthly precipitation data. The Mill Island ice core record covers the period 1913 – 2009. Thus, this method was applied to the overlap period of 1979 – 2009. Also, the climatology of the CFSR precipitation was used for applying this method to the entire ice core record.

a. Precipitation-weighted monthly dating using the CFSR precipitation time series (1979 – 2009)

Firstly, the proportion of annual precipitation occurring in each month was calculated on an annual basis. Then, the δ^{18}O time series was resampled to 12 points per year based on this proportional time series. Monthly mean δ^{18}O was calculated using data points in the same monthly bin. Figure 4.2 shows the precipitation-weighted monthly dating using the CFSR precipitation time series for 2009. The inset figure shows the corresponding monthly precipitation proportion from CFSR output. This clearly demonstrates that snowfall is not constant throughout the year. Thus the layer thickness for each month varies.

b. Precipitation-weighted monthly dating using the CFSR precipitation climatology (1979 – 2009)

First, the climatology of monthly CFSR precipitation was computed for the period of 1979 – 2009. Then the precipitation proportion was derived based

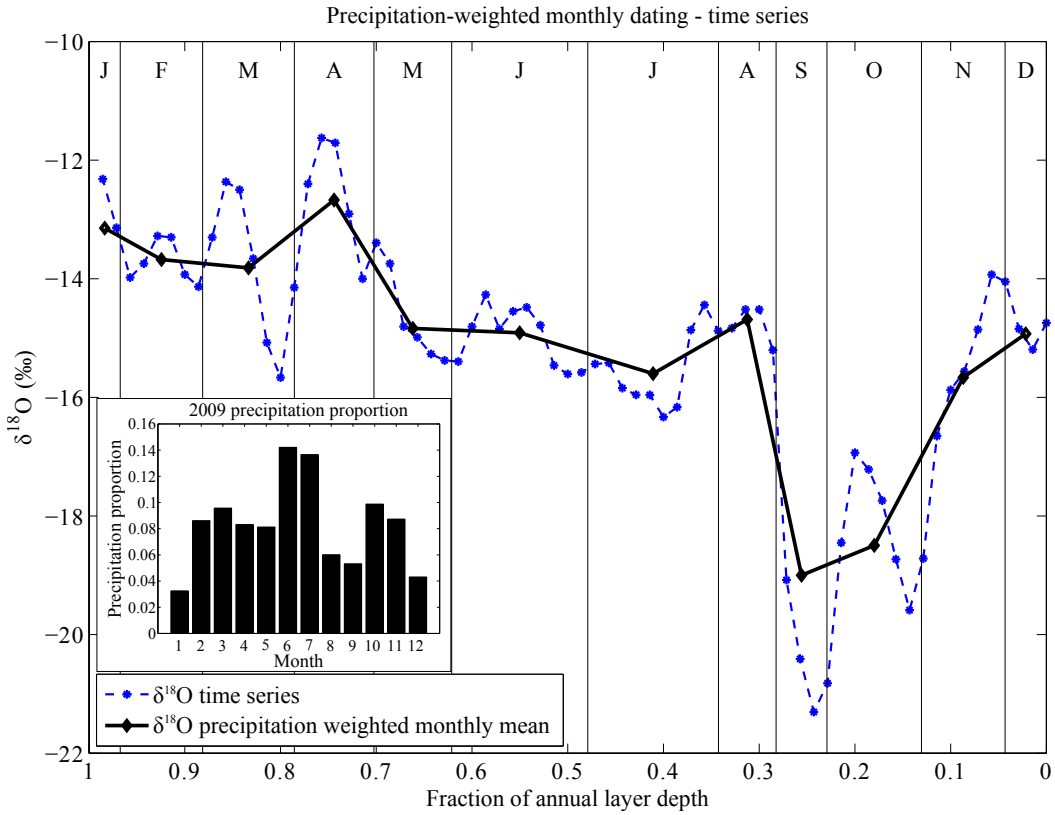

Figure 4.2: An example showing the precipitation-weighted monthly dating method using the CFSR precipitation time series for 2009. The dashed line shows the δ^{18}O ratio time series, and the solid line shows the monthly mean δ^{18}O ratio. The vertical lines partition the year according to the proportion of precipitation in each month. Inset: Monthly precipitation proportion from CFSR output in 2009.

on the precipitation climatology. The climatology represents a more realistic simplification than assuming constant precipitation, and thus may be suitable for use prior to the start of the CFSR time series in 1979. Finally, the proportion climatology was applied to the entire δ^{18}O record. Figure 4.3 shows the

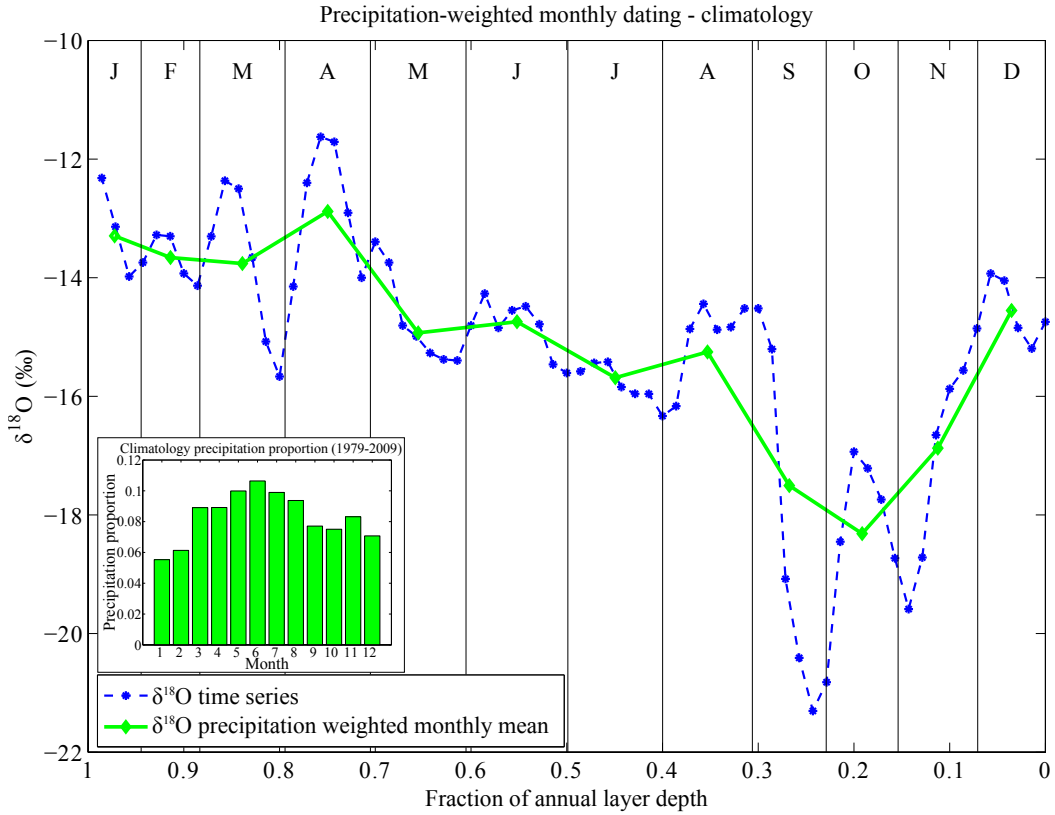

Figure 4.3: An example showing the precipitation-weighted monthly dating method using the CFSR precipitation climatology for 2009. The dashed line shows the δ^{18}O ratio time series, and the solid line shows the monthly mean δ^{18}O ratio. The vertical lines partition the year according to the climatological precipitation proportion over the period 1979 – 2009. Inset: CFSR climatological monthly precipitation proportion.

climatology precipitation-weighted monthly dating for 2009. The inset figure shows the climatology of monthly CFSR precipitation. The precipitation cli-

matology shows lower monthly variability than most years in the precipitation time series (Figure 4.2). However it still shows non-consistent precipitation. Though only based on a precipitation climatology, this method likely provides better sub-annual timing than the linear precipitation assumption method.

4.3 Results and discussion

4.3.1 Snow accumulation rate

Figure 4.4 shows density- and strain- corrected Mill Island annual snow accumulation (dashed blue line), along with a Gaussian-smoothed ($\sigma = 1.5$ points) version (solid blue line). A Gaussian filter of width $\sigma = 1.5$ years gives a half-power filter response for a period of approximately five years. The annual mean accumulation does not show a statistically significant trend. However the Mudelsee (2009) break function regression demonstrates a gradual decreasing trend between 1913 to 1999 (slope $= -0.001$ mIE/yr), followed by an increasing trend (slope $= +0.023$ mIE/yr) after 1999 (dash-dotted magenta line). The mean snow accumulation rate of 1.34 mIE/yr between 1913 and 1999 increases to 1.43 mIE/yr between 2000 and 2009. Visual inspection suggests this breakpoint in 1999 is no more significant than other sifts within the time series (e.g., those at 1930 and 1965). However as discussed previously (Section 3.3.1), there is a change in regime in the trace chemistry records around 1999, therefore it cannot be ruled out that this shift is real and therefore related to

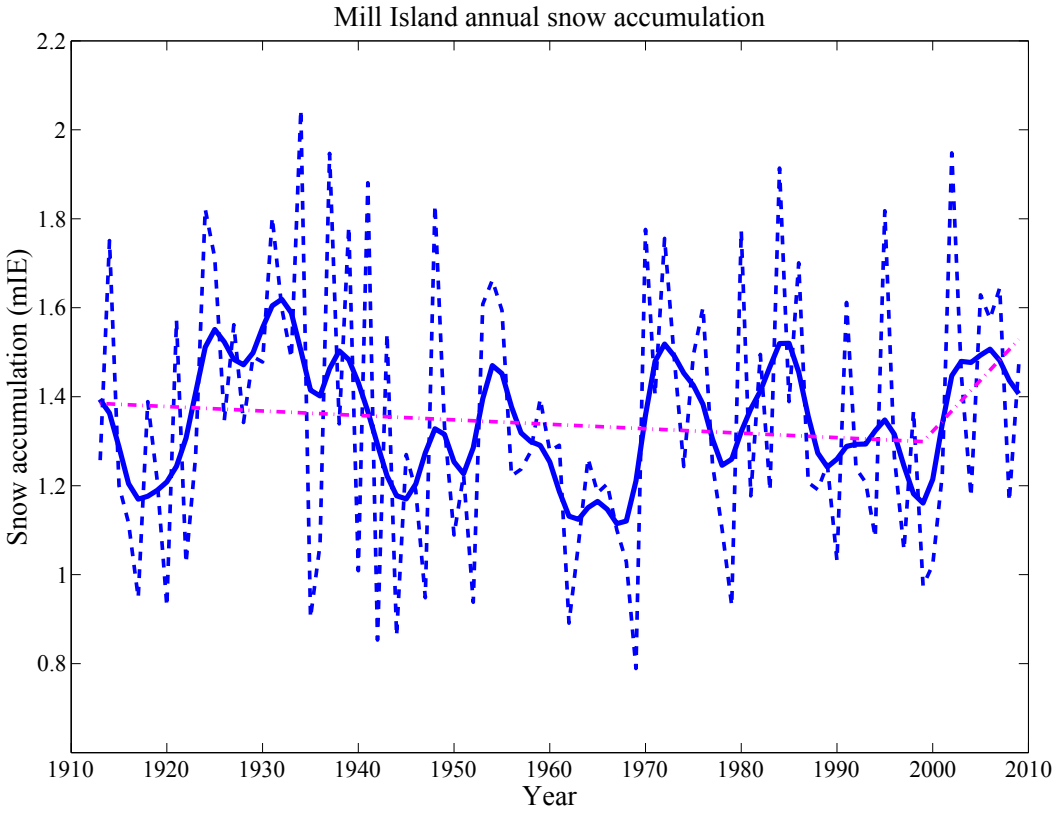

Figure 4.4: Mill Island density and strain-corrected annual snow accumulation (dashed line) and Gaussian smoothed ($\sigma = 1.5$ year) accumulation (solid line). The dash-dotted line shows the line of best fit before and after the break point (1999). The break point was calculated using the Mudelsee (2009) break function regression.

the change in regime discussed in Section 3.3.1.

The snow accumulation record demonstrates both decadal and multi-decadal variability. This is further discussed in Section 4.3.4.

The MI910 annual snow accumulation rate averages 1.35 mIE/yr for the period from 1913 to 2009, with a minimum of 0.79 mIE/yr in 1969 and a maximum of 2.04 mIE/yr in 1934. With a 4 cm sample spacing, there are, on average, 30 samples per year. This accumulation rate is sufficient to investigate sub-annual climate records for chemical species and water stable isotopes.

4.3.2 Validation of atmospheric reanalysis model precipitation output

Figure 4.5 shows a comparison between the Mill Island snow accumulation record and atmospheric model output precipitation datasets. The AMPS record is available only from March 2007. Because the 2007 AMPS data (i.e., March – December 2007) comprise only 10 months' data, the total of the 10 months record for 2007 was multiplied by a factor of 1.2, under the assumption that precipitation occurs equally in each month (as with Fraser et al., 2015, submitted). The Mill Island snow accumulation was converted to millimetres of water equivalent (mmWE/yr) for comparison with the model data.

Table 4.2 shows correlation coefficients between the annual Mill Island snow accumulation record and the precipitation record from each atmospheric

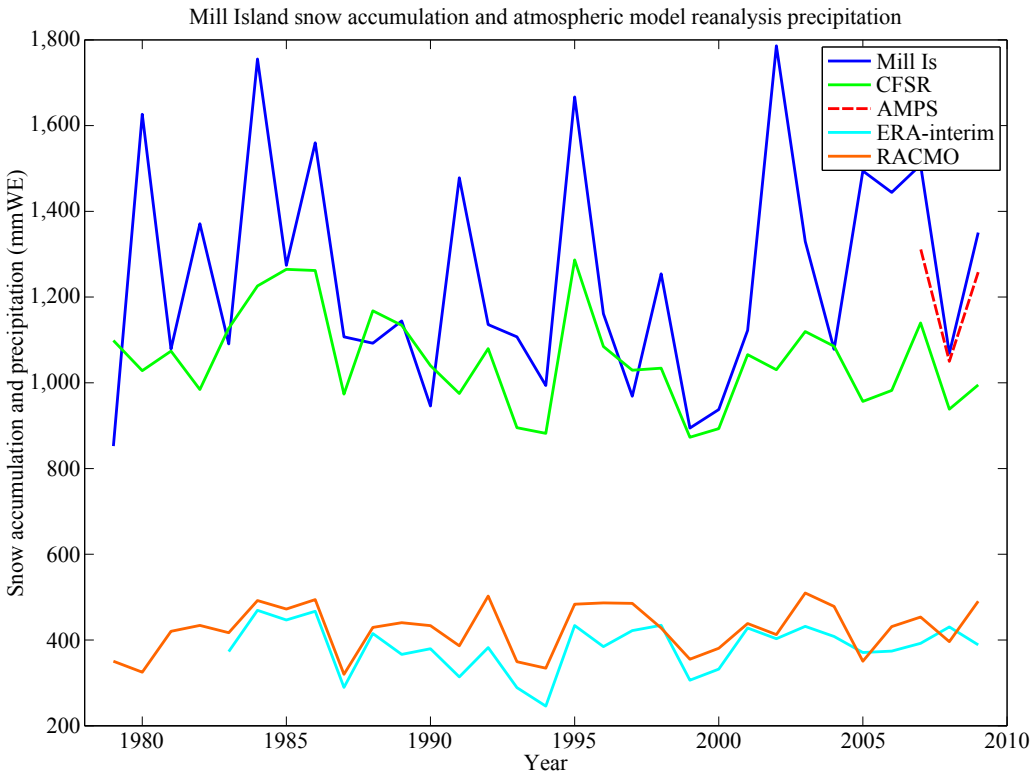

Figure 4.5: Annual snow accumulation and precipitation records from Mill Island (blue line), CFSR (green line), AMPS (red dashed line), ERA-interim (light blue line) and RACMO (orange line). Mill Island snow accumulation was converted into millimetres of water equivalent (mmWE).

Model	r	95 %confidence	p	df	% of Mill Island prcp
ERA-interim	0.43	[0.133; 0.660]	< 0.03	25	31
CFSR	0.39	[0.049; 0.647]	< 0.05	29	85
RACMO	0.24	$[-0.155; 0.574]$	> 0.05	29	34
AMPS	0.99	[N/A]	> 0.05	1	92

Table 4.2: The correlation coefficient between Mill Island snow accumulation and each atmospheric model dataset assessed in this chapter, the range of r with 95 % confidence, and the percentage of mean precipitation compared to the Mill Island mean precipitation. The p value and number of degrees of freedom used is also shown in here. The AMPS time series is too short for a meaningful significant test.

model. The correlation coefficients were calculated using the Mudelsee (2003) PearsonT3 function to focus on the range in the r value rather than the p value. The PearsonT3 function gives a range in r by repeating the correlation calculation with randomly removed data points, with compensation for autocorrelated signals. If the range does not span zero, it indicates that the correlation is significant. The highest correlation coefficient is between Mill Island and ERA-interim ($r = 0.43$ [0.133; 0.660]). However, the magnitude of the mean annual ERA-interim precipitation is a factor of 3.2 lower than the mean Mill Island snow accumulation (mean precipitation is 384 mmWE/yr and 1,247 mmWE/yr respectively), indicating somewhat poor model performance for this location (Figure 4.5). RACMO shows similar mean precipitation (425 mmWE/yr) to ERA-interim. However there is no significant correlation between the RACMO and Mill Island precipitation records ($r = 0.24$ $[-0.155$;

0.574]), although the ERA-interim and RACMO precipitation records are significantly correlated with each other (r = 0.78 [0.558; 0.901]). AMPS mean precipitation is similar to Mill Island snow accumulation, with a mean precipitation of 1,207 mmWE/yr. However the data are available only from March 2007, thus the length of the time series is insufficient to make a statistically-meaningful comparison with the Mill Island record. CFSR data show a similar mean precipitation rate (1,055 mmWE/yr) to the Mill Island record. CFSR also shows a good correlation with Mill Island accumulation (r = 0.39 [0.049; 0.647]). The CFSR time series runs from 1979 to present, which gives 31 years of overlap with the Mill Island record.

This comparison suggests that models with high spatial resolution may perform better for precipitation at Mill Island. This is likely due to high resolution models being better able to represent the local topography. Due to the similar precipitation rate, good correlation with the Mill Island record, and the 31 years of overlap, CFSR was chosen as the preferred model for further analysis in this study.

4.3.3 Comparison between Mill Island snow accumulation and precipitation records from nearby sites

Figure 4.6 shows a comparison between Mill Island annual snow accumulation (blue line), DSS snow accumulation (red line), Casey Station precipitation (or-

ange line), Mirny Station precipitation (black line), and CFSR precipitation at Mill Island (green line). Mill Island shows the highest snow accumulation of all the datasets presented. The annual mean snow accumulation at Mill Island (1,236 mmWE/yr, 1913 – 2009) is approximately twice that of DSS (631 mmWE/yr, 1248 – 2005), and it has higher inter-annual variability ($\sigma = 272$ and 113 mmWE, respectively). Mirny Station precipitation is a factor of 2.4 lower than at Mill Island (518 mmWE/yr), but it has similar variability ($\sigma = 220$ mmWE). Casey Station shows the lowest precipitation (193 mmWE/yr). A detailed comparison between Mill Island, DSS and Mirny Station precipitation records is described in Section 4.3.4. The Casey Station record is relatively short (1977 – 2009), so it is excluded from further comparisons.

It appears that Mill Island snowfall does not have a strong connection with the rest of the continent. This indicates that nearby observational data are not suitable to use for the Mill Island climate proxy calibration. The record best representing the Mill Island precipitation is the closest CFSR grid point.

4.3.4 Regional snow accumulation variability

In this section, a detailed comparison between annual snow accumulation from Mill Island and DSS and annual precipitation record from Mirny Station is presented in order to document the regional snow accumulation variability, and

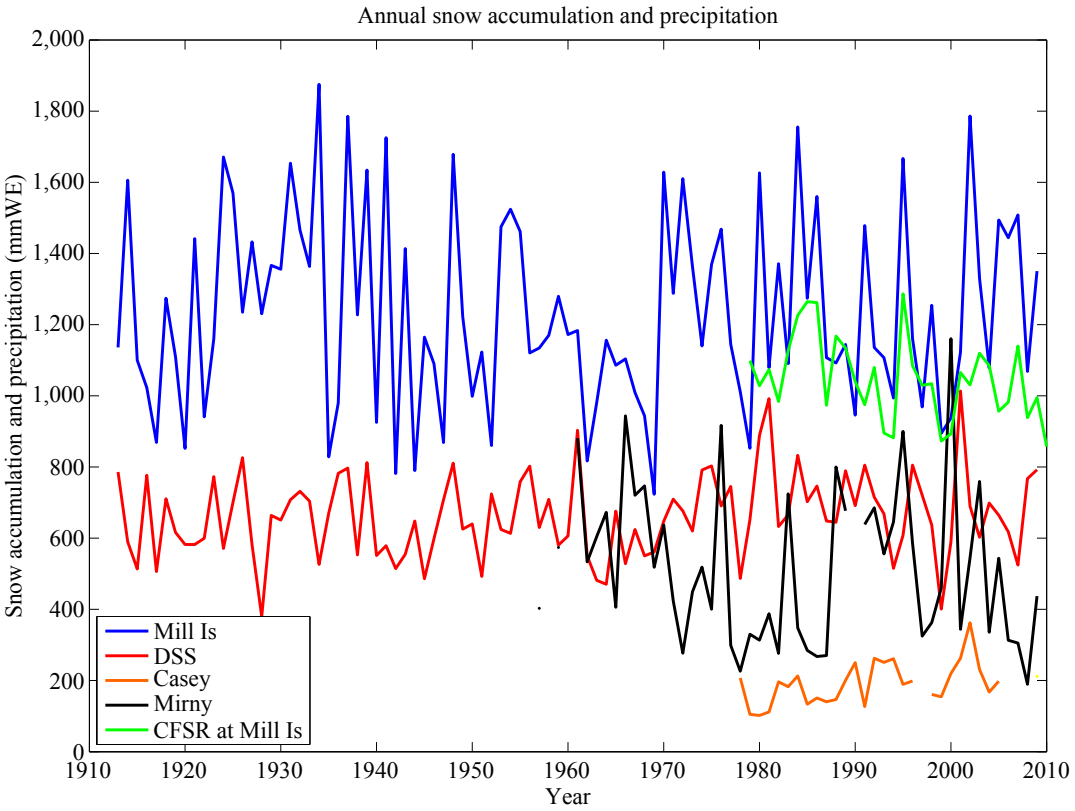

Figure 4.6: Annual snow accumulation and precipitation records from Mill Island (blue line), DSS (red line), Casey Station (orange line), Mirny Station (black line), and CFSR at Mill Island (green line). Snow accumulation was converted into millimeters of water equivalent (mmWE).

to suggest potential drivers of this variability. To investigate annual anomalies and long-term variability, annual accumulation records were filtered with high- and low-pass filters, respectively.

Comparison between Mill Island and Law Dome Summit South snow accumulation

Figure 4.7 shows high- and low-pass filtered annual snow accumulation records from Mill Island and DSS. The top panel shows high-pass filtered precipita-

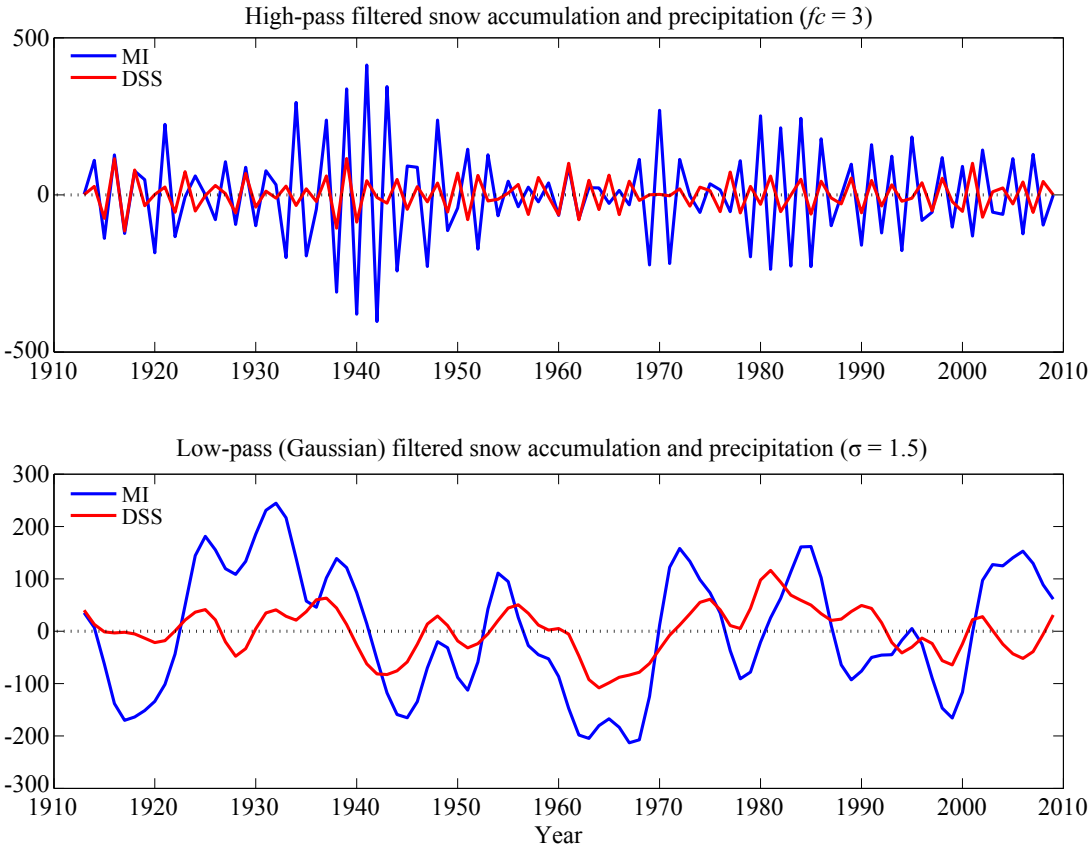

Figure 4.7: High- and low-pass filtered annual accumulation records from Mill Island (blue line) and DSS (red line). Top panel: High-pass filtered accumulation, using a cut-off frequency of $fc = 3$ years; Bottom panel: Low-pass (Gaussian) filtered accumulation ($\sigma = 1.5$ years).

tion. The detrended data were filtered with a Butterworth filter with a cut-off frequency $fc = 3$ years, and order $= 2$. The effective degrees of freedom for high-pass filtered data are often difficult to estimate. To address this, the Mudelsee (2003) estimation of a 95 % confidence internal for r was used, as described earlier. There is no significant correlation between Mill Island and DSS snow accumulation (r = 0.192 [-0.023; 0.389]). This lack of high-frequency correlation may indicate that annual anomalies are mainly driven by local-scale systems. The possibility of sastrugi noise influencing the Mill Island record can be discounted here due to significant correlation (r = 0.585 [0.285; 0.781]) between high-pass filtered snow accumulation from MI0910 and MIp0809.

The bottom panel shows low-pass filtered accumulation using a Gaussian filter with a width of $\sigma = 1.5$ years, which gives a half-power response period of approximately five years. The correlation between Mill Island low-pass filtered snow accumulation and DSS low-pass filtered snow accumulation is significant (r = 0.523 [0.521; 0.525]). This may indicate that larger-scale atmospheric circulation patterns influence both Mill Island and DSS in the same way on an inter-annual (or longer) basis.

Comparison between Mill Island snow accumulation and Mirny Station precipitation

Figure 4.8 shows high- and low-pass filtered annual snow accumulation records from Mill Island and Mirny Station. Note that there are several gaps in the

Mirny Station monthly precipitation record (in 1956, 1958, 1960, and 1990). These monthly gaps were filled by assuming that the same precipitation occurred in every month, i.e., total annual precipitation throughout that year was divided by the number of months with valid data in that year, then multiplied by 12. The high-pass filtered records (top panel) shows no significant

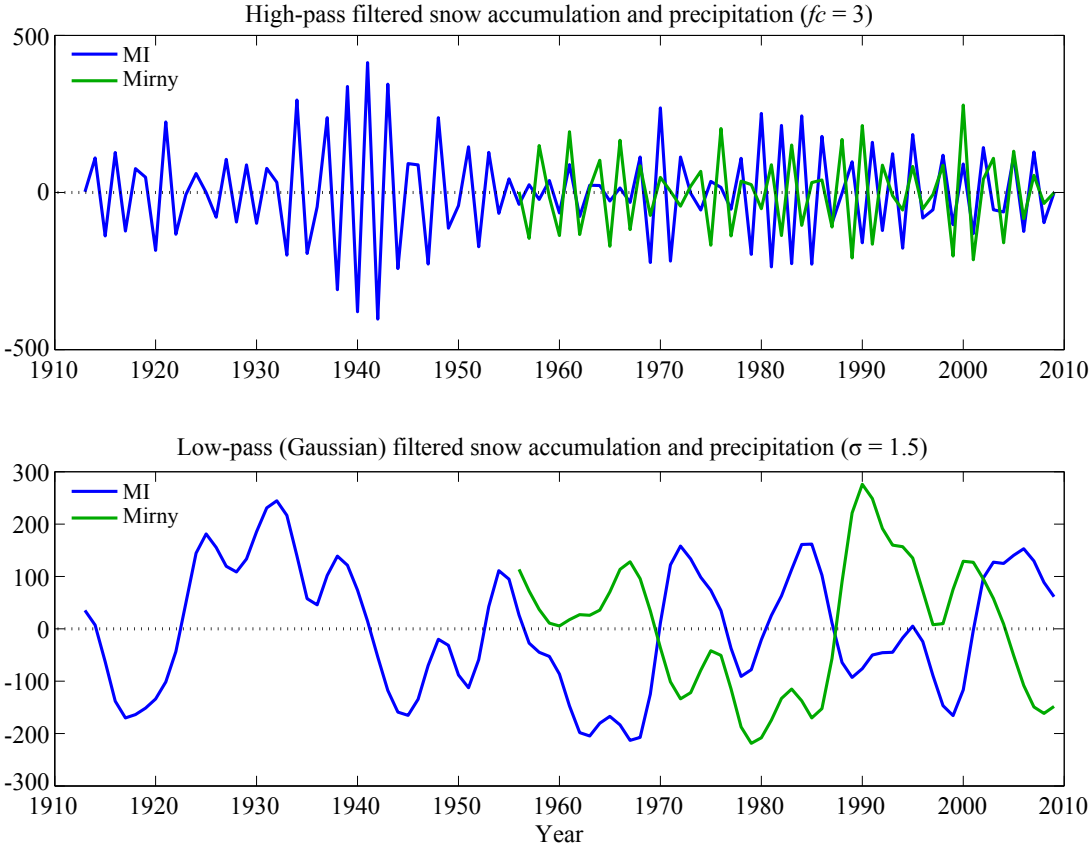

Figure 4.8: The high- and low-pass filtered annual accumulation records from Mill Island (blue line) and Mirny Station (green line). Top panel: High-pass filtered accumulation, cut-off frequency $fc = 3$ years; Bottom panel: Low-pass (Gaussian) filtered accumulation ($\sigma = 1.5$ years).

correlation (r = 0.035 [− 0.194; 0.259]). This, again, may indicate that annual anomalies at Mill Island and Mirny Station are driven by local scale events.

The low-pass filtered record shows significant anti-correlation between Mill Island snow accumulation and Mirny Station precipitation ($r = -0.491$ $[-0.519; -0.463]$). In contrast to DSS, this anti correlation likely suggests that large-scale atmospheric circulation patterns influence snowfall at Mill Island and Mirny Station oppositely on an inter-annual (or longer) time scale.

Relationship between Mill Island snow and DSS snow accumulation, and Mirny Station precipitation

The positive correlation between the low-pass filtered Mill Island and DSS records, together with the anti correlation between the low-pass filtered Mill Island and Mirny Station records (Figures 4.7 and 4.8), and the fact that the low-pass filtered DSS and Mirny Station are also negatively correlated ($r = -0.329$ $[-0.381; -0.274]$, not shown), suggests that Mirny Station is in a different regional climate regime to Mill Island and DSS. This is probably a consequence of topographically driven continental climate variations and synoptic scale influences of cyclonic systems. Mill Island is located along the eastern side of the Denman glacier, and Mirny Station is located in the western side of the Denman glacier. Figure 4.9, modified from the Parish and Bromwich (1987) study, shows the strong katabatic streamline along the eastern edge of the Denman glacier which divides Mill Island and Mirny Station. This division seems to be reflected in apparent snowfall differences. Monaghan et al. (2006) studied the annual mean precipitation co-variability between 16 ice

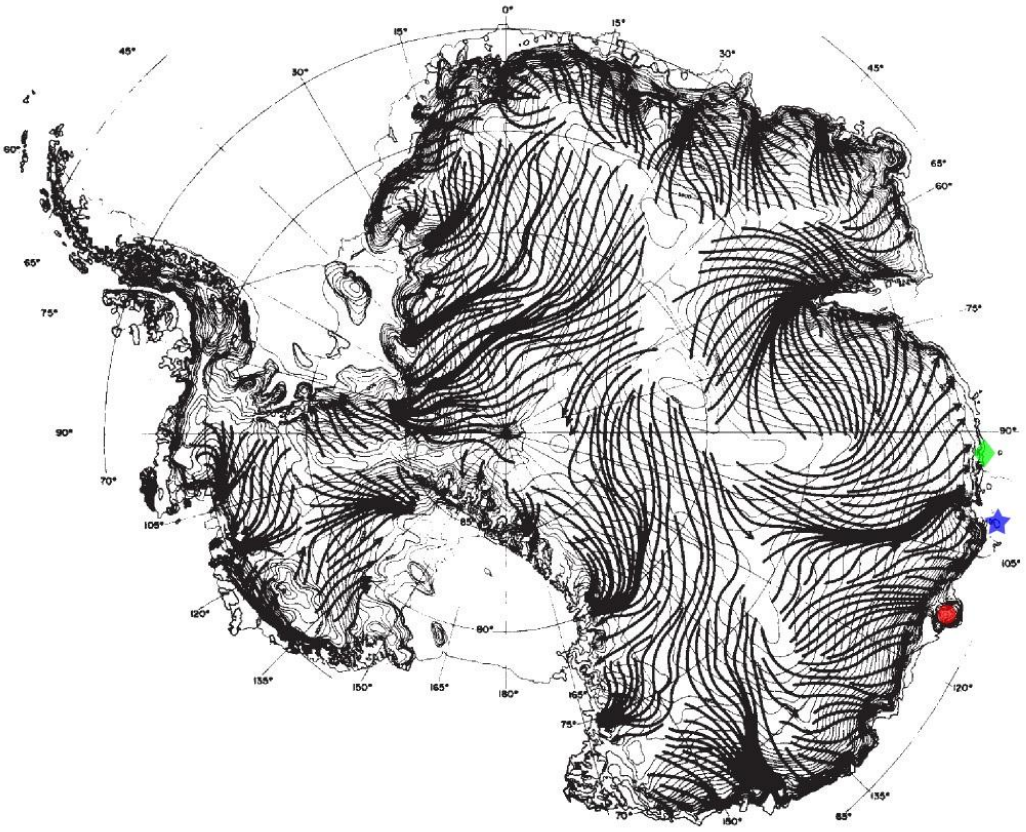

Figure 4.9: Katabatic wind streamlines overlaid with the locations of Mirny Station (green diamond), Mill Island (blue star), and Law Dome (red circle). The figure was obtained and modified from Figure 3, Parish and Bromwich (1987).

coring sites throughout Antarctica, and the rest of the continent at a 1 degree resolution using ERA-interim reanalysis data, from 1985 to 2004. Figure 4.10 is modified from the Monaghan et al. (2006) study. It presents the composite map of precipitation co-variability. It appears that the accumulation record in the vicinity of Mill Island is not necessarily representative of regions to the immediate east or west (i.e., LD or Mirny).

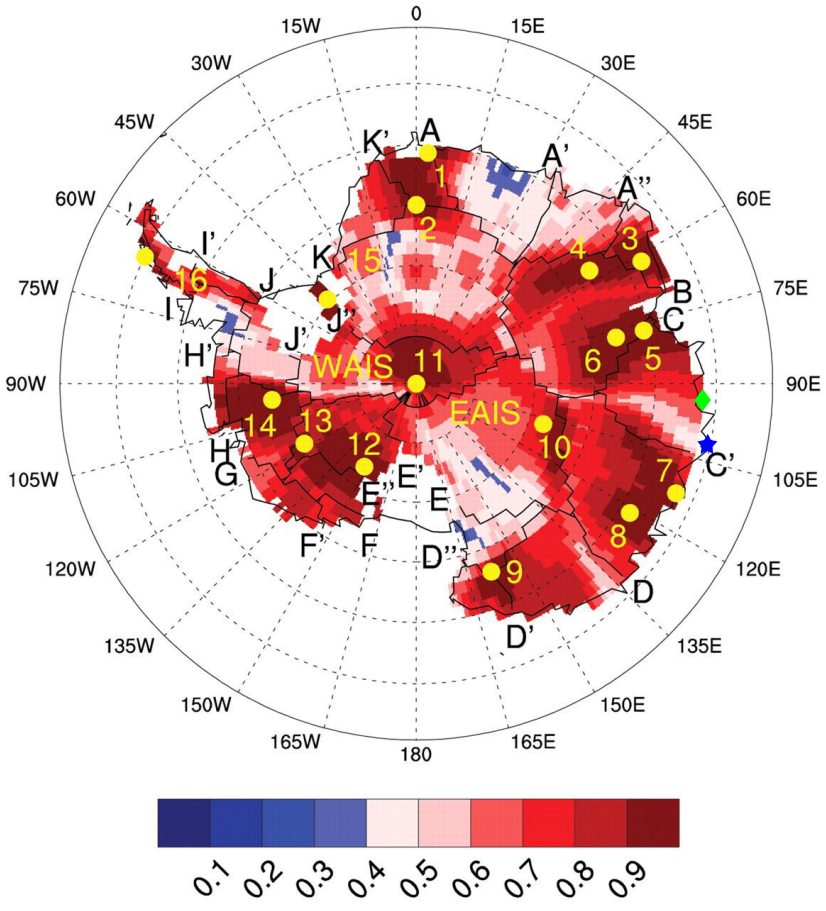

Figure 4.10: The composite map of precipitation co-variability modified from Figure 1, Monaghan et al. (2006), overlaid with the locations of Mirny Station (green diamond), Mill Island (blue star), and Law Dome (yellow circle number 7). Detailed information for this figure is given in Monaghan et al. (2006).

Large scale atmospheric modes constitute another process governing precipitation in Antarctica. The Zonal Wave Three (ZW3) pattern is a large-scale atmospheric mode characterised by quasi-stationary mid-latitude pressure centres. ZW3 is expected to play an important role governing precipitation in this region (Raphael, 2007; van Ommen and Morgan, 2010; Roberts et al., 2015). ZW3 is associated with zonally-quasi-stationary changes in meridional flow at around 50° S. ZW3 atmospheric pressure ridges occur in the longitudinal vicinity of the three continents of South America, Africa, and Australia. The presence of these continents establishes quasi-stationary high pressure centres in the upwind direction, i.e., west of each continent. The strength of these high pressure centres defines the ZW3 index strength. With a high ZW3 strength, meridional wind anomalies become stronger, in a pattern related to the pressure centre location (Figure 4.11). ZW3 contributes to monthly and interannual circulation variability and is associated with cyclonic system blocking in the Southern Hemisphere. The southern edges of the ZW3 circulation pattern extend south to reach the Antarctic continent, which influences the meridional transport of maritime air (van Loon and Jenne, 1972; Raphael, 2004, 2007).

The longitude of LD places it in a region of enhanced northerly flow in times of a strong ZW3 index. This is also true to a lesser extent for Mill Island. On the other hand, Mirny Station is located near a region where southerly flow

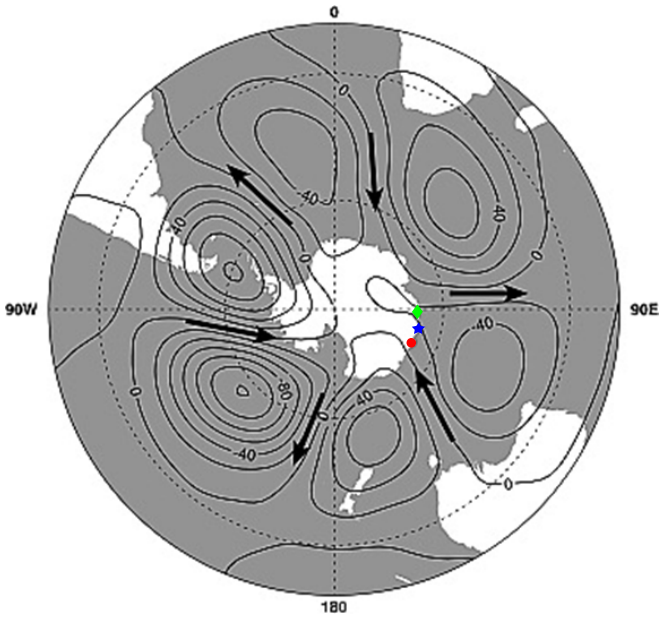

Figure 4.11: The phase of ZW3 at the 500-hPa geopotential height field with the locations of Mirny Station (green diamond), Mill Island (blue star), and Law Dome (red circle) indicated. Arrows indicate directions of anomalous airflow associated with the circulation pattern. Units are geopotential metres. The figure was obtained from Raphael (2007) and reproduced with permission from M. Raphael.

is enhanced when ZW3 is strong. Thus, ZW3 likely modulates the snowfall at each site, i.e., Mill Island and LD are in the same snowfall regime but Mirny Station is in the opposite regime. These differences in the snowfall regime may explain the positive correlation between Mill Island and DSS, and the negative correlation between Mill Island and Mirny Station precipitation records. However Mill Island is located near the edge of the ZW3 flow centres (Figure 4.11, blue star). This is confirmed by correlating the snowfall each stations with the Australian sector zonal wave three (AZ3) index (van Ommen and Morgan, 2010). The correlation coefficients between the AZ3 index and Mill Island, DSS and Mirny Station annual snow accumulation/precipitation data are $r = -0.00$ $[-0.07;\ 0.06]$, $r = 0.28$ $[0.23;\ 0.32]$, $r = -0.31$ $[-0.56;\ -0.01]$, respectively. This suggests that the ZW3 pattern likely modulates LD and Mirny Station snowfall to a similar but opposing, extent. Mill Island snowfall, however, is not strongly controlled by ZW3, probably because it lies close to the boundary between enhanced southerly and northerly ZW3 flow.

4.3.5 Intercomparison of temperature datasets

In order to assess whether CFSR temperature record is the most representative the Mill Island temperature record, the Mill Island annual mean $\delta^{18}O$ record (blue) was compared with annual mean DSS $\delta^{18}O$ (red), Casey Station temperature (yellow), Mirny Station temperature (black), CFSR temperature

at Mill Island (green), and GF08 (AWS) temperature (magenta) (Figure 4.12).

The GF08 temperature in 2007 is abnormally high, indicating that there may be some problem with the AWS data, and there are only three months' of data in 1986. Thus 1986 and 2007 were excluded from this analysis. There are no data for October to December in 1998. These missing values were filled with the climatology values.

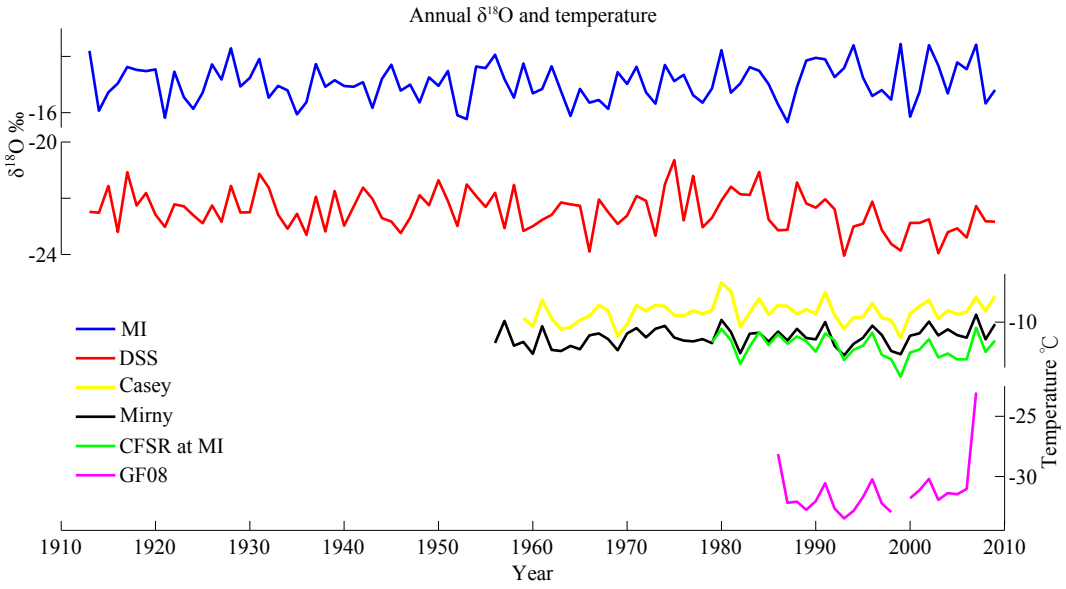

Figure 4.12: Annual mean Mill Island δ^{18}O (blue), DSS δ^{18}O (red), Casey Station temperature (yellow), Mirny Station temperature (black), CFSR temperature at Mill Island (green), GF08 (AWS) temperature (magenta).

A correlation table relating all δ^{18}O and temperature datasets is given in Table 4.3. Mill Island annual mean δ^{18}O is poorly correlated with CFSR temperature at the nearest CFSR grid point ($r \simeq 0.0$), and with other nearby temperature records (DSS, Casey Station, Mirny Station, and GF08). Con-

versely, CFSR temperature at Mill Island correlates significantly with all other nearby records except Mill Island δ^{18}O and GF08. The nearest observational temperature data to the east and west of Mill Island, i.e., Casey and Mirny Stations are significantly correlated ($r = 0.83$, $p < 0.05$). Therefore, it is reasonable to expect that the Mill Island temperature should reflect nearby observational records. Although precipitation is highly uncorrelated across the region, temperature appears to be well-correlated.

		p-value					
	Site	MI	DSS	Casey	Mirny	CFSR at MI	GF08
r	Mill Island	–	> 0.05	> 0.05	> 0.05	> 0.05	> 0.05
	DSS	0.11	–	**= 0.01**	> 0.05	**<0.01**	> 0.05
	Casey	0.05	**0.35**	–	**<0.01**	**<0.01**	**<0.01**
	Mirny	0.15	0.20	**0.83**	–	**<0.01**	**<0.01**
	CFSR at MI	− 0.00	**0.64**	**0.83**	**0.74**	–	> 0.05
	GF08	− 0.00	0.27	**0.77**	**0.82**	0.36	–

Table 4.3: The correlation coefficient (r) and significance (p value) between each pair of annual mean δ^{18}O and annual mean temperature records. Bold font indicates a significant correlation ($p < 0.05$).

The poor correlation between annual mean Mill Island δ^{18}O and annual mean CFSR temperature indicates that the raw Mill Island annual mean δ^{18}O record is not suitable for use as a temperature proxy. The next section investigates the potential use of monthly Mill Island δ^{18}O as a sub-annual temperature proxy. Since none of the temperature or δ^{18}O datasets correlate

well with Mill Island δ^{18}O, the CFSR temperature record was used for further analysis because the CFSR precipitation record was the most representative of the Mill Island climate.

4.3.6 δ^{18}O as a sub-annual temperature proxy

Since Mill Island annual mean δ^{18}O record is unsuitable as an annual mean temperature proxy (Section 4.3.5), and monthly temperature data are available from the most representative Mill Island climate record (i.e., CFSR), the use of δ^{18}O as a sub-annual temperature proxy is investigated in this section. A study of the δ^{18}O temperature construction at a monthly resolution also has the potential to reveal any temperature biases arising from non-constant precipitation through each year.

Comparison of dating techniques

Figure 4.13 shows (a) the monthly mean CFSR temperature, (b) the monthly mean δ^{18}O record computed using the linear precipitation assumption, (c) the monthly mean δ^{18}O calculated using the precipitation time series to weight the δ^{18}O dating, and (d) the monthly mean δ^{18}O calculated using the precipitation climatology to weight the δ^{18}O dating. Under the linear precipitation assumption (Figure 4.13 b, blue solid line), the correlation coefficient (r) between monthly δ^{18}O and the CFSR temperature record is 0.49 [0.418; 0.553].

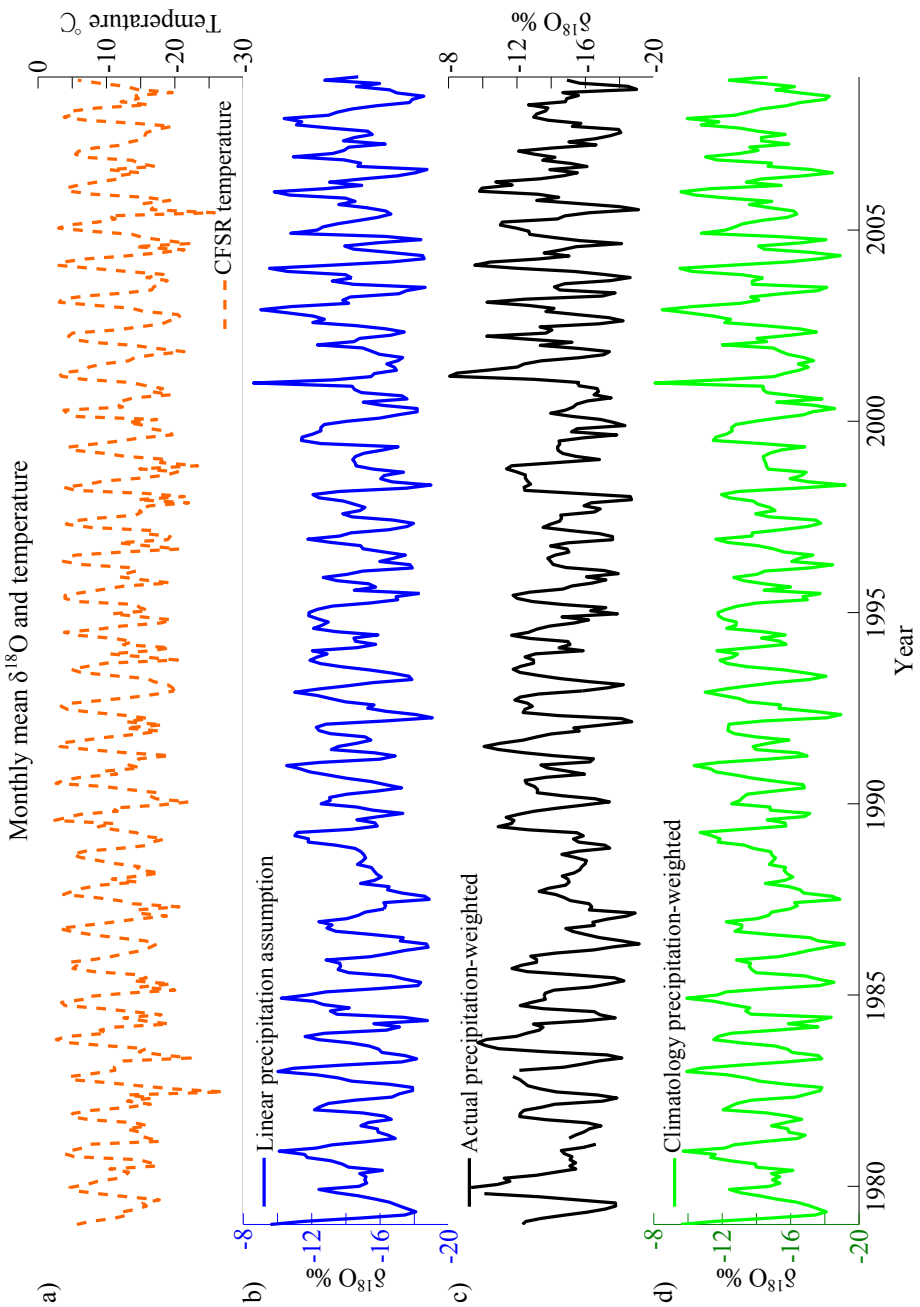

Figure 4.13: Left panel: The monthly mean temperature from CFSR (a, orange dashed line) and monthly mean δ^{18}O record derived from the linear precipitation assumption (b, blue solid line), from the precipitation time series-weighted dating method (c, black line), and the precipitation climatology-weighted dating method (d, green line).

This correlation improves to r = 0.59 [0.528; 0.654] with the precipitation time series-weighted dating method (Figure 4.13 c, black line). With the precipitation climatology-weighted dating method (Figure 4.13 d, green line), the correlation coefficient between the monthly mean δ^{18}O and CFSR temperature record is slightly higher than the linear monthly dating method but still lower than the method using the CFSR precipitation time series, as expected (r = 0.51 [0.434; 0.571]).

However, when the monthly δ^{18}O anomaly for each method is compared (i.e., when the average seasonal cycle is removed), each correlation to the temperature anomaly record is much lower. Figure 4.14 shows the monthly mean CFSR temperature anomaly and the monthly mean δ^{18}O anomalies computed by each method. The climatology of the temperature and δ^{18}O calculated by each method is also shown in right panel. The correlation between CFSR temperature monthly anomaly and δ^{18}O monthly anomaly becomes much lower in each case: r = − 0.066 [− 0.140; 0.008] for the linear assumption method, r = 0.076 [0.030; 0.123] for the precipitation time series-weighted dating method, r = − 0.078 [− 0.157; 0.001] for the climatology-weighted dating method. Though the precipitation time series-weighted timing method is still significant (i.e., the range in r does not span zero), the correlation coefficient is so low that it becomes hard to argue that it represents monthly Mill Island temperature. Neither the precipitation climatology-weighted nor lin-

ear dating methods are significantly correlated with the temperature anomaly. The reason for the low anomaly correlations is discussed next.

The climatology of the monthly mean CFSR temperature at Mill Island (Figure 4.14, e) shows a "coreless" winter from April to October, however the climatology of the monthly mean δ^{18}O (Figure 4.14, f, g, and h) shows a winter trough. The precipitation time series-weighted timing method (third panel, black line), in particular, shows a clear winter trough in July and August. The reason for the apparent lack of a coreless winter in the δ^{18}O may be due to the nearby open water bias: During summer, the open water around Mill Island provides a local source of moisture. The local moisture is less fractionated than moisture from lower latitude due to the proximity to moisture source, so that the summer δ^{18}O ratio appears higher (i.e., warmer) than it is. As nearby open water diminishes, Mill Island receives less local moisture. As winter progresses, even though there may be no change in temperature, the local moisture source becomes smaller (i.e., there is less open water), so δ^{18}O becomes progressively lower (colder). Then finally when the temperature increases the δ^{18}O reflects both the genuine warming signal and more local moisture from the increasing open water nearby Therefore, the open water bias potentially removes the coreless winter in the δ^{18}O seasonal cycle. δ^{18}O diffusion may also remove the coreless winter signal in low accumulation sites. However with the high snow accumulation rate at Mill Island, the influence of δ^{18}O diffusion is negligible.

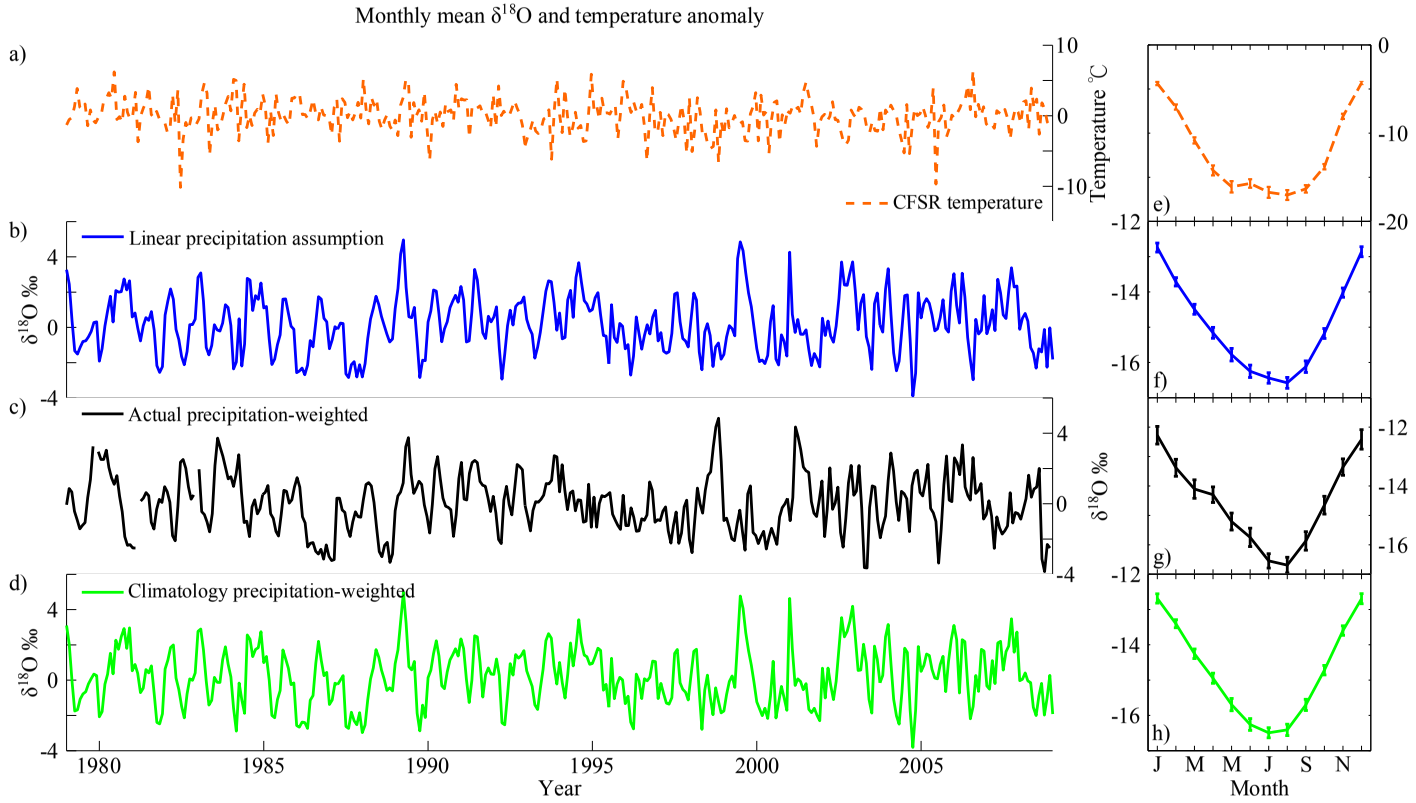

Figure 4.14: Left panel: The monthly mean temperature anomaly from CFSR at Mill Island (a, orange dashed line) and the monthly mean δ^{18}O anomaly record derived from the linear precipitation assumption (b, blue solid line), from the precipitation time series-weighted dating method (c, black line), and the precipitation climatology-weighted dating method (d, green line). Right panel: climatologies of the CFSR temperature at Mill Island (orange dashed line) and monthly mean δ^{18}O calculated with the linear precipitation assumption (blue line), the precipitation time series-weighted dating method (black line), and the precipitation climatology-weighted dating method (green line). The error bars show the standard error of the mean.

These results indicate that Mill Island δ^{18}O may require more care for use as a site temperature proxy. Mill Island δ^{18}O does capture the seasonal cycle of temperature, but it does not capture the details of winter particularly well. The noise of monthly anomalies is about the same magnitude as the annual cycle ($\sim \pm 4$ ‰). The coreless winter (Apr – Oct) demonstrated in the CFSR temperature climatology suggests that the coldest month can be any month from April to October, however the open water bias affects the δ^{18}O seasonal cycle in such a way that the coreless winter does not appear in the seasonal cycle. This could be the reason that the climatology-weighted method does not improve monthly dating. Therefore, Mill Island δ^{18}O may be useful as a sub-annual temperature proxy if it is partitioned into summer and winter periods.

In addition to the considerable effect of the open water bias, it appears that monthly snowfall variability also dominates the δ^{18}O climatology. Figure 4.15 shows the climatology of monthly CFSR precipitation proportion during 1979 – 1989 (blue), 1990 – 1999 (green), 2000 – 2009 (magenta), and 1979 – 2009 (black). The error bars show the standard error of the mean, and the horizontal dotted line shows the equivalent linear monthly precipitation proportion. January is the minimum precipitation month in all periods, but otherwise the three different climatology periods show significant differences. The overall climatology (Figure 4.15 d) shows higher precipitation in autumn

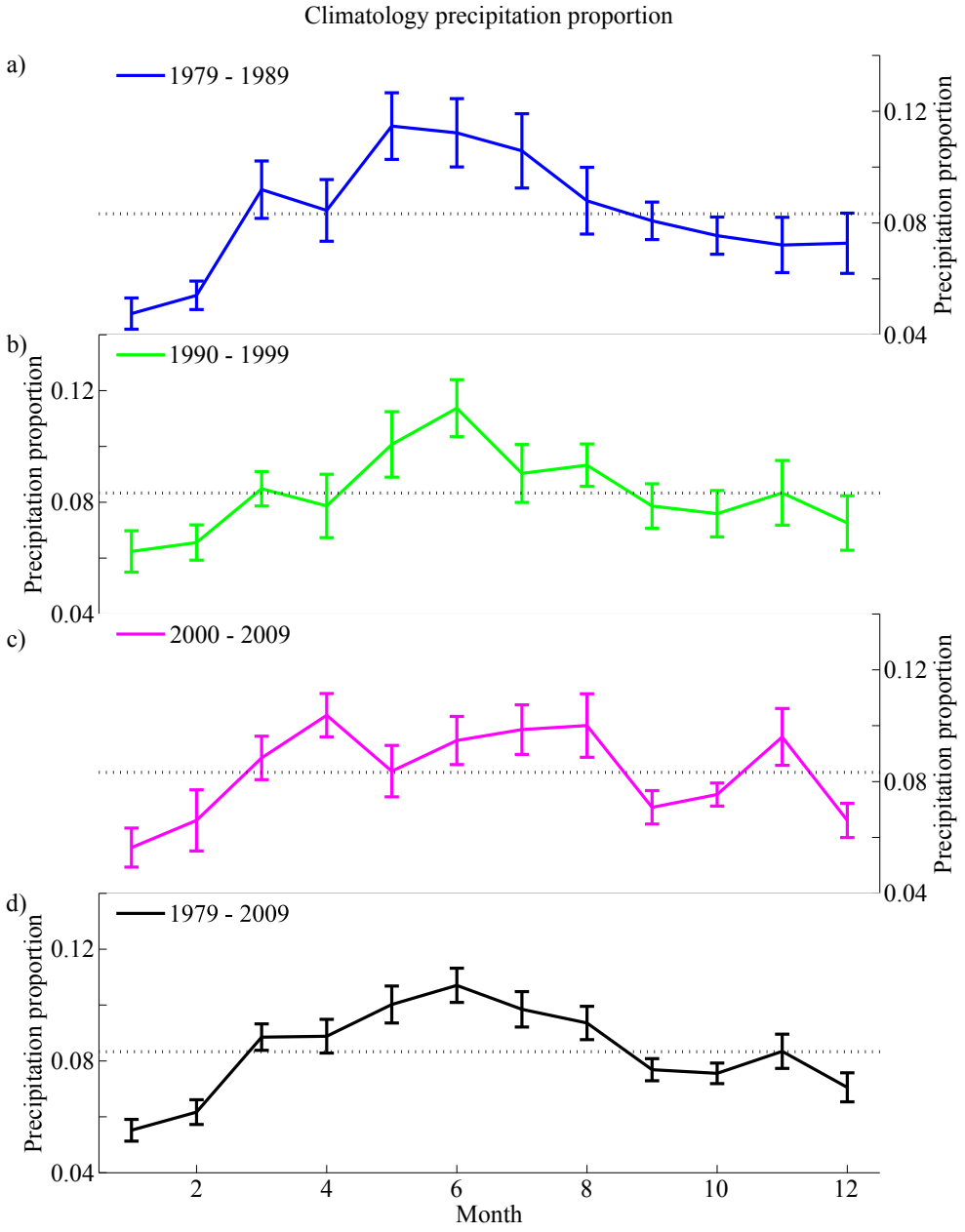

Figure 4.15: Climatology of the precipitation proportion for the period of a) 1979 – 1989 (blue), b) 1990 – 1999 (green), c) 2000 – 2009 (magenta), and d) 1979 – 2009 (black). The error bars show the standard error of the mean. The horizontal dotted line shows the linear monthly precipitation proportion (~ 0.0833).

and winter (March to August) and lower precipitation in spring and summer (September to February). This indicates a bias to colder autumn/winter temperatures if unweighted (linear monthly or annual mean) δ^{18}O is used as a temperature proxy.

Figure 4.16 shows the annual mean δ^{18}O calculated from the mean of all data points within an annual layer (blue) and annual mean δ^{18}O corrected with precipitation-weighted monthly δ^{18}O (black). The corrected annual mean δ^{18}O ($-$ 14.56 ‰) is slightly higher than the non-corrected annual mean δ^{18}O ($-$ 14.76 ‰ [1979 – 2009]). These differences in precipitation timing may thus bias Antarctic temperature reconstructions using ice cores (Jones et al., 2009). Ligtenberg et al. (2012) also demonstrated the seasonal bias in Antarctic ice sheet volume change. Ice sheet mass increases in winter and decreases in summer across most of Antarctica. Thus, throughout the continent, temperature reconstructions from ice cores are likely biased to be cooler than actual temperatures. Such biases need to be kept in mind when considering Antarctic temperature reconstructions from ice cores (e.g., PAGES 2k Consortium et al., 2013), particularly where precipitation biases change or climate trends differ with season. These biases also needed to be taken into account for comparisons between ice core reconstructions and other temperature reconstructions from terrestrial or ocean based records (e.g., tree rings, corals).

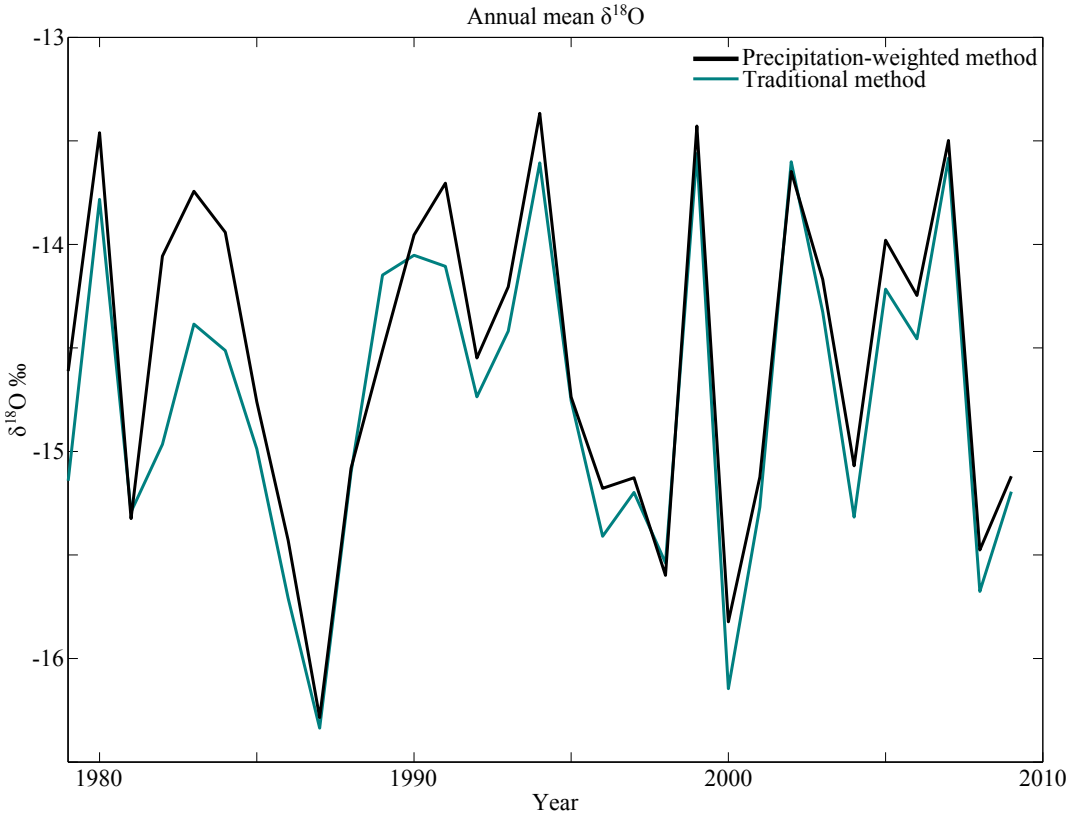

Figure 4.16: Annual mean δ^{18}O (blue) and annual mean δ^{18}O corrected using the precipitation-weighted monthly dating method (black), from 1979 – 2009.

4.3.7 Optimal temperature reconstruction from the Mill Island δ^{18}O record

In order to generate summer and winter temperature reconstructions, the δ^{18}O record must be segmented into representative portions based on proximity to mid-summer and winter markers. Since it is impossible to know accurately which depth corresponds to which date, the technique used to divide the δ^{18}O time series into summer and winter is critical for accurate sub-annual reconstruction. It is clear that summer is warmer (higher δ^{18}O ratio) and winter is colder (lower δ^{18}O ratio). Thus the annually dated δ^{18}O time series was divided into summer and winter portions.

For summer, since the beginning of a year is near mid-summer, the year marker was used as the mid-summer marker. For winter, it was assumed that the coldest date is in the middle of winter, so the lowest δ^{18}O value within a year was chosen as the mid-winter marker. Summer "windows" were configured centred on mid-summer marker. For example, the 10 % summer window was setup as 10 % of the depth between the mid-summer marker and the deeper side of the adjacent mid-winter marker, and between the mid-summer marker and the surface side of the adjacent mid-winter marker. This technique was repeated for 20, 30, 40, and 50 % summer windows. Winter windows were configured in same way but centred on a mid-winter marker. A narrower window provides more certainty that the snow within that window

contains only summer/winter snow.

The percentage window technique is demonstrated in Figure 4.17, top panel. The black solid line shows the δ^{18}O time series between 2007 and 2009. The x axis shows the depth of the ice core, and the y axis shows the δ^{18}O ratio (‰). The vertical red dashed lines show the beginning of each year, i.e., the mid-summer markers, and the vertical blue dotted lines show mid-winter markers. The associated depth of sodium (orange, left y axis) and MSA (purple, right y axis) records are shown in Figure 4.17 bottom panel to confirm the summer and winter windows. Case a) shows a summertime 30 % window. The mid-summer marker is at the same position as the beginning of 2009 (depth 2.82 m). The lowest δ^{18}O value within 2009 was found at depth 0.70 m, indicating the location of the 2009 mid-winter marker. Thirty percent of the snow/ice between the mid-winter marker and the 2008/09 year marker, starting from the 2009 year marker (i.e., depth between 2.184 and 2.82 m) was considered as the upper half of the 2009 summer 30 % window. The lowest δ^{18}O value within 2008 was identified at a depth of 3.94 m, indicating the 2008 mid-winter marker. 30 % of the depth between the 2008/09 year marker and the 2008 mid-winter marker, starting from the 2009 year marker, was considered as the lower half of the 2009 summer 30 % window (depth between 2.82 and 3.156 m). The mean summer 30 % window δ^{18}O was thus calculated using all samples between depth 2.184 and 3.156 m.

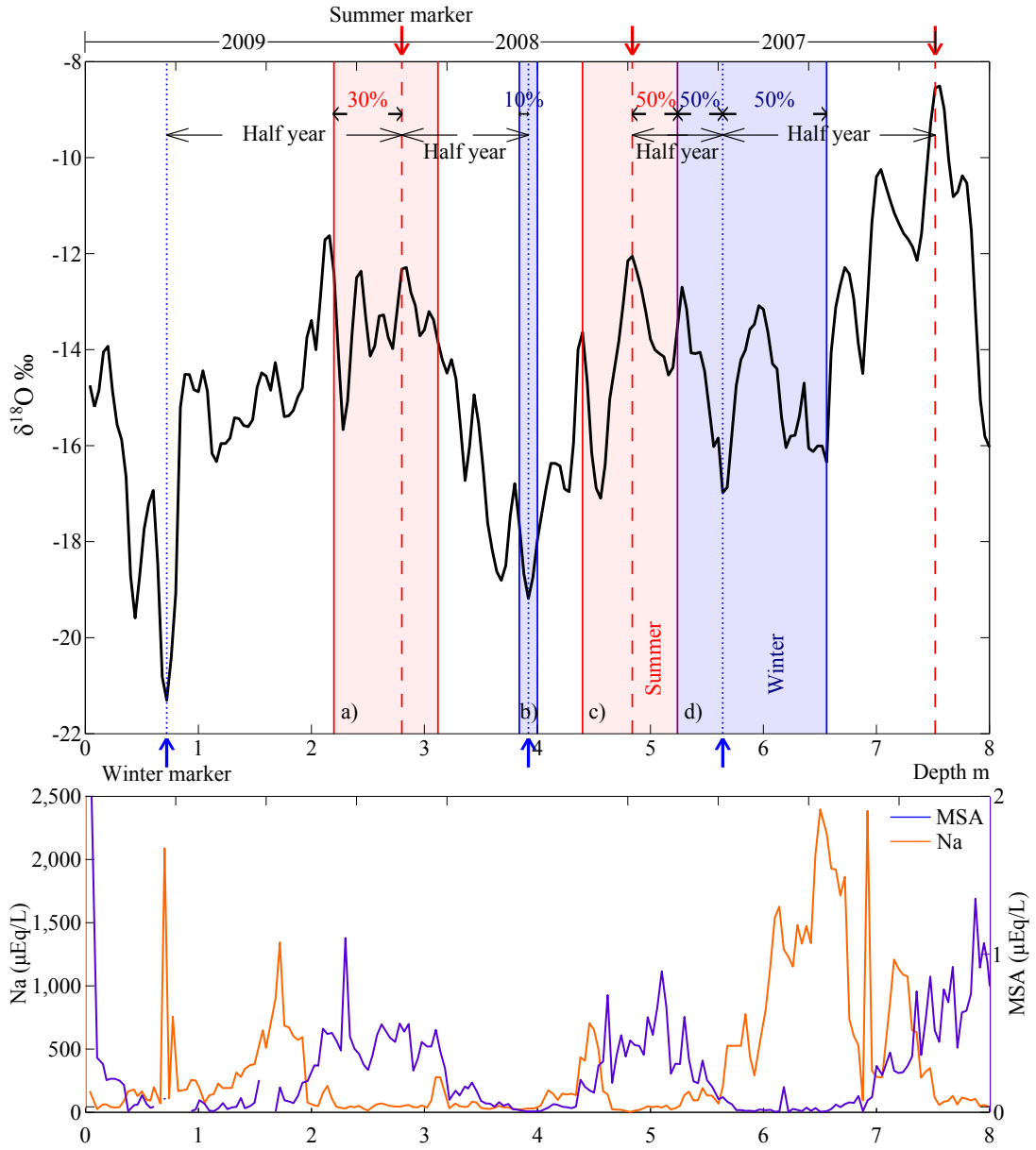

Figure 4.17: An example showing the summer and winter windows: Top panel, Black solid line shows δ^{18}O record. X axis is ice core depth, y axis is δ^{18}O ratio (‰). The vertical red dashed lines show the beginning of each year, i.e., the mid-summer markers, and the vertical blue dotted lines show mid-winter markers; bottom panel, associated depth of sodium (orange, left y axis) and MSA (purple, right y axis) records.

Case b) in Figure 4.17 shows calculation of the winter 10 % window in 2008. It was calculated similarly to Case a), but was centred on a mid-winter marker (depth 3.94 m) with a width of ± 10 % (depth 3.828 to 4.032 m). In the same way, cases c) and d) were calculated for summer and winter 50 % windows, respectively.

The sodium and MSA records shown in bottom panel confirm that the summer and winter windows are in the correct locations. Even though the trace chemistry is complicated over the entire Mill Island record, the agreement between summer and winter windows and sodium and MSA seasonality in the top 20 m of the ice core provides confidence for the remainder of the record.

The summer and winter window mean δ^{18}O records were then assessed by comparing with CFSR monthly/seasonal temperatures at Mill Island. CFSR "seasonal" mean temperature was calculated using a period of two, three, four, five, or six months mean from each starting month. For example, if the starting month was October, the mean of October and November δ^{18}O is the two months summer mean. Table 4.4 shows the starting month and two-to-six months combinations for summer and winter.

4.3.8 Summer and winter temperature reconstructions

Table 4.5 shows the correlation coefficient of each summer window mean δ^{18}O with each combination of monthly seasonal mean temperature from CFSR.

		Month window				
	Starting month	2	3	4	5	6
Summer	Oct to ..	Nov	Dec	Jan	Feb	Mar
	Nov to ..	Dec	Jan	Feb	Mar	Apr
	Dec to ..	Jan	Feb	Mar	Apr	May
	Jan to ..	Feb	Mar	Apr	May	Jun
Winter	Apr to ..	May	Jun	Jul	Aug	Sep
	May to ..	Jun	Jul	Aug	Sep	Oct
	Jun to ..	Jul	Aug	Sep	Oct	Nov
	Jul to ..	Aug	Sep	Oct	Nov	Dec

Table 4.4: CFSR mean periods for summer and winter windows. The left column shows the starting month.

The 10 % summer window is most highly correlated with "summer" months mean temperature. The December to April mean temperature and January to April mean temperature both correlate well with 10 to 50 % seasonal mean δ^{18}O values. The best correlation here is between the 10 % summer window δ^{18}O mean and December to April mean temperature (r = 0.46 [0.435; 0.486]).

Table 4.6 shows the correlation coefficient between each winter window mean δ^{18}O and each combination of monthly seasonal mean temperatures from CFSR. The best correlation here is between the 10 % winter window δ^{18}O mean and May to July mean temperature (r = 0.44 [0.081; 0.702]).

Figure 4.18 shows a scatter plot of the best summer and winter correla-

CFSR mean period	Window width 10 %	20 %	30 %	40 %	50 %
Oct-Nov	− 0.14	− 0.20	− 0.22	− 0.20	− 0.16
Oct-Dec	− 0.02	− 0.06	− 0.10	− 0.08	− 0.06
Oct-Jan	0.09	0.03	− 0.03	− 0.03	− 0.03
Oct-Feb	0.21	0.15	0.10	0.11	0.12
Oct-Mar	0.26	0.20	0.15	0.16	0.17
Nov-Dec	− 0.02	− 0.06	− 0.11	− 0.11	− 0.08
Nov-Jan	0.10	0.04	− 0.03	− 0.05	− 0.05
Nov-Feb	0.26	0.19	0.13	0.12	0.14
Nov-Mar	0.29	0.23	0.18	0.18	0.19
Nov-Apr	0.41	0.38	0.34	0.33	0.32
Dec-Jan	0.33	0.28	0.21	0.18	0.14
Dec-Feb	0.40	0.35	0.30	0.29	0.29
Dec-Mar	0.39	0.34	0.29	0.29	0.29
Dec-Apr	0.46	0.44	0.41	0.40	0.37
Dec-May	0.39	0.36	0.35	0.34	0.33
Jan-Feb	0.37	0.32	0.28	0.27	0.27
Jan-Mar	0.35	0.30	0.27	0.26	0.26
Jan-Apr	0.44	0.42	0.40	0.39	0.36
Jan-May	0.37	0.33	0.33	0.33	0.31
Jan-Jun	0.39	0.36	0.34	0.33	0.32

Table 4.5: The correlation coefficient between "summer" percentage window mean $\delta^{18}O$ (columns) and "summer" CFSR temperature (rows) for each monthly combination. Red coloured cells indicate $p < 0.05$, dark red coloured cells indicate $p \leq 0.01$.

CFSR mean period	Window width 10 %	20 %	30 %	40 %	50 %
Apr-May	0.12	− 0.00	− 0.03	− 0.03	− 0.06
Apr-Jun	0.25	0.13	0.09	0.08	0.05
Apr-Jul	0.31	0.23	0.16	0.10	0.02
Apr-Aug	0.25	0.19	0.14	0.09	− 0.01
Apr-Sep	0.32	0.27	0.20	0.12	0.01
May-Jun	0.41	0.30	0.25	0.21	0.18
May-Jul	0.44	0.37	0.29	0.20	0.11
May-Aug	0.37	0.32	0.26	0.18	0.09
May-Sep	0.42	0.39	0.31	0.20	0.08
May-Oct	0.43	0.40	0.32	0.22	0.10
Jun-Jul	0.38	0.38	0.30	0.19	0.11
Jun-Aug	0.26	0.28	0.24	0.16	0.07
Jun-Sep	0.33	0.36	0.29	0.18	0.07
Jun-Oct	0.34	0.38	0.30	0.20	0.09
Jun-Nov	0.30	0.33	0.26	0.15	0.04
Jul-Aug	0.12	0.17	0.13	0.06	− 0.05
Jul-Sep	0.22	0.28	0.21	0.10	− 0.04
Jul-Oct	0.25	0.30	0.23	0.12	− 0.00
Jul-Nov	0.20	0.26	0.18	0.08	− 0.05
Jul-Dec	0.16	0.22	0.16	0.06	− 0.07

Table 4.6: The correlation coefficient between winter percentage window mean $\delta^{18}O$ (columns) and winter temperature (rows) for each monthly combination. Blue coloured cells indicate $p < 0.05$, dark blue coloured cells indicate $p \leq 0.01$.

tion combinations, i.e., CFSR mean temperature for December to April versus the summer 10 % δ^{18}O window (red square); and CFSR mean temperature for May to July versus the winter 10 % δ^{18}O window (blue circle). The linear relation between temperature and δ^{18}O (line of best fit) gives the parameters for the calibration of equation 4.1.

$$\delta^{18}O = \alpha T + \beta$$

where $\alpha = 0.67$ ‰$/K$, $\beta = -6.7$ ‰ for summer, and $\alpha = 0.21$ ‰$/K$, $\beta = -14.4$ ‰ for winter. The calibration slope α for summer is broadly consistent with central Antarctica and Greenland (~ 0.67 ‰/K, Paterson, 1994), and for winter is lower than DSS (0.44 ‰/K, van Ommen and Morgan, 1997).

It appears that the winter calibration slope is much lower than summer calibration slope. This is not unexpected, since the "coreless" winter was not well represented in the δ^{18}O seasonal cycle, and the winter snowfall shows more variability than summer in each 10 year period climatology (see Section 4.3.6). Blowing snow redistribution may also impact the winter record more than the summer record: Figure 2.16 c) in Chapter 2 shows more frequent occurrence of strong wind (wind speed ≥ 15 m/s) during winter months. The strong wind may mix δ^{18}O signals, or even completely remove layers of fresh snow. However, because the lowest δ^{18}O value was set as the mid-winter marker, instead of being based on depth or date, it is likely still able to represent winter snow

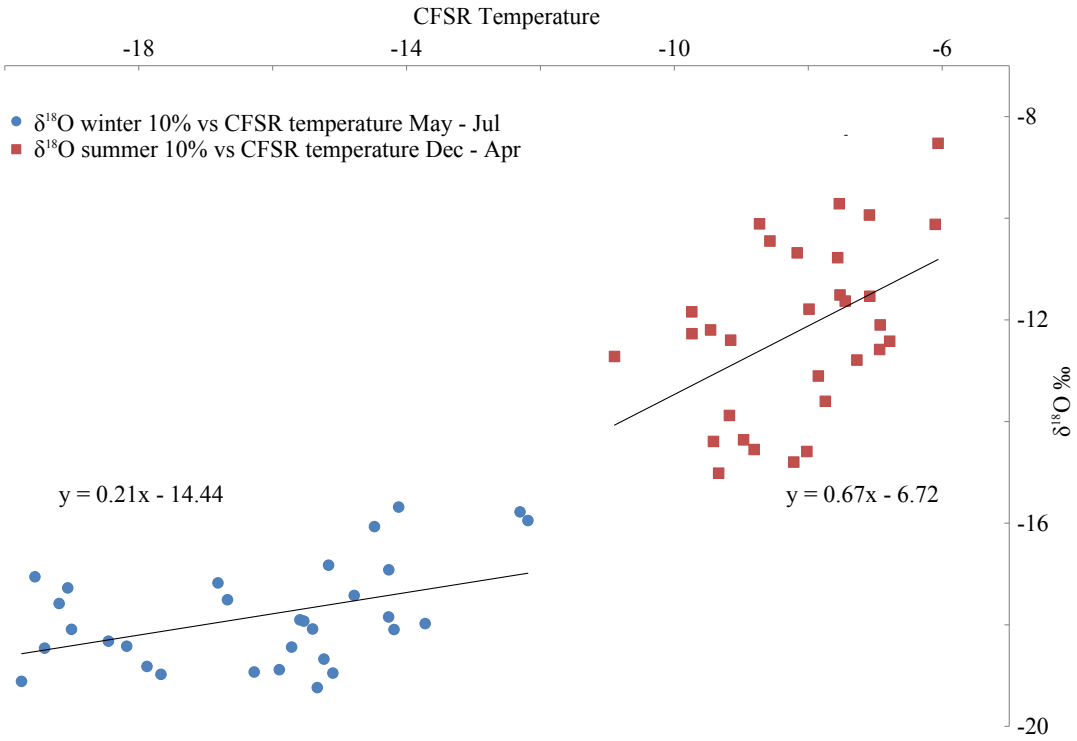

Figure 4.18: A scatter plot of CFSR mean temperature for December to April versus summer 10 % window δ^{18}O (red squares), and CFSR mean temperature for May to July versus winter 10 % window δ^{18}O (blue circles).

associated with low δ^{18}O values. Therefore, the percentage window technique may be the optimal method for summer and winter temperature reconstruction based on high-resolution δ^{18}O sample data. Thus, 10 % summer and winter window mean δ^{18}O values are used to generate a reconstruction of summer and winter temperatures in the following section.

4.3.9 Mill Island temperature reconstruction

Figure 4.19 shows a) the Mill Island borehole temperature (green solid, Roberts et al., 2013), b) CFSR temperature at Mill Island (November to April [magenta dashed line], May to October [cyan dashed line], November to October [black dashed line], and January to December [orange dashed line]), and c) the Mill Island δ^{18}O ratio (summer 10 % window mean [red], winter 10 % window mean [blue], mean of summer 10 % and winter 10 % windows [black], and annual mean [orange]). Note that CFSR mean temperature records were calculated using November to April as summer and May to October as winter mean temperature, instead of the best correlation combination, in order to form a complete year temperature proxy.

"Annual" δ^{18}O was computed as the mean δ^{18}O of summer 10 % and winter 10 % windows (Figure 4.19 c, black line) and compared with the mean temperature from November to October (Figure 4.19 b, black dashed line). The correlation between the "annual" δ^{18}O and Nov to Oct temperature mean

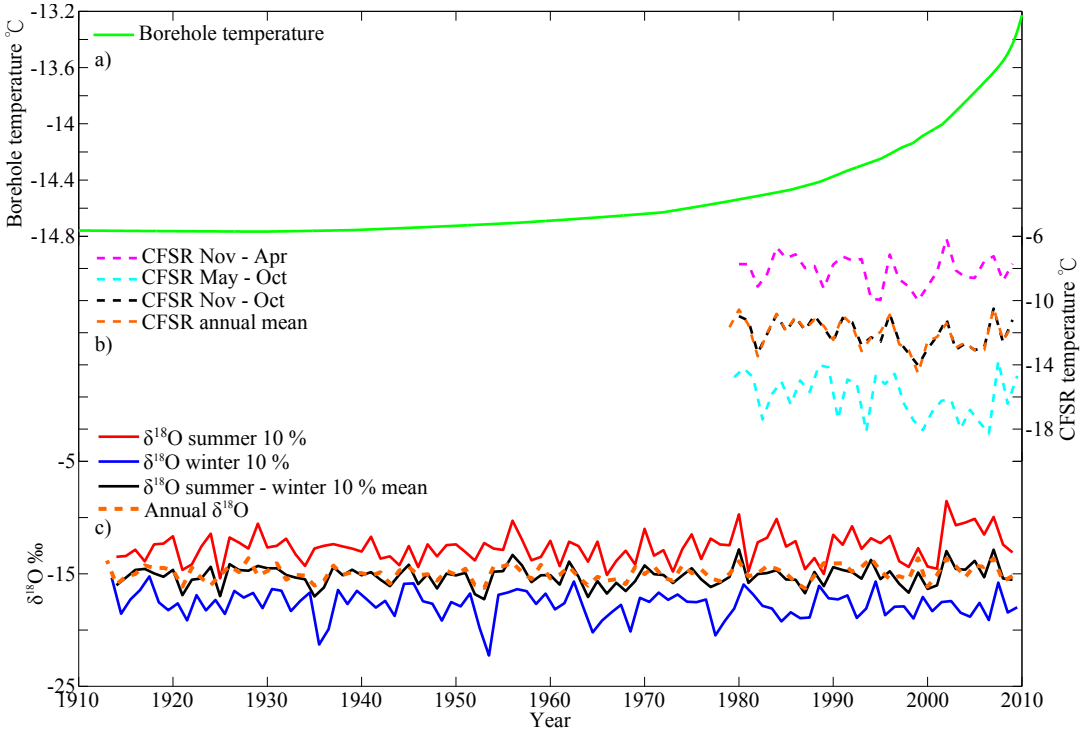

Figure 4.19: a) Mill Island borehole temperature (green solid, Roberts et al., 2013), b) CFSR temperature at Mill Island (November to April [magenta dashed line], May to October [cyan dashed line], November to October [black dashed line], and January to December [orange dashed line]), and c) Mill Island δ^{18}O ratio (summer 10 % window mean [red], winter 10 % window mean [blue], mean of summer 10 % and winter 10 % windows [black], and annual mean [orange]).

is marginally significant (r = 0.31 [− 0.06; 0.61]). While there is no significant trend for summer, winter, or "annual" δ^{18}O (Figure 4.19 c, red, blue, and black, respectively), there is a suggestion of a change in slope (slope = 0.004 ‰/yr to 0.155 ‰/yr) from the Mudelsee (2009) BREAKFIT function from 1998, with almost no trend between 1913 and 1998. Although the change is small, this break point is in almost the same location as the changes observed in trace ion chemistry (Chapter 3) and snow accumulation (Section 4.3.1). Thus, it may indicate environmental changes around this time.

Roberts et al. (2013) observed a warming trend in the Mill Island borehole temperature after 1980 ± 5 years (Figure 4.19 a), which is not observed in the CFSR temperature (Figure 4.19 b) or Mill Island δ^{18}O records (Figure 4.19 c). This suggests one of three possibilities. Firstly, the CFSR temperature may not be representative of the temperature at the summit of Mill Island. Secondly, δ^{18}O at Mill Island may not be a good proxy for site temperature. Lastly there may be factors which influence borehole temperature, in addition to air temperature.

The Mill Island δ^{18}O record does represent the CFSR temperature to some extent, as shown in Tables 4.5 and 4.6, and Figure 4.18. However, if CFSR poorly represents temperature at Mill Island, this δ^{18}O reconstruction is of limited use. Mill Island δ^{18}O is more closely associated with air temperature than with surface temperature, since δ^{18}O reflects a precipitation

process. On the other hand, borehole temperature may be influenced by surface temperature or latent heat. Thus, δ^{18}O and borehole temperature may not represent the same parameter.

The interpretation of the lack of δ^{18}O trend in conjunction with the observed borehole warming trend implies that either of the following has occurred, in conjunction with no change to the surface air temperature: The net incoming shortwave radiation flux to the ice has increased, either through a reduction in summertime cloud cover or a decrease in albedo at the site; the net incoming longwave radiation flux to the ice has increased, probably via an increase in cloud cover; or a net increase in latent heat to the ice has occurred, probably via an increase in fog rime accretion. Such an increase in rime accretion would also lead to an increase in sea salt concentration in the Mill Island ice core, as hypothesised in Section 3.3.6. All three processes are closely tied to the cloud conditions around the site, which are difficult to model reliably, especially at very small scales. At an ice cap site such as this, cloud is likely to be orographically-driven, so a very high (possibly sub-km) grid resolution atmospheric model would be required to accurately model the cloud field here. Furthermore, model validation would be required, likely in the form of an AWS equipped with a full radiometer suite. This work is suggested in order to resolve the apparent discrepancy between the borehole and δ^{18}O temperature proxy records.

4.4 Conclusion

This chapter presented an investigation of the use of the δ^{18}O proxy as a palaeothermometer. The high snow accumulation rate (1.35 mIE/yr) at Mill Island enables the study of the δ^{18}O record at a sub-annual resolution.

Mill Island snow accumulation was calculated and compared with snow accumulation/precipitation data from nearby sites and atmospheric model output. The comparison with precipitation records from DSS snow accumulation, Casey Station, Mirny Station and atmospheric models (RACMO, AMPS, ERA-interim, and CFSR) demonstrates that CFSR is the most representative model for precipitation at Mill Island.

The five year mean snow accumulation record at Mill Island shows a positive correlation with the five year mean snow accumulation record at DSS ($r = 0.523$ [0.521; 0.525]), and a negative correlation with the five year mean precipitation record at Mirny Station ($r = -0.491$ [-0.519; -0.463]). These opposing correlations between Mill Island and DSS, and Mill Island and Mirny Station may reflect the influence of mid-latitude continental topography and subsequent formation of the ZW3 circulation pattern. The ZW3 index correlates oppositely with DSS snow accumulation ($r = 0.28$ [0.23; 0.32]) and Mirny Station precipitation ($r = -0.31$ [-0.56; -0.01]), but shows no correlation with the Mill Island snow accumulation record ($r = -0.00$ [-0.07; 0.06]).

This indicates that Mill Island lies between regions influenced oppositely by ZW3. Furthermore, the orography around Mill Island strongly influences the precipitation regime. The location of the Denman Glacier and associated katabatic flow partition the precipitation regime between Mill Island and Mirny Station.

The annual mean δ^{18}O record does not correlate well with the annual CFSR temperature record (r = 0.0), so another technique to reconstruct temperature using δ^{18}O was sought. To calibrate Mill Island δ^{18}O as a site temperature proxy, δ^{18}O was compared with CFSR temperature and investigated at a sub-annual resolution. Using the high resolution Mill Island δ^{18}O record, summer and winter temperature reconstructions were achieved by computing progressively narrower summer and winter "windows" centred around the maximum and minimum δ^{18}O values during each year. The mean δ^{18}O of the "summer" 10 % width window correlates well with December to April mean CFSR temperature (r = 0.46 [0.435; 0.486]), and the mean δ^{18}O of the "winter" 10 % width window correlates well with May to July CFSR temperature (r = 0.44 [0.081; 0.702]).

The derived summer and winter mean δ^{18}O records do not show significant trends throughout the record, indicating no significant air temperature trends, in agreement with the CFSR record. This result stands in contrast to Roberts et al. (2013), which shows a recent warming trend in the Mill Island

borehole temperature record. It would appear that the δ^{18}O and borehole temperature proxies each respond to distinct parameters. While the δ^{18}O temperature record is also influenced by open ocean proximity, timing of precipitation, and conditions at the site of evaporation, the borehole temperature record is also influenced by changes in radiation fluxes and latent heat processes. As such, neither proxy is an ideal record for air temperature at the core site, and each proxy gives a somewhat independent account of the environmental conditions.

The impact of a seasonal bias in precipitation on interpreting the δ^{18}O record was considered by comparing the monthly dating techniques to the simple assumption of linear precipitation ice core dating. Using the actual precipitation proportion per year to compute monthly mean δ^{18}O was found to be the best monthly dating technique. It was found that Mill Island tends to have more snowfall during winter than during summer, as with most of the Antarctic continent and the Greenland Ice Sheet (Lee et al., 2012; Thomas et al., 2008). The temperature proxy using the Mill Island δ^{18}O record shows a negative bias of 0.2 ‰. Using the summer and winter calibration slopes in Section 4.3.8, this corresponds to a cold bias of 0.3 and 1 K, respectively. By extension, a comparable negative bias is also applicable to temperature records derived from most other Antarctic and Greenland ice cores.

Chapter 5

General conclusions

One of the most northerly ice cores in East Antarctica, the Mill Island ice core (MI0910), was drilled in the 2009/2010 field season. Measurements of hydrogen peroxide (H_2O_2), stable water isotopes (δD, δ^{18}O), and major trace ion chemistry (Na^+, Cl^-, MSA, SO_4^{2-}, Mg^{2+}, Ca^{2+}, NO_3^-) were completed, and the results are presented in this thesis.

The main outcomes of this thesis are:

- The Mill Island 120 m main ice core contains 97 years of climate record (from 1913 to 2009, Chapter 2).
- Sea salt concentration is the highest of all Antarctic ice core records (Chapter 2).
- Sea ice concentration to the east of Mill Island significantly influences the Mill Island ice core record (Chapter 3).
- Post-depositional migration of sodium and chloride were observed for the first time in an ice core. MSA and magnesium post-depositional migration were also observed (Chapter 3).

- The Mill Island snow accumulation is most likely influenced by local orography with a weaker influence from ZW3 modulation (Chapter 4).

- Not accounting for the stronger winter precipitation leads to a cold bias in temperatures reconstructed from the δ^{18}O record (Chapter 4).

- Summer and winter temperature proxies were produced from the δ^{18}O record that cover the period 1913 to 2009 (Chapter 4).

The Mill Island ice core was dated by counting annual layers of δ^{18}O, with support of the H_2O_2 and Deuterium excess (D-ex) records as required. The dating uncertainties are + 2.4, − 3.5 years. The trace ion chemistry of the Mill Island core was investigated by comparison with other nearby ice cores and instrumental data. The Mill Island ice core record is characterised by a unique chemistry record with a mixture of clear and ambiguous seasonality, and high and low trace ion concentration periods with regime changes in 1934 and 2000. The mean concentration of all major ion species except nitrate is much higher than in other nearby ice core records, e.g, Law Dome Summit South (DSS). In particular, sea salt concentration (Na^+ and Cl^-) is remarkably high (254 and 290 $\mu Eq/L$, respectively), which is the highest sea salt concentration values reported from an Antarctic ice core. The sulphate most likely originated from sea salt, and is highly depleted relative to sodium. Overall, 59 % of sulphate is fractionated, and non sea salt sulphate was calculated using the equation

$[\text{nss}SO_4^{2-}] = [SO_4^{2-}] - 0.049[Na^+]$ (Chapter 2).

Trace ion species, especially sodium, sulphate, and magnesium, were investigated in Chapter 3 in conjunction with records of environmental conditions around Mill Island. According to atmospheric model output, an easterly wind is dominant at this site, and the wind speed was unlikely related to sea salt concentration. Instead, sea ice concentration between Mill Island and Bowman Island was found to influence the sodium and sulphate records, at least from 1979 onward (when sea ice satellite observation data became available). The abrupt change observed in the sea salt record in 1934 suggests that there may have been significant changes to the ice shelf or sea ice configuration east of Mill Island during the mid-1930s. However, there are no historical records which support this hypothesis.

It was discussed that the extremely high sea salt concentration could result in ambiguous seasonality due to post-depositional migration. Post-depositional migration of sodium, chloride, magnesium, and MSA are observed in the MI0910 record. This is the first report of sodium post-depositional migration in an ice core. The chloride post-depositional migration from a high accumulation site ice core was also reported for the first time in this thesis. Because the chloride concentration in the MI0910 core exceeds its solubility limit (300 – 400 $\mu Eq/L$), the excess chloride probably migrates to locations of lower Cl^- value over time. As Cl^- moves, Na^+ likely follows as the coupling

species. As a consequence, lengthy "plateau"s in Cl^- and Na^+ were observed in the record. If this hypothesis is correct, Cl^- and Na^+ in periods of high sea salt concentration with clear seasonality (2000 – 2009) will smooth out with time, creating another "plateau" in the record similar to the period of 1934 – 1999. Since Na^+ occupies the limited space between the grain boundaries, Mg^{2+} likely moves to lower Na^+ concentration areas. MSA post-depositional migration may form magnesium methanesulphonate salt in parts of the ice core (Chapter 3).

The reason for the extremely high sea salt concentration was discussed, and a hypothetical sea salt deposition mechanism was proposed in Chapter 3. The high concentrations may be due to the combined influences of nearby low sea ice concentration in adjacent polynyas, wind speed and direction, production of frost flowers, and fog and rime accretion, in addition to the proximity to the coast.

The snow accumulation record was investigated by comparing with precipitation records from other sites. It was found that the Mill Island precipitation does not correlate strongly with the rest of the continent. The Zonal Wave 3 large scale atmospheric mode likely weakly modulates precipitation at Mill Island. The local orography combined with the maritime climate system is most likely a stronger influence. The snow accumulation rate at Mill Island is 1.35 mIE/yr, which enables the study of ice core samples at sub-annual res-

olution. Using high resolution δ^{18}O samples and an atmospheric model precipitation and temperature record at Mill Island, a new technique for monthly ice core dating was proposed. The precipitation climatology shows more snowfall during winter than summer, such that the annual mean δ^{18}O tends to preserve more winter time δ^{18}O than summer time. It was subsequently argued that temperature reconstructions using Antarctic ice cores show a seasonal cold bias (Chapter 4).

Taking account of the seasonal precipitation bias, the optimal use of the Mill Island δ^{18}O record as a temperature proxy was investigated. Instead of using all δ^{18}O points within a year boundary as a temperature proxy, only those points within a certain vicinity of the maximum and minimum δ^{18}O value data were used to reconstruct summer (November to April) and winter (May to October) temperatures. Combining these, "annual" temperature (mean of November to October temperature) was effectively reconstructed. The reconstructed annual temperature does not show the warming trend observed in the Mill Island borehole temperature record from 1980 onward. This suggests that the proposed borehole temperature warming is probably caused by radiation or latent heat changes due to changes in cloud cover, fog or rime accretion, rather than air temperature warming (Chapter 4).

Both annual mean snow accumulation and annual mean temperature records show no significant trend during the period covered by the ice core

(1913 – 2009). However, there are slight changes observed in 1999 and 1998, respectively, with positive trends in both parameters thereafter. These changes are not overt, yet they occur at around the same time as the trace ion record changes in 2000. This suggests that environmental changes may have occurred around this time (Chapter 4).

Overall, the Mill Island ice core is quite a challenging record to interpret, given its unique features, i.e., ambiguous seasonality, remarkably high chemical concentration, high resolution records, strong local influence on snowfall regime. This uniqueness makes difficult to simply compare it to the DSS record. However, the Mill Island record provides important evidence for significant regional changes that could prove valuable in understanding the longer term pre-industrial variability in sea ice in this region of East Antarctica.

Despite the ambiguous chemical record, the top part of the ice core (2000 – 2009) where the seasonality is still clear, could be useful for short term (interannual scale) variability studies. Moreover, Mill Island presents an ideal natural laboratory to study microphysics of ice, and the ice core may contain samples suitable for studying the behavior of impurities in firn and ice. To elucidate whether the increasing trends observed in Mill Island trace ions, snow accumulation and reconstructed temperature records since $\sim$2000 are real environmental signals or just natural variability will require further research, including new ice core drilling from Mill Island to update the record. Also

installation of an AWS (including a relative humidity sensor, and shortwave and longwave radiometers) at this site is crucial for accurate interpretation. Although the AWS may soon be buried due to the high snow accumulation at the summit, to obtain an observational record including precipitation, temperature and fog events is necessary to improve the understanding of the Mill Island climate. With this record, it may be possible to reconstruct the local maritime climate and to answer some of the outstanding questions raised by this study. Together with high resolution snow pit sampling, continued snow sample collections, and ongoing laboratory experiments, this will contribute to understanding sea salt deposition mechanisms, the influence of fog and rime accretion on the trace ion record, the relationship between oxygen isotope ratios and temperature, changes in the moisture source, and the microphysics of snow, firn and ice. With these further studies, the Mill Island ice core will further close the knowledge gap of the southern hemisphere climate.

Appendix A

Ambiguous dating years

The MI0910 record was dated using the H_2O_2, $\delta^{18}O$ and D-ex records. There are eight ambiguous cases in the dating. Three examples were demonstrated in Section 2.3.2. This appendix presents all the ambiguous cases. As in Figures 2.4 and 2.5, the figures presented in this appendix were re-sampled to a regular 12 cm grid for H_2O_2, and 5 cm grid for $\delta^{18}O$ and D-ex. These were then smoothed with a Gaussian filter of width $\sigma = 1$ point for H_2O_2, $\sigma = 2.4$ points for $\delta^{18}O$ and D-ex, to match the smoothing between the records.

A.1 Depth 10 – 20 m

Figure A.1 shows an anomaly in H_2O_2 at 18 m (indicated by the dashed ellipse). However this was not counted as a new year marker because $\delta^{18}O$ does not show a clear peak, as expected at mid-summer. Thus the small H_2O_2 peak was assumed to be associated with a late summer or autumn deposition which contained low-level H_2O_2. The lack of a D-ex trough also points to this being a non-summer feature. Then the highest $\delta^{18}O$ in the peak area (18 m to 20 m) was chosen as the beginning of the year 2002. This decision was

supported by the large D-ex trough at the same depth.

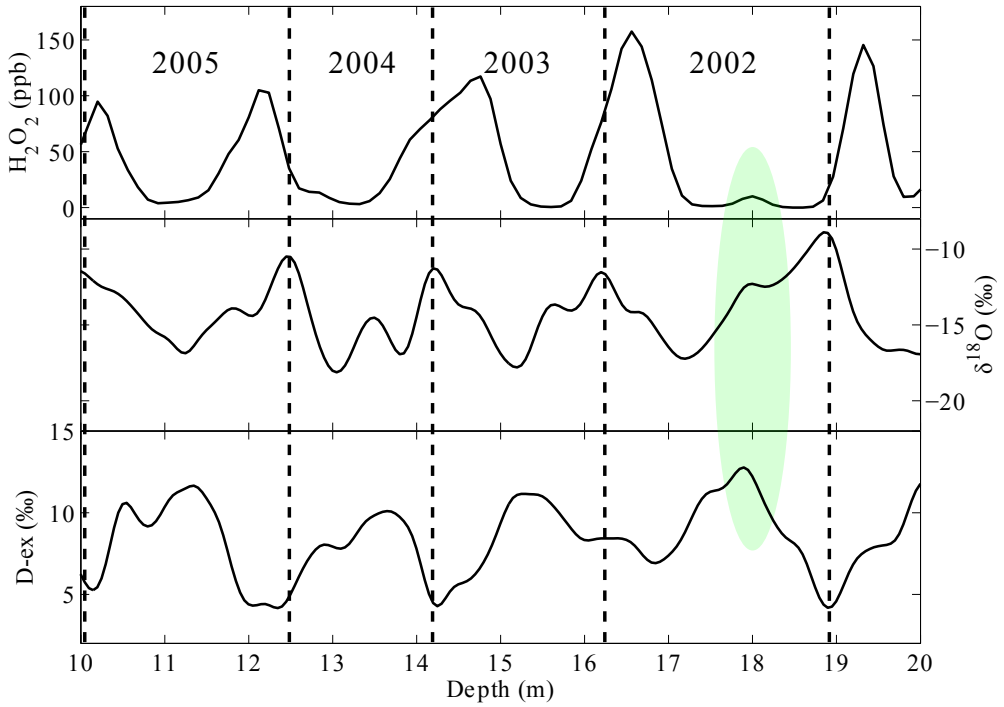

Figure A.1: The ambiguous part of the H_2O_2, δ^{18}O and D-ex records from depth 10 – 20 m. The dashed vertical line represents the beginning of each year.

A.2 Depth 50 – 60 m

Figure A.2 shows two ambiguous cases. At a depth of ∼51 m, δ^{18}O does not show any obvious peak (within the dashed circle). However there is a clear H_2O_2 peak and D-ex trough. Thus this was counted as a new year marker.

The depth between 52 and 57 m shows no H_2O_2 seasonality (within the grey circle). However δ^{18}O shows annual cycles, and corresponding D-ex troughs are present. Therefore, four years were counted in this section.

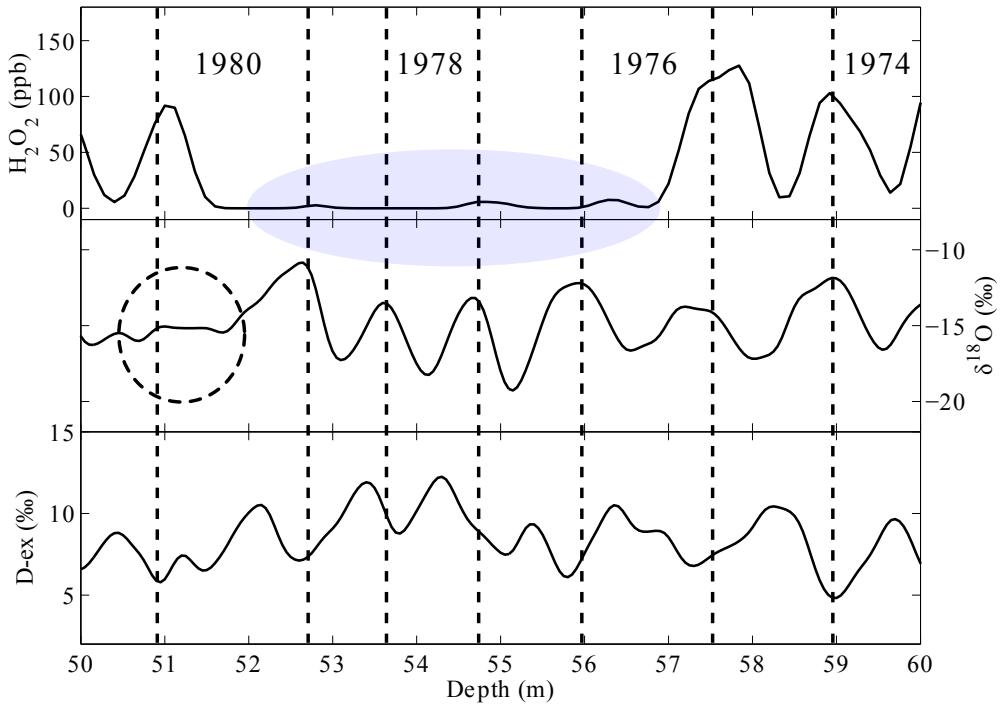

Figure A.2: The ambiguous part of the H_2O_2, $\delta^{18}O$ and D-ex records from depth 50 – 60 m. The dashed vertical line represents the beginning of each year.

A.3 Depth 80 – 90 m

The seasonality in H_2O_2 between 82 m and 87 m (indicated by the blue ellipse in Figure A.3) is unclear. However, the presence of $\delta^{18}O$ peaks and D-ex troughs indicate yearly seasonality, so these peaks were counted as years. Thus, the record between 82 and 87 m resembles the record between 52 and 57 m, as discussed in Section A.2.

The clear peak in H_2O_2 between 81 m and 82 m (indicated by the green ellipse) was not counted as a year, because there is no concurrent clear $\delta^{18}O$ peak nor D-ex trough. Likewise, the $\delta^{18}O$ peak between 87.5 m (indicated by the grey ellipse) was not counted as a year, because there is no concurrent H_2O_2 peak nor clear D-ex trough.

A.4 Depth 95 – 105 m

Figure A.4 shows the record of H_2O_2, $\delta^{18}O$ and D-ex from depth 95 to 105 m. The blue ellipse shows a region with no peak in H_2O_2. However, $\delta^{18}O$ shows a clear peak, and a D-ex trough is nearby. Thus, this was counted as a year.

A H_2O_2 peak is evident at $\sim$ 101 m (indicated by the green ellipse). However the small $\delta^{18}O$ peak is inconclusive, and there is no D-ex trough. Thus this was not counted as a year.

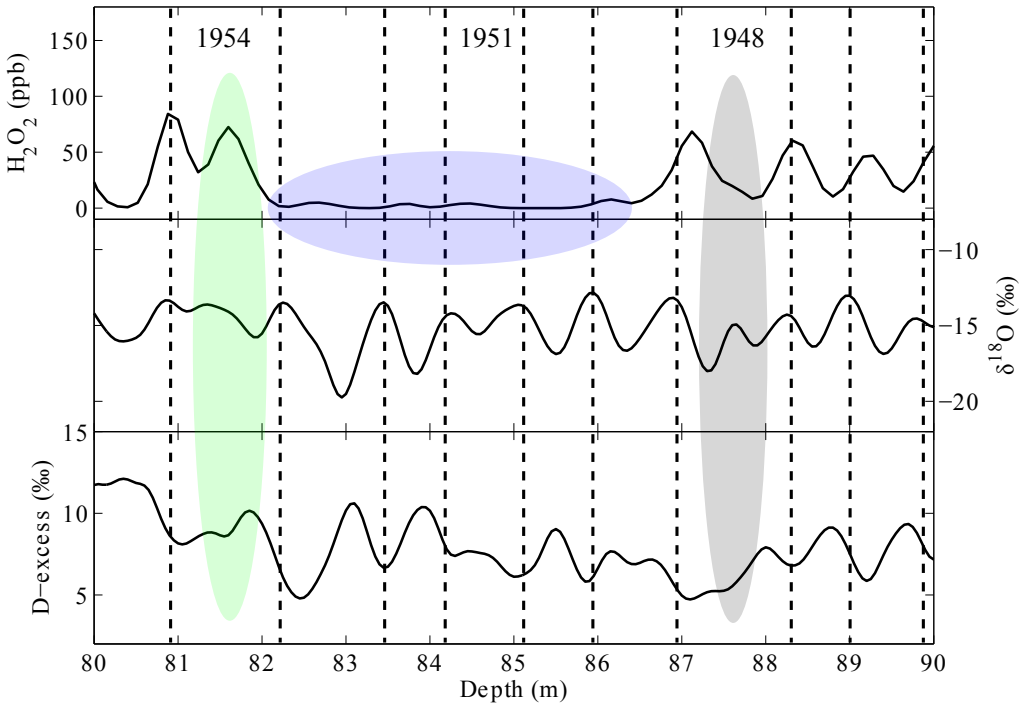

Figure A.3: The ambiguous part of the H_2O_2, $\delta^{18}O$ and D-ex records from depth 80 to 90 m. The dashed vertical line represents the beginning of each year.

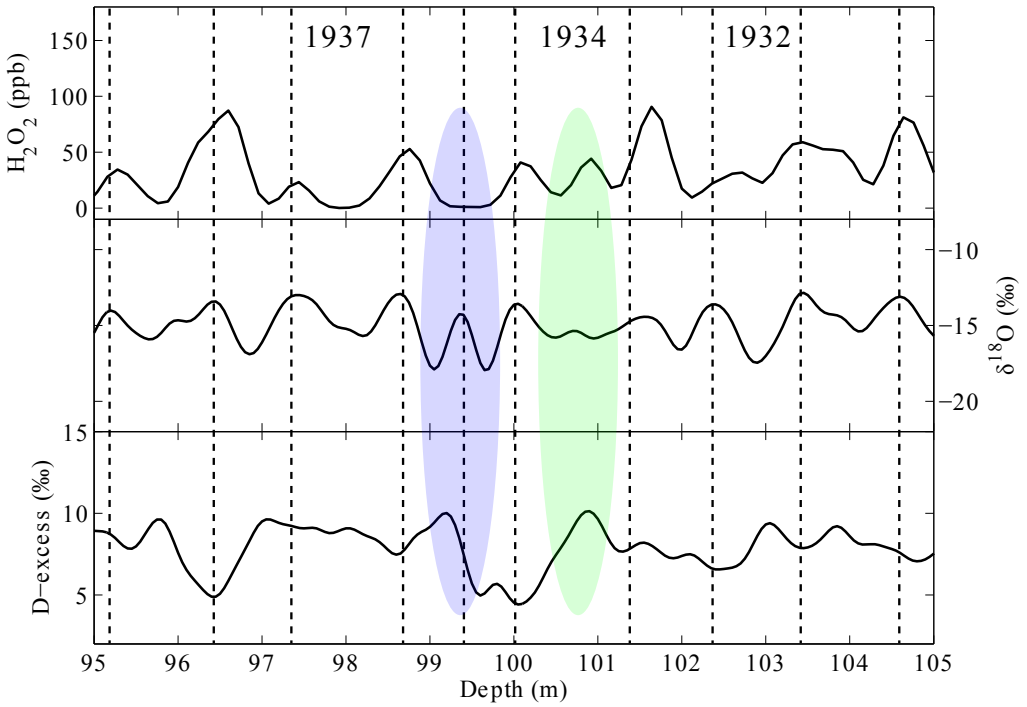

Figure A.4: The ambiguous part of the H_2O_2, $\delta^{18}O$ and D-ex records from depth 95 to 105 m. The dashed vertical line represents the beginning of each year.

BIBLIOGRAPHY

Abram, N. J., Curran, M. A. J., Mulvaney, R., and Vance, T.: The preservation of methanesulphonic acid in frozen ice-core samples, Journal of Glaciology, 54, 680–684, doi:10.3189/002214308786570890, 2008.

Abram, N. J., Mulvaney, R., and Arrowsmith, C.: Environmental signals in a highly resolved ice core from James Ross Island, Antarctica, Journal of Geophysical Research (Atmospheres), 116, D20116, doi:10.1029/2011JD016147, 2011.

Abram, N. J., Wolff, E. W., and Curran, M. A. J.: A review of sea ice proxy information from polar ice cores, Quaternary Science Reviews, 79, 168–183, doi:10.1016/j.quascirev.2013.01.011, 2013.

Alley, R. B.: Concerning the deposition and diagenesis of strata in polar firn, Journal of Glaciology, 34, 18, 1988.

Alley, R. B., Saltzman, E. S., Cuffey, K. M., and Fitzpatrick, J. J.: Summertime formation of Depth Hoar in central Greenland, Geophysical Research Letters, 17, 2393–2396, doi:10.1029/GL017i013p02393, 1990.

Alley, R. B., Shuman, C. A., Meese, D. A., Gow, A. J., Taylor, K. C., Cuffey, K. M., Fitzpatrick, J. J., Grootes, P. M., Zielinski, G. A., Ram, M., Spinelli, G., and Elder, B.: Visual-stratigraphic dating of the GISP2 ice core: Basis, reproducibility, and application, Journal of geophysical research, 102, 26 367, doi:10.1029/96JC03837, 1997.

Angert, A., Cappa, C. D., and DePaolo, D. J.: Kinetic ^{17}O effects in the hydrologic cycle: Indirect evidence and implications, Geochimica et cosmochimica acta, 68, 3487–3495, doi:10.1016/j.gca.2004.02.010, 2004.

Arthern, R. J., Winebrenner, D. P., and Vaughan, D. G.: Antarctic snow accumulation mapped using polarization of 4.3-cm wavelength microwave emission, Journal of Geophysical Research (Atmospheres), 111, D06107, doi:10.1029/2004JD005667, 2006.

Barkan, E. and Luz, B.: High precision measurements of $^{17}O/^{16}O$ and $^{18}O/^{16}O$ ratios in H_2O, Rapid Communications in Mass Spectrometry, 19, 3737–3742, 2005.

Barlow, R. J.: Statistics: a guide to the use of statistical methods in the physical sciences, vol. 29, John Wiley & Sons, 1989.

Barnes, P. R. F. and Wolff, E. W.: Distribution of soluble impurities in cold glacial ice, Journal of Glaciology, 50, 311–324, doi:10.3189/172756504781829918, 2004.

Benassai, S., Becagli, S., Gragnani, R., Magand, O., Proposito, M., Fattori, I., Traversi, R., and Udisti, R.: Sea-spray deposition in Antarctic coastal and plateau areas from ITASE traverses, Annals of Glaciology, 41, 32–40, doi: 10.3189/172756405781813285, 2005.

Blake, E. W., Wake, C. P., and Gerasimoff, M. D.: The ECLIPSE drill: a field-portable intermediate-depth ice-coring drill, Journal of Glaciology, 44, 175–178, 1998.

Bradley, R. S.: Paleoclimatology: reconstructing climates of the Quaternary, vol. 68, Academic Press, 1999.

Charles, C. D., Rind, D., Jouzel, J., Koster, R. D., and Fairbanks, R. G.: Seasonal Precipitation Timing and Ice Core Records, Science, 269, 247–248, doi: 10.1126/science.269.5221.247, 1995.

Cohen, L. and Dean, S.: Snow on the Ross Ice Shelf: comparison of reanalyses and observations from automatic weather stations, The Cryosphere, 7, 1399–1410, doi:10.5194/tc-7-1399-2013, URL `http://www.the-cryosphere.net/7/1399/2013/`, 2013.

Cole-Dai, J., Mosley-Thompson, E., and Thompson, L. G.: Annually resolved southern hemisphere volcanic history from two Antarctic ice cores, Journal of geophysical research, 102, 16 761, doi:10.1029/97JD01394, 1997.

Cole-Dai, J., Mosley-Thompson, E., Wight, S. P., and Thompson, L. G.: A 4100-year record of explosive volcanism from an East Antarctica ice core, Journal of geophysical research, 105, 24 431, doi:10.1029/2000JD900254, 2000.

Comiso, J.: Bootstrap Sea Ice Concentrations from Nimbus-7 SMMR and DMSP SSM/I-SSMIS. Version 2. Five pixels between Mill Island and Bowman Island, 1979 - 2009. Boulder, Colorad USA: NASA DAAC at the National Snow and Ice Data Center, 2000. Updated 2014.

Curran, M. A. J. and Palmer, A. S.: Suppressed ion chromatography methods for the routine determination of ultra low level anions and cations in ice cores, Journal of Chromatography A, 919, 17–113, 2001.

Curran, M. A. J., van Ommen, T. D., and Morgan, V.: Seasonal characteristics of the major ions in the high-accumulation Dome Summit South ice core, Law Dome, Antarctica, Annals of Glaciology, 27, 385–390, 1998.

Curran, M. A. J., Palmer, A. S., van Ommen, T. D., Morgan, V. I., Phillips, K. L., McMorrow, A. J., and Mayewski, P. A.: Post-depositional movement of methanesulphonic acid at Law Dome, Antarctica, and the influence of accumulation rate, Annals of Glaciology, 35, 333–339, doi:10.3189/172756402781816528, 2002.

Curran, M. A. J., van Ommen, T. D., Morgan, V. I., Phillips, K. L., and Palmer, A. S.: Ice Core Evidence for Antarctic Sea Ice Decline Since the 1950s, Science, 302, 1203–1206, doi:10.1126/science.1087888, 2003.

Dansgaard, W.: Stable isotopes in precipitation, Tellus, 16, 436–468, 1964.

Dansgaard, W., Clausen, H. B., Gundestrup, N., Hammer, C. U., Johnsen, S. F., Kristinsdottir, P. M., and Reeh, N.: A New Greenland Deep Ice Core, Science, 218, 1273–1277, doi:10.1126/science.218.4579.1273, 1982.

Das, I., Bell, R. E., Scambos, T. A., Wolovick, M., Creyts, T. T., Studinger, M., Frearson, N., Nicolas, J. P., Lenaerts, J. T. M., and van den Broeke, M. R.: Influence of persistent wind scour on the surface mass balance of Antarctica, Nature Geoscience, 6, 367–371, doi:10.1038/ngeo1766, 2013.

Das, S. B. and Alley, R. B.: Characterization and formation of melt layers in polar snow: observations and experiments from West Antarctica, Journal of Glaciology, 51, 307–312, doi:10.3189/172756505781829395, 2005.

Dee, D. P., Uppala, S. M., Simmons, A. J., Berrisford, P., Poli, P., Kobayashi, S., Andrae, U., Balmaseda, M. A., Balsamo, G., Bauer, P., Bechtold, P., Beljaars, A. C. M., van de Berg, L., Bidlot, J., Bormann, N., Delsol, C., Dragani, R., Fuentes, M., Geer, A. J., Haimberger, L., Healy, S. B., Hersbach, H., Hólm, E. V., Isaksen, L., Kållberg, P., Köhler, M., Matricardi, M., McNally, A. P., Monge-Sanz, B. M., Morcrette, J.-J., Park, B.-K., Peubey, C., de Rosnay, P., Tavolato, C., Thépaut, J.-N., and Vitart, F.: The ERA-Interim reanalysis: configuration and performance of the data assimilation system, Quarterly Journal of the Royal Meteorological Society, 137, 553–597, doi:10.1002/qj.828, 2011.

Delmotte, M., Masson, V., Jouzel, J., and Morgan, V. I.: A seasonal deuterium excess signal at Law Dome, coastal eastern Antarctica: A southern ocean signature, Journal of Geophysical Research, 105, 7187–7197, doi:10.1029/1999JD901085, 2000.

Domensino, B.: Using synoptic climate pattern typing to resolve snow accumulation and glaciochemical variability at Mill Island, East Antarctica, department of Environment and Geography, Macquarie University, Honours thesis, 2010.

Environmental Modeling Center, National Centers for Environmental Prediction, N. W. S. N. U. D. o. C.: NCEP Climate Forecast System Reanalysis (CFSR) Selected Hourly Time-Series Products, January 1979 to December 2010, URL `http://rda.ucar.edu/datasets/ds093.1/`, 2010.

Evers, L. G., Green, D. N., Young, N. W., and Snellen, M.: Remote hydroacoustic sensing of large icebergs in the southern Indian Ocean: Implications for iceberg monitoring, Geophysical Research Letters, 40, 4694–4699, doi:10.1002/grl.50914, 2013.

Favier, V., Agosta, C., Parouty, S., Durand, G., Delaygue, G., Gallée, H., Drouet, A.-S., Trouvilliez, A., and Krinner, G.: An updated and quality controlled surface mass balance dataset for Antarctica, The Cryosphere, 7, 583–597, doi:10.5194/tc-7-583-2013, 2013.

Ferrier, R. C., Jenkins, A., and Elston, D. A.: The composition of rime ice as an indicator of the quality of winter deposition, Environmental Pollution, 87, 259–266, 1995.

Fraser, A. D., Massom, R. A., Michael, K. J., Galton-Fenzi, B. K., and Lieser, J. L.: East Antarctic Landfast Sea Ice Distribution and Variability, 2000-08, Journal of Climate, 25, 1137–1156, doi:10.1175/JCLI-D-10-05032.1, 2012.

Fraser, A. D., Nigro, M. A., Ligtenberg, S. R. M., Legresy, B., Inoue, M., Cassano, J. J. andKuipers Munneke, P., Lenaerts, J. T. M., Young, N. W., Treverrow, A., Van den Broeke, M., and Enomoto, H.: Characterisation and investigation of drivers of Antarctic dry snow zone C band backscatter variability using ASCAT, 2015, submitted.

Gjessing, Y.: Excess and deficit of sulfate in polar snow, Atmospheric Environment (1967), 23, 155–160, 1989.

Goodwin, I., de Angelis, M., Pook, M., and Young, N. W.: Snow accumulation variability in Wilkes Land, East Antarctica, and the relationship to atmospheric ridging in the 130°-170°E region since 1930, Journal of Geophysical Research (Atmospheres), 108, 4673, doi:10.1029/2002JD002995, 2003.

Goodwin, I. D.: Snow accumulation and surface topography in the katabatic zone of Eastern Wilkes Land, Antarctica, Antarctic science, 2, 235–242, 1990.

Goodwin, I. D., van Ommen, T. D., Curran, M. A. J., and Mayewski, P. A.: Mid latitude winter climate variability in the South Indian and southwest Pacific regions since 1300 AD, Climate Dynamics, 22, 783–794, doi:10.1007/s00382-004-0403-3, 2004.

Hall, J. S. and Wolff, E. W.: Causes of seasonal and daily variations in aerosol sea-salt concentrations at a coastal Antarctic station, Atmospheric Environment, 32, 3669–3677, doi:10.1016/S1352-2310(98)00090-9, 1998.

IPCC: Fifth Assessment Report. Climate Change 2013. The AR5 Synthesis Report, Geneva IPCC, URL `http://www.ipcc.ch/report/ar5/wg1/#.UoSDJflmiSo`, 2013.

IPCC: Climate Change 2014: Synthesis Report. Contribution of Working Groups I, II and III to the Fifth Assessment Report of the Intergovernmental Panel on Climate Changet, Geneva: IPCC, URL http://www.ipcc.ch/report/ar5/wg1/#.UoSDJflmiSo, 2014.

Jones, P. D., Briffa, K. R., Osborn, T. J., Lough, J. M., van Ommen, T. D., Vinther, B. M., Luterbacher, J., Wahl, E. R., Zwiers, F. W., Mann, M. E., Schmidt, G. A., Ammann, C. M., Buckley, B. M., Cobb, K. M., Esper, J., Goosse, H., Graham, N., Jansen, E., Kiefer, T., Kull, C., Küttel, M., Mosley-Thompson, E., Overpeck, J. T., Riedwyl, N., Schulz, M., Tudhope, A. W., Villalba, R., Wanner, H., Wolff, E., and Xoplaki, E.: High-resolution palaeoclimatology of the last millennium: a review of current status and future prospects, The Holocene, 19, 3–49, doi:10.1177/0959683608098952, URL http://hol.sagepub.com/content/19/1/3.abstract, 2009.

Kaleschke, L., Richter, A., Burrows, J., Afe, O., Heygster, G., Notholt, J., Rankin, A. M., Roscoe, H. K., Hollwedel, J., Wagner, T., and Jacobi, H.-W.: Frost flowers on sea ice as a source of sea salt and their influence on tropospheric halogen chemistry, Geophysical Research Letters, 31, L16114, doi:10.1029/2004GL020655, 2004.

Kinnard, C., Koerner, R. M., Zdanowicz, C. M., Fisher, D. A., Zheng, J., Sharp, M. J., Nicholson, L., and Lauriol, B.: Stratigraphic analysis of an ice core from the Prince of Wales Icefield, Ellesmere Island, Arctic Canada, using digital image analysis: High-resolution density, past summer warmth reconstruction, and melt effect on ice core solid conductivity, Journal of Geophysical Research (Atmospheres), 113, D24120, doi:10.1029/2008JD011083, 2008.

Kreutz, K. J., Mayewski, P. A., Whitlow, S. I., and Twickler, M. S.: Limited migration of soluble ionic species in a Siple Dome, Antarctica, ice core, Annals of Glaciology, 27, 371–377, 1998.

Krinner, G. and Werner, M.: Impact of precipitation seasonality changes on isotopic signals in polar ice cores: a multi-model analysis, Earth and Planetary Science Letters, 216, 525–538, doi:10.1016/S0012-821X(03)00550-8, 2003.

Laj, P., Sigurdsson, H., Drummey, S. M., Spencer, M. J., and Palais, J. M.: Depletion of H_2O_2 in a Greenland ice core - Implications for oxidation of volcanic SO_2, Nature, 346, 45–48, doi:10.1038/346045a0, 1990.

Landais, A., Barkan, E., and Luz, B.: Record of $\delta^{18}O$ and ^{17}O-excess in ice from Vostok Antarctica during the last 150,000 years, Geophysical Research Letters, 35, L02709, doi:10.1029/2007GL032096, 2008.

Landais, A., Ekaykin, A., Barkan, E., Winkler, R., and Luz, B.: Seasonal variations of ^{17}O-excess and D-excess in snow precipitation at Vostok station, East Antarctica, Journal of Glaciology, 58, 725–733, doi:10.3189/2012JoG11J237, 2012.

Langway, C. C.: Stratigraphic analysis of a deep ice core from Greenland, vol. 125, Geological Society of America, 1970.

Lee, H., Shum, C. K., Howat, I. M., Monaghan, A., Ahn, Y., Duan, J., Guo, J.-Y., Kuo, C.-Y., and Wang, L.: Continuously accelerating ice loss over Amundsen Sea catchment, West Antarctica, revealed by integrating altimetry and GRACE data, Earth and Planetary Science Letters, 321, 74–80, doi:10.1016/j.epsl.2011.12.040, 2012.

Legrand, M. and Mayewski, P.: Glaciochemistry of polar ice cores: A review, Reviews of Geophysics, 35, 219–244, doi:10.1029/96RG03527, 1997.

Lenaerts, J. T. M., van den Broeke, M. R., van de Berg, W. J., van Meijgaard, E., and Kuipers Munneke, P.: A new, high-resolution surface mass balance map of Antarctica (1979-2010) based on regional atmospheric climate modeling, Geophysical Research Letters, 39, L04501, doi:10.1029/2011GL050713, 2012.

Lenaerts, J. T. M., Meijgaard, E., Broeke, M. R., Ligtenberg, S. R. M., Horwath, M., and Isaksson, E.: Recent snowfall anomalies in Dronning Maud Land, East Antarctica, in a historical and future climate perspective, Geophysical Research Letters, 40, 2684–2688, doi:10.1002/grl.50559, 2013.

Ligtenberg, S. R. M., Horwath, M., van den Broeke, M. R., and Legrésy, B.: Quantifying the seasonal "breathing" of the Antarctic Ice Sheet, Geophysical Research Letters, 39, L23501, doi:10.1029/2012GL053628, 2012.

Linow, S., Hörhold, M. W., and Freitag, J.: Grain-size evolution of polar firn: a new empirical grain growth parameterization based on X-ray microcomputer tomography measurements, Journal of Glaciology, 58, 1245–1252, doi:10.3189/2012JoG11J256, 2012.

Livingston, F. E. and George, S. M.: Effect of sodium on HCl hydrate diffusion in ice: Evidence for anion-cation trapping, The Journal of Physical Chemistry A, 106, 5114–5119, 2002.

Logan, J. A., Prather, M. J., Wofsy, S. C., and McElroy, M. B.: Tropospheric chemistry - A global perspective, Journal of Geophysical Research, 86, 7210–7254, doi:10.1029/JC086iC08p07210, 1981.

Long, M.: Icebergs: useful archives for climate information, institute of Antarctic and Southern Ocean Studies, University of Tasmania, Honours thesis, 2004.

Magand, O., Genthon, C., Fily, M., Krinner, G., Picard, G., Frezzotti, M., and Ekaykin, A. A.: An up-to-date quality-controlled surface mass balance data set for the 90°-180°E Antarctica sector and 1950-2005 period, Journal of Geophysical Research (Atmospheres), 112, D12106, doi:10.1029/2006JD007691, 2007.

Martin, S., Yu, Y., and Drucker, R.: The temperature dependence of frost flower growth on laboratory sea ice and the effect of the flowers on infrared observations of the surface, Journal of Geophysical Research, 101, 12 111, doi: 10.1029/96JC00208, 1996.

Massom, R. A., Giles, A. B., Fricker, H. A., Warner, R. C., LegréSy, B., Hyland, G., Young, N., and Fraser, A. D.: Examining the interaction between multi-year landfast sea ice and the Mertz Glacier Tongue, East Antarctica: Another factor in ice sheet stability?, Journal of Geophysical Research (Oceans), 115, C12027, doi:10.1029/2009JC006083, 2010.

McConnell, J. R., Winterle, J. R., Bales, R. C., Thompson, A. M., and Stewart, R. W.: Physically based inversion of surface snow concentrations of H_2O_2 to atmospheric concentrations at South Pole, Geophysical Research Letters, 24, 441–444, doi:10.1029/97GL00183, 1997.

McMorrow, A. J., Curran, M. A. J., van Ommen, T. D., Morgan, V., Pook, M. J., and Allison, I.: Intercomparison of firn core and meteorological data, (Antarctic Science), 13, 329–337, doi:10.1017/S0954102001000463, 2001.

Minikin, A., Legrand, M., Hall, J., Wagenbach, D., Kleefeld, C., Wolff, E., Pasteur, E. C., and Ducroz, F.: Sulfur-containing species (sulfate and methanesulfonate) in coastal Antarctic aerosol and precipitation, Journal of Geophysical Research, 103, 10 975, doi:10.1029/98JD00249, 1998.

Monaghan, A. J., Bromwich, D. H., Fogt, R. L., Wang, S.-H., Mayewski, P. A., Dixon, D. A., Ekaykin, A., Frezzotti, M., Goodwin, I., Isaksson, E., Kaspari, S. D., Morgan, V. I., Oerter, H., Van Ommen, T. D., Van der Veen, C. J., and Wen, J.: Insignificant Change in Antarctic Snowfall Since the International Geophysical Year, Science, 313, 827–831, doi:10.1126/science.1128243, 2006.

Moore, J. C., Reid, A. P., and Kipfstuhl, J.: Microstructure and electrical properties of marine ice and its relationship to meteoric ice and sea ice, Journal of geophysical research, 99, 5171–5180, doi:10.1029/93JC02832, 1994.

Morgan, V. I.: Antarctic Ice Sheet surface oxygen isotope values, Journal of Glaciology, 28, 315–323, 1982.

Morgan, V. I.: An oxygen isotope: Climate record from the Law Dome, Antarctica, Climatic Change, 7, 415–426, 1985.

Morgan, V. I., Wookey, C. W., Li, J., van Ommen, T. D., Skinner, W., and Fitzpatrick, M. F.: Site information and initial results from deep ice drilling on Law Dome, Antarctica, Journal of Glaciology, 43, 3–10, 1997.

Mudelsee, M.: Estimating Pearson's correlation coefficient with bootstrap confidence interval from serially dependent time series, Mathematical Geology, 35, 651–665, 2003.

Mudelsee, M.: Break function regression. A tool for quantifying trend changes in climate time series, European Physical Journal Special Topics, 174, 49–63, doi: 10.1140/epjst/e2009-01089-3, 2009.

Mulvaney, R. and Wolff, E. W.: Spatial variability of the major chemistry of the Antarctic Ice Sheet, Annals of Glaciology, 20, 440–447, 1994.

Mulvaney, R., Pasteur, E. C., Peel, D. A., Saltzman, E. S., and Whung, P.: The ratio of MSA to non-sea-salt sulphate in Antarctic Peninsula ice cores, Tellus B, 44, 295–303, 1992.

Nihashi, K. and Ohshima, K, I.: Circumpolar mapping of Antarctic coastal polynyas and landfast sea ice: relationship and variability, Journal of Climate, doi: 10.1175/JCLI-D-14-00369.1, 2015.

O'Dowd, C. D. and de Leeuw, G.: Marine aerosol production: a review of the current knowledge, Royal Society of London Philosophical Transactions Series A, 365, 1753–1774, doi:10.1098/rsta.2007.2043, 2007.

PAGES 2k Consortium, Ahmed, M., Anchukaitis, K. J., Asrat, A., Borgaonkar, H. P., Braida, M., Buckley, B. M., Büntgen, U., Chase, B. M., Christie, D. A., Cook, E. R., Curran, M. A. J., Diaz, H. F., Esper, J., Fan, Z.-X., Gaire, N. P., Ge, Q., Gergis, J., González-Rouco, J. F., Goosse, H., Grab, S. W., Graham, N., Graham, R., Grosjean, M., Hanhijärvi, S. T., Kaufman, D. S., Kiefer, T., Kimura, K., Korhola, A. A., Krusic, P. J., Lara, A., Lézine, A.-M., Ljungqvist, F. C., Lorrey, A. M., Luterbacher, J., Masson-Delmotte, V., McCarroll, D., McConnell, J. R., McKay, N. P., Morales, M. S., Moy, A. D., Mulvaney, R., Mundo, I. A., Nakatsuka, T., Nash, D. J., Neukom, R., Nicholson, S. E., Oerter, H., Palmer, J. G., Phipps, S. J., Prieto, M. R., Rivera, A., Sano, M., Severi, M., Shanahan, T. M., Shao, X., Shi, F., Sigl, M., Smerdon, J. E., Solomina, O. N., Steig, E. J., Stenni, B., Thamban, M., Trouet, V., Turney, C. S. M., Umer, M., van Ommen, T., Verschuren, D., Viau, A. E., Villalba, R., Vinther, B. M., von Gunten, L., Wagner, S., Wahl, E. R., Wanner, H., Werner, J. P., White, J. W. C., Yasue, K., and Zorita, E.: Continental-scale temperature variability during the past two millennia, Nature Geoscience, 6, 503, doi:10.1038/ngeo1849, 2013.

Palmer, A. S., van Ommen, T. D., Curran, M. A. J., Morgan, V., Souney, J. M., and Mayewski, P. A.: High-precision dating of volcanic events (AD 1301–1995) using ice cores from Law Dome, Antarctica, Journal of Geophysical Research, 106, 28–089, 2001.

Palmer, A. S., Morgan, V. I., Curran, M. A. J., van Ommen, T. D., and Mayewski, P. A.: Antarctic volcanic flux ratios from Law Dome ice cores, Annals of Glaciology, 35, 329–332, doi:10.3189/172756402781816771, 2002.

Parish, T. R. and Bromwich, D. H.: The surface windfield over the Antarctic ice sheets, Nature, 328, 51–54, doi:10.1038/328051a0, 1987.

Pasteur, E. C. and Mulvaney, R.: Migration of methane sulphonate in Antarctic firn and ice, Journal of Geophysical Research, 105, 11 525–11 534, doi: 10.1029/2000JD900006, 2000.

Paterson, W. S. B.: The physics of glaciers, Pergamon, UK, 3rd edn., 1994.

Perovich, D. K. and Richter-Menge, J. A.: Surface characteristics of lead ice, Journal of Geophysical Research, 99, 16 341, doi:10.1029/94JC01194, 1994.

Persson, A., Langen, P. L., Ditlevsen, P., and Vinther, B. M.: The influence of precipitation weighting on interannual variability of stable water isotopes in Greenland, Journal of Geophysical Research (Atmospheres), 116, D20120, doi: 10.1029/2010JD015517, 2011.

Plummer, C. T., Curran, M. A. J., van Ommen, T. D., Rasmussen, S. O., Moy, A. D., Vance, T. R., Clausen, H. B., Vinther, B. M., and Mayewski, P. A.: An independently dated 2000-yr volcanic record from Law Dome, East Antarctica, including a new perspective on the dating of the 1450s CE eruption of Kuwae, Vanuatu, Climate of the Past, 8, 1929–1940, doi:10.5194/cp-8-1929-2012, 2012.

Powers, J. G., Manning, K. W., Bromwich, D. H., Cassano, J. J., and Cayette, A. M.: A decade of Antarctic science support through AMPS, Bulletin of the American Meteorological Society, 93, 1699–1712, doi:10.1175/BAMS-D-11-00186.1, 2012.

Rankin, A. M., Auld, V., and Wolff, E. W.: Frost flowers as a source of fractionated sea salt aerosol in the polar regions, Geophysical Research Letters, 27, 3469–3472, doi:10.1029/2000GL011771, 2000.

Rankin, A. M., Wolff, E. W., and Martin, S.: Frost flowers: Implications for tropospheric chemistry and ice core interpretation, Journal of Geophysical Research (Atmospheres), 107, 4683, doi:10.1029/2002JD002492, 2002.

Raphael, M. N.: A zonal wave 3 index for the Southern Hemisphere, Geophysical Research Letters, 31, n/a–n/a, doi:10.1029/2004GL020365, URL `http://dx.doi.org/10.1029/2004GL020365`, l23212, 2004.

Raphael, M. N.: The influence of atmospheric zonal wave three on Antarctic sea ice variability, Journal of Geophysical Research: Atmospheres (1984–2012), 112, 2007.

Roberts, J., Plummer, C., Vance, T., van Ommen, T., Moy, A., Poynter, S., Treverrow, A., Curran, M., and George, S.: A 2000-year annual record of snow accumulation rates for Law Dome, East Antarctica, Climate of the Past, 11, 697–707, doi:10.5194/cp-11-697-2015, 2015.

Roberts, J. L., Moy, A. D., van Ommen, T. D., Curran, M. A. J., Worby, A. P., Goodwin, I. D., and Inoue, M.: Borehole temperatures reveal a changed energy budget at Mill Island, East Antarctica, over recent decades, The Cryosphere, 7, 263–273, doi:10.5194/tc-7-263-2013, 2013.

Sakurai, T., Ohno, H., Genceli, F. E., Horikawa, S., Iizuka, Y., Uchida, T., and Hondoh, T.: Magnesium methanesulfonate salt found in the Dome Fuji (Antarctica) ice core, Journal of Glaciology, 56, 837–842, doi:10.3189/002214310794457335, 2010.

Schneider, D. P., Steig, E. J., van Ommen, T. D., Dixon, D. A., Mayewski, P. A., Jones, J. M., and Bitz, C. M.: Antarctic temperatures over the past two centuries from ice cores, AGU Fall Meeting Abstracts, 2006.

Sigg, A. and Neftel, A.: Seasonal variations in hydrogen peroxide in polar ice cores, Annals of Glaciology, 10, 157–162, 1988.

Sigg, A. and Neftel, A.: Evidence for a 50 percent increase in H2O2 over the past 200 years from a Greenland ice core, Nature, 351, 557–559, doi:10.1038/351557a0, 1991.

Sinclair, K. E., Bertler, N. A. N., and van Ommen, T. D.: Twentieth-century surface temperature trends in the Western Ross Sea, Antarctica: Evidence from a high-resolution ice core, Journal of Climate, 25, 3629–3636, doi:10.1175/JCLI-D-11-00496.1, 2012.

Steig, E. J., Ding, Q., White, J. W. C., Küttel, M., Rupper, S. B., Neumann, T. A., Neff, P. D., Gallant, A. J. E., Mayewski, P. A., Taylor, K. C., Hoffmann, G., Dixon, D. A., Schoenemann, S. W., Markle, B. R., Fudge, T. J., Schneider, D. P., Schauer, A. J., Teel, R. P., Vaughn, B. H., Burgener, L., Williams, J., and Korotkikh, E.: Recent climate and ice-sheet changes in West Antarctica compared with the past 2,000 years, Nature Geoscience, 6, 372–375, doi:10.1038/ngeo1778, 2013.

Thomas, R., Davis, C., Frederick, E., Krabill, W., Li, Y., Manizade, S., and Martin, C.: A comparison of Greenland ice-sheet volume changes derived from altimetry measurements, Journal of Glaciology, 54, 203–212, doi:10.3189/002214308784886225, 2008.

Turner, J. and Pendlebury, S., eds.: The International Antarctic Weather Forecasting Handbook, British Antarctic Survey, 2004.

Uemura, R., Matsui, Y., Yoshimura, K., Motoyama, H., and Yoshida, N.: Evidence of deuterium excess in water vapor as an indicator of ocean surface conditions, Journal of Geophysical Research (Atmospheres), 113, D19114, doi:10.1029/2008JD010209, 2008.

Uemura, R., Masson-Delmotte, V., Jouzel, J., Landais, A., Motoyama, H., and Stenni, B.: Ranges of moisture-source temperature estimated from Antarctic ice cores stable isotope records over glacial-interglacial cycles, Climate of the Past, 8, 1109–1125, doi:10.5194/cp-8-1109-2012, 2012.

van Loon, H. and Jenne, R. L.: The zonal harmonic standing waves in the southern hemisphere, Journal of Geophysical Research, 77, 992, doi: 10.1029/JC077i006p00992, 1972.

van Ommen, T. D. and Morgan, V.: Peroxide concentrations in the Dome Summit South ice core, Law Dome, Antarctica, Journal of Geophysical Research, 101, 15 147–15 152, doi:10.1029/96JD00838, 1996.

van Ommen, T. D. and Morgan, V.: Calibrating the ice core paleothermometer using seasonality, Journal of Geophysical Research, 102, 9351–9358, doi: 10.1029/96JD04014, 1997.

van Ommen, T. D. and Morgan, V.: Snowfall increase in coastal East Antarctica linked with southwest Western Australian drought, Nature Geoscience, 3, 267–272, doi:10.1038/ngeo761, 2010.

Vance, T. R., van Ommen, T. D., Curran, M. A. J., Plummer, C. T., and Moy, A. D.: A millennial proxy record of ENSO and eastern Australian rainfall from the Law Dome ice core, East Antarctica, Journal of Climate, 26, 710–725, doi: 10.1175/JCLI-D-12-00003.1, 2013.

Vance, T. R., Roberts, J. L., Plummer, C. T., Kiem, A. S., and van Ommen, T. D.: Interdecadal Pacific variability and eastern Australian megadroughts over the last millennium, Geophysical Research Letters, 42, 129–137, doi: 10.1002/2014GL062447, 2015.

Wagenbach, D.: Coastal Antarctica: Atmospheric chemical composition and atmospheric transport, in: Chemical Exchange between the Atmosphere and polar snow, pp. 173–199, Springer, 1996.

Wagenbach, D., Ducroz, F., Mulvaney, R., Keck, L., Minikin, A., Legrand, M., Hall, J. S., and Wolff, E. W.: Sea-salt aerosol in coastal Antarctic regions, Journal of Geophysical Research, 103, 10 961–10 974, doi:10.1029/97JD01804, 1998a.

Welch, K. A., Mayewski, P. A., and Whitlow, S. I.: Methanesulfonic acid in coastal Antarctic snow related to sea-ice extent, Geophysical Research Letters, 20, 443–446, doi:10.1029/93GL00499, 1993.

Winkler, R., Landais, A., Sodemann, H., Dümbgen, L., Prié, F., Masson-Delmotte, V., Stenni, B., and Jouzel, J.: Deglaciation records of ^{17}O-excess in East Antarctica: reliable reconstruction of oceanic normalized relative humidity from coastal sites, Climate of the Past, 8, 1–16, doi:10.5194/cp-8-1-2012, 2012.

Wolff, E. W.: Location, movement and reactions of impurities in solid ice, in: Chemical Exchange Between the Atmosphere and Polar Snow, edited by Wolff, E. W. and Bales, R., vol. 43 of *NATO Advanced Sciences Institutes*, pp. 541–560, Springer-Verlag, 1996.

Wolff, E. W., Rankin, A. M., and Röthlisberger, R.: An ice core indicator of Antarctic sea ice production?, Geophysical Research Letters, 30, 2158, doi: 10.1029/2003GL018454, 2003.

Wong, G. J.: Investigating the Dominant Source of sea salt to Antarctica: The sea salt signal in ice core GD17, university of Tasmania, Honours thesis, 2007.

Yang, X., Pyle, J. A., and Cox, R. A.: Sea salt aerosol production and bromine release: Role of snow on sea ice, Geophysical Research Letters, 35, L16815, doi: 10.1029/2008GL034536, 2008.

Young, N. and Gibson, J.: A century of change in the Shackleton and West ice shelves, East Antarctica, Global and Planetary Change, submitted, 2013.